MODELING OF HEMODIALYSIS OPERATION

A Thesis Submitted to
the Graduate School of Engineering and Sciences of
İzmir Institute of Technology
in Partial Fulfillment of the Requirements for the Degree of

MASTER OF SCIENCE

in Chemical Engineering

by
Hasan Erbil ABACI

August 2008
İZMİR

We approve the thesis of **Hasan Erbil ABACI**

_____

Prof. Dr. Sacide Alsoy ALTINKAYA
Supervisor

_____

Assoc. Prof. Dr. Ali İhsan NESLİTÜRK
Committee Member

_____

Assist. Prof. Dr. *Erol ŞEKER*
Committee Member

01 August 2008

_____

Prof. Dr. Devrim BALKÖSE
Head of the Chemical Engineering Department

_____

Prof. Dr. Hasan BÖKE
Dean of the Graduate School
of Engineering and Sciences

ACKNOWLEDGMENTS

First and foremost, I would like to thank my advisor Dr. Sacide Alsoy Altınkaya, who has shown a large and consistent interest in my project during the times. Beside this work, I have learned so many useful things from her, that will help me to become a part of academia.

I would also like to express my appreciation to my thesis committee; Dr. Erol Şeker, and Dr. Ali İhsan Neslitürk. Their constructive comments have greatly improved this work.

All of my friends, thank you for your patience and understanding throughout my study. One of my most special thanks goes to my dear friend, Pınar, who had always time to help me and let me use her personal computer no matter how busy she is.

Last but not least, my family, I feel so privileged to have parents like you, giving me your unconditional support and love through all this work.

ABSTRACT

MODELING OF HEMODIALYSIS OPERATION

Recent studies have shown that the effectiveness of hemodialysis is based on module geometry, membrane properties and operating conditions. Various experimental work exist in the literature concentrated on the synthesis of new hemodialysis membranes. However, optimization of membrane structure requires extensive and time consuming experimentations. Therefore, mathematical models are neccessary that can be used to predict the performance of hemodialysis operation.

In this study, a predictive theoretical model was developed to predict the solute concentrations in patient's blood and optimize the efficiency of hemodialysis operation. The model takes into account simultaneous mass and momentum transfer along with the adsorption of rejected protein molecules on the surface of the membrane.

Model predictions show that blood and dialysate flowrates are effective for all sizes of molecules. The change in structural properties of the membrane makes no effect on the total removal of urea beacause of its high clearance. On the other hand, a considerable increment in the clearance of larger molecular weight solutes occurs as the pore size and porosity of the membrane increases. The most important design parameter for dialysis unit which influence the solute clearances significantly is found to be the effective diameter among the fibers in the dialyzer.

The model is extended to investigate the use of urease immobilized membranes on the efficiency of the hemodialysis operation. The results have shown that urease immobilization enhances the removal of urea from the blood and decreases the protein adsorption capacity of the polysulfone membrane.

Model predictions are compared with different sets of clearance data available in the literature. The agreement is found to be satisfactory which suggests that the model can be used as a tool to design or test the performance of dialysis units.

ÖZET

HEMODİYALİZ İŞLEMİNİN MODELLENMESİ

Son çalışmalar, hemodiyaliz işleminin verimliliğinin, model geometrisine, membran özelliklerine ve işlem koşullarına bağlı olduğunu göstermiştir. Literatürde, yeni diyaliz membranları sentezlemek amacıyla yapılmış çeşitli deneysel çalışmalar yer almaktadır. Ancak membran yapısının optimizasyonu, kapsamlı ve uzun süreli deneyler gerektirmektedir. Bu nedenle, hemodiyaliz işleminin performansını öngörebilmek için matematiksel modellere ihtiyaç duyulmaktadır.

Bu çalışmada, hasta kanındaki çözünen madde konsantrasyonunu tahmin etmek ve hemodiyaliz işleminin verimini optimize edebilmek amacıyla teorik bir model geliştirilmiştir. Model içerisinde, kütle ve momentum transferi eşzamanlı olarak ele alınmakla birlikte, membran yüzeyi tarafından reddedilen protein moleküllerinin adsorpsiyonu da dikkate alınmıştır.

Model sonuçları, kan ve diyalizat çözeltisi hızlarının, tüm boyuttaki moleküller için etkili olduğunu göstermiştir. Ürenin yüksek temizlenme hızından ötürü, membranın yapısal özelliklerindeki değişikliğin, üre uzaklaştırılmasında etkisiz olduğu saptanmıştır. Öte yandan, gözenek boyutu ve gözeneklilik arttırıldıkça, daha büyük boyutlardaki moleküllerin uzaklaştırılmasında artış gözlenmiştir. Kandan madde uzaklaştırılmasını belirgin bir şekilde etkileyen en önemli dizayn parametresinin, fiberlerin arasıdaki efektif çap olduğu bulunmuştur.

Model, üreaz tutturulmuş membranların, hemodiyaliz işleminin verimini arttırmak için kullanımını incelemek amacıyla genişletilmiştir. Sonuçlar, üreaz tutturulmasının, üre uzaklaştırılmasına katkıda bulunduğunu ve polisülfon membranının protein adsorpsiyon kapasitesini azalttığını göstermiştir.

Model tahminleri, literatürdeki farklı deneysel sonuçlarla karşılaştırılmıştır. Tutarlılık, tatmin edici olup, modelin diyaliz ünitelerinin tasarlanması ve performansının sınanması için bir araç olarak kullanılabileceğini göstermiştir.

TABLE OF CONTENTS

LIST OF TABLES

Table..... ...

LIST OF FIGURES

Figure .....

NOMENCLATURE

ϕ = Partition coefficient

σ = Staverman coefficient

Γ = Adsorption coefficient, cm^{-1}

ρ_i = Concentration of species *i,* g/cm^3

κ = Debye screening length, cm^{-1}

$\rho_{\substack{ads. \\ layer}}$ = Density of adsorbed protein layer, g/cm^3

ς = Dielectric constant

ε_o = Dielectric permittivity, $C^2 / N.m^2$

D_∞ = Diffusion coefficient in free space, cm^2/sec

y_s = Dimensionless particle electrical potential

ψ_s = Dimensionless surface electrical potential

μ = Dimensionless viscosity

y_{eff} = Effective particle electrical potential

ΔU^{el} = Electrostatic interaction energy, joule

ξ = Fiber length to diameter ratio, $L / 2R_i$

β = Mass transfer coefficient, cm/sec

δ = Membrane thickness, cm

π = Oncotic Pressure, mmHg

λ_s = Pore size, cm

$\hat{v}_p$ = Specific volume of protein, cm^3/g

γ = Stoichiometric coefficient

ΔU^{vdw} = Van der Waals interaction energy, joule

a = Protein radius, cm

A_s= Membrane surface area, cm^2

a_v = Specific surface area, cm^2

d_B = Fiber inner diameter, cm

d_{hous}= Housing diameter, cm

e = Electron charge, C

F = Force acting on particles, N

ΔG = Gibbs free energy, joule

I = Ionic strength, M

J_v= Total volumetric flux, cm/sec

k = Boltzman Constant, $cm^2.g/sec^2$.Kelvin

K= Proportionality Coefficient

K_C = Convective hindrance factor

K_D = Diffusive hindrance factor

K^{IE} = Intercompartmental solute clearance, cm^3/sec

K_{ov}= Overall mass transfer coefficient, cm/sec

L= Fiber length, cm

υ = Local fluid velocity, cm/sec

L_p= Hydraulic permeability, cm/sec.mmHg

m_p=Amount of protein adsorbed, g

N_p= Protein flux towards membrane, g/cm^2.sec

N_s = Solute flux through porous layer , g/cm^2.sec

N_{tube}= Number of fibers

P = Pressure, mmHg

Pe= Peclet number, $U_{avg} R_i^2 / D_{AB} L$

P_{em}= Diffusive permeability, cm^2/sec

q = Amount of protein adsorbed per specific area, g/cm^2

Q = Volumetric flow rate, cm^3/sec

Q_{max1} = Adsorption capacity for primary adsorption, g/cm^2

Q_{max2}= Adsorption capacity for secondary adsorption, g/cm^2

Re = Reynold's Number, $d_{hous} U_{avg} \rho / \mu$

R_i = Fiber radius, cm

R_{pore}= Pore radius, cm

T = Absolute temperature, Kelvin

U = Dimensionless axial blood velocity, cm/sec

V = Dimensionless radial blood velocity, cm/sec

V^E = Volume of extracellular water, cm^3

V^I = Volume of intracellular water, cm^3

z_o= Closest approach between protein-surface, cm

Subscripts

B = Blood

D = Dialysate

1 = Dense layer of membrane

2 = Porous layer of membrane

w = Membrane wall

b = Bulk solution

UF = Ultrafiltration

i = Species

p = Protein

enz = Enzyme

avg=Average

INTRODUCTION

Chronic renal failure is the final common pathway of a number of kidney diseases. The choices for a patient suffering from renal failure are chronic dialysis treatments (either hemodialysis or peritoneal dialysis), and renal transplantation. Worldwide, hundreds of thousands of patients are currently treated with hemodialysis, due to the limited number of donors, age or coexistent disease of the patient. Routine clinical dialysis therapies are still expensive and long lasting. Many facets of the uraemic syndrome are not improved, causing high mortality on dialysis (Pandya and Farrington 2003) and this is usually attributed to the insufficient hemocompatibility of the hemodialysis membranes.

To minimize undesirable reaction between blood and the membrane surface and to shorten the treatment time, numerous high flux membranes and membrane modules are being developed for hemodialyzers. The structural properties of newly developed membranes and module design should be optimized by testing their performances before using in clinical applications. The optimization requires extensive trial and error experimentation which is usually costly and time consuming. This difficulty can be greatly overwhelmed by accurate and reliable mathematical models which can also be used to optimize both operating conditions for routine clinical applications.

Various efforts have been made to develop theoretical models for predicting the performance of hemodialysis operation. In many of these studies, total solute flux J_v is assumed constant (Jaffrin, et al. 1981; Kunimoto, et al. 1977; Sigdell 1982; Stiller, et al. 1985) and mass transfer of solutes through the membrane is defined with an overall mass transfer coefficient (Werynski and Wanieski 1995; Wüpper, et al.1996), to include blood, membrane and dialysate resistances for the given solute. In some cases, the transmembrane solute flux is defined in terms of both diffusive and convective transport (Raff, et al. 2003). The empirical and correlative nature of these models limit their practical application.

In addition, they assume that the solute concentrations are uniformly distributed in the cross-section so that the diffusional mass transfer of solutes are caused by the concentration difference between the bulk and membrane phases (Legallais, et al. 2000; Wüpper, et al. 1997) and they do not consider the momentum transport in blood and dialysate sides.

In a few studies, momentum and mass transfer are considered together (Moussy 2000; Noda et al. 1978). However, the use of these models are also limited due to assumptions utilized either for obtaining analytical solutions or for neglecting mass transfer resistance of the membrane.

In the first part of the study a theoretical model is developed to predict the in vitro performance of commercial hemodialysis units. The model takes into account simultaneous momentum and mass transfer on the blood side both in radial and axial directions. Mass transfer is assumed to take place both by diffusion and convection in the radial direction, while convection is considered to be dominant mass transfer mechanism in the axial direction. Furthermore, adsorption of large blood molecules on the membrane surface is taken into account. Model predictions for the clearances of creatinine, vitamin B12 and myoglobin are compared with the experimental data available in the literature (Bosch, et al. 1985; Jaffrin, et al. 1981).

In the second part of the study, the model was extended to evaluate the influence of urease enzyme immobilization on the performance of hemodialysis units. Urease enzyme can catalyze the hydrolysis of urea to ammonia and carbon dioxide. Yang and Lin (2003) have shown that urease immobilized on the surface of hydrolyzed PAN hollow fibers enhanced the rate of removal of urea compared with that of the regular dialyzer. Mahlicli (2007) has found that urease immobilization into cellulose acetate membrane not only increased the rate of removal of urea but also decreased the protein adsorption capacity of these membranes.

The objective of the second model is to be able to predict experimentally observed advantages of urease immobilized hemodialysis membranes. For this purpose, enzyme layer immobilized on the membrane surface is considered as a porous gel layer in which decomposition of urea takes place. In order to exhibit the difference between the protein adsorption capacity of plain and enzyme immobilized membrane, electrostatic and Van der Waals forces between the protein-protein and protein-surface are taken into account with Derjaguin-Landau-Verwey-Overbeek(DLVO) theory. Both models were used to investigate the influences of the operating conditions, structural characteristics of the membrane, surface charge of the membrane and dimensions of the dialyzer on the performance of the hemodialysis operation. The clearance values of the model toxic compounds at the end of 4 hours, typical treatment time, was chosen as performance criteria. For each model, the effect of neglecting protein adsorption on the predictions was determined.

This thesis consists of 7 Chapters. In Chapter 1, the necessity of this study and the main objectives are mentioned. In following Chapter, basic principles of the hemodialysis operation is given including the different module geometries, common types of hemodialysis membranes and classification of hemodialysis. The previous studies concentrated on developing theoretical models of hemodialysis operation are involved in Chapter 3, from the simplest to more complex models available in the literature. The drawbacks of these mathematical models are also discussed. In Chapter 4, protein fouling in the case of the blood-contact membranes and the parameters effecting the protein adsorption during the hemodialysis operation are mentioned. Model development and assumptions are given under the title of "Theory" in Chapter 5 where the model development is divided into two main sections; Plain membrane model and enzyme immobilized membrane model. Estimation of the model parameters and numerical methods used in the solution of model equations are also included in theory chapter. In Chapter 6, simulation results obtained by the numerical solution of resulting model equations are illustrated and discussed in detail. The effect of structural parameters of membrane, operating conditions and design parameters on the overall efficiency of hemodialysis operation is investigated. Model validation and comparison of plain and enzyme immobilized cases are also given. Finally in Chapter 7, conclusions of this thesis and its contributions either to ongoing researchs or clinical applications are stated.

CHAPTER 2

GENERAL INFORMATION ABOUT HEMODIALYSIS

Hemodialysis is a blood purifying therapy in which the blood of a patient is circulated through an artificial kidney, also called hemodialyzer. This is realized in an extracorporeal circuit(Figure 2.1) where one or two needles (or catheters) can be used to access patient's vascular system. A general hemodialysis therapy lasts about 9-15 hours a week, mostly spread over three sessions. It can take place in a hospital, in a low care unit or at home.

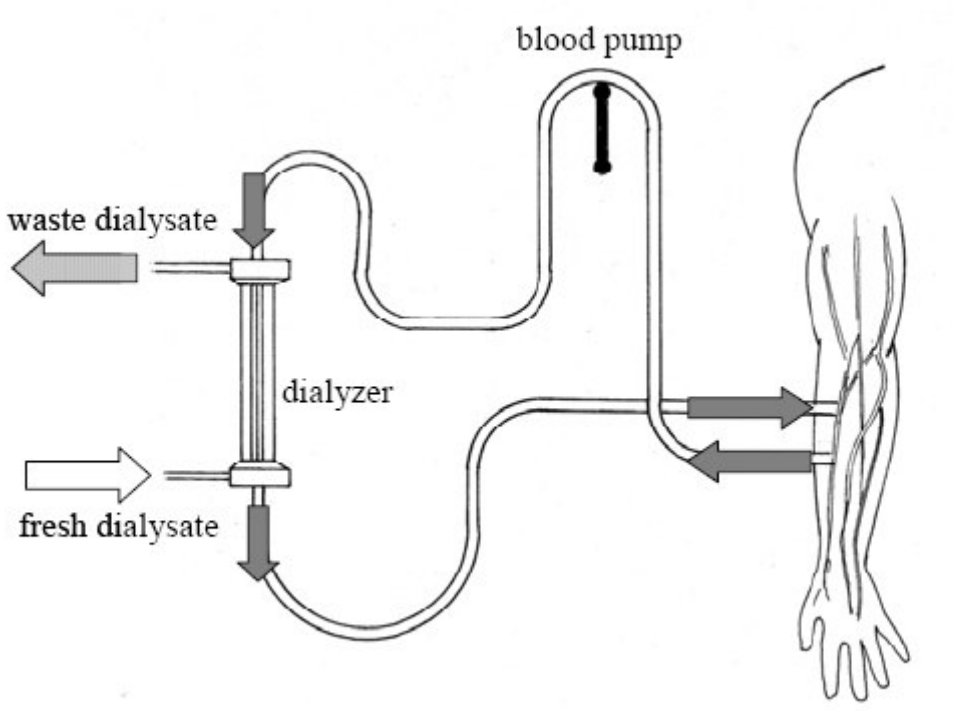

Figure 2.1. Extracorporeal curcuit in hemodialysis.

Blood is withdrawn from the fistula via the 'A' needle by a peristaltic pump, circulated through the dialyser, and returned to the fistula downstream through the 'V' needle. Heparin is infused downstream from the blood pump. The venous pressure monitor protects against blood loss from the circuit and detects downstream obstruction to flow. The bubble trap level detector protects against air embolus. The arterial pressure monitor protects the fistula by detecting excessive negative pressure (Eloot 2005).

Dialysis procedures remove nitrogenous end-products of catabolism and begin the correction of the salt, water, and acid-base derangements associated with renal failure. Dialysis is an imperfect treatment for the myriad abnormalities that occur in renal failure, as it does not correct the endocrine functions of the kidney. Indications for starting dialysis for chronic renal failure are empiric and vary among physicians. Some begin dialysis when residual glomerular filtration rate (GFR) falls below 10 mL/min/1.73 m^2 body surface area (15 mL/min/1.73 m^2 in diabetics.)

Diffusive and convective mass transfer occur across a semipermeable membrane, allowing changes in the composition of body fluids. Diffusive transport depends on solute molecular weight and charge, transmembrane concentration gradients, blood and dialysis fluid flow rates and membrane characteristics. Small molecules (e.g. urea) are cleared well through diffusive transport. Convection is the bulk movement of solvent and dissolved solute (by solvent drag) across the membrane, caused by the transmembrane hydrostatic pressure gradient. Convection improves the clearance of poorly diffusible middle sized molecules (e.g. β2- microglobulin). Ultrafiltration is convective movement of water across the membrane.

Dialyzers comprise semipermeable membranes arranged to form separate adjacent paths for blood and dialysis fluid, which flow in opposite directions to optimize diffusion gradients. Dialysers are classified by membrane composition, surface area, permeability characteristics (diffusion and ultrafiltration coefficients) and biocompatibility characteristics, reflecting the degree of complement activation and cytokine release provoked by blood–membrane contact.

Two types of hemodialyzers are in use: plate and hollow fiber dialyzers. In a plate dialyzer, membrane sheets are packed together and blood and dialysate flow in subsequent layers. The priming volume is around 30% larger than in a hollow fiber dialyzer. Hollow fiber type hemodialyzer consists of thousands of small capillaries (inner diameter in the range of 200μm and wall thickness of 8-40μm) as shown in Figure 2.2. Blood flows inside the capillaries whereas dialysate flows counter currently around them. Typical blood flow rates are in the range of 200 up to 350mL/min (Waeleghem and Lindley 2000), while dialysate flows are preferably twice the blood flow (Sigdell and Tersteegen 1986).

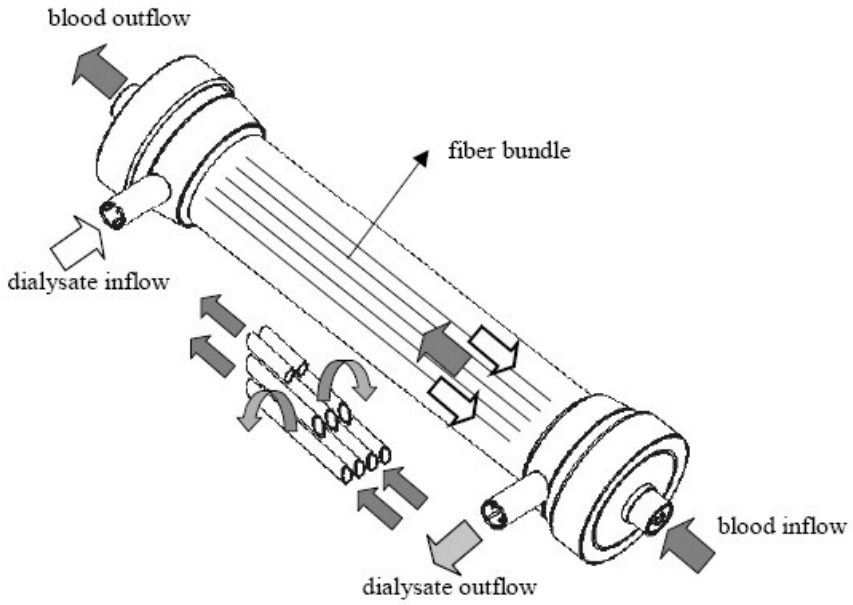

Figure 2.2. Hollow fiber dialyzer.

Hemodialysis can be divided into four main categories due to degree of flux and molecular size range of clearances. Today conventional hemodialysis, hemofiltration, high-flux hemodialysis and hemodiafiltration therapies are applied to 2,000,000 patients worldwide. Main properties of each type of hemodialysis can be summarized as (Pandya and Farrington 2003):

- Conventional hemodialysis uses low-flux (low ultrafiltration coefficient), regenerated cellulose dialysers, allowing diffusive but little convective solute removal. Middle molecule clearance is poor.
- Hemofiltration is a convective treatment. Clearance of middle molecules is greatly improved, but that of small molecules is poor.
- High-flux haemodialysis uses biocompatible membranes with high ultrafiltration coefficients, allowing convective and diffusive solute removal.
- Hemodiafiltration adds a greater convective component to high-flux hemodialysis; 12–20 litres of water per session, in excess of prescribed ultrafiltration volumes, are removed and replaced by substitution fluid, which is prepared by on-line filtration of dialysis fluid. Middle molecule clearance is excellent.

The first hollow fiber hemodialyzers were used clinically in the 1960s (Lipps, et al. 1969). These units contained about 1.0m^2 of an unmodified cellulosic membrane. Cellulose membranes are still widely used for hemodialysis because their hydrogel structure and small thickness provide very effective removal of small solutes like urea. However, these membranes provide relatively little clearance for larger "middle" molecules like β_2-microglobulin that are known to be associated with many dialysis-related disorders. In addition, the cellulosic structure contains a high density of hydroxyl groups, which are known to cause complement activation upon contact with blood (Baeyer, et al. 1988).

The shortcomings in cellulose membranes have led to the development of hemodialyzers based on a variety of synthetic polymers (e.g. polysulfone, polyamide, and polyacrylonitrile) and modified cellulosic materials (e.g. cellulose triacetate and Hemophan). By 1992 the registry form of the European Dialysis Transplant Association–European Renal Association listed more than 400 dialyzers having different base materials, pore size, and surface area (Woffindin and Hoenich 1995). Modified cellulose membranes are produced by replacing the hydroxyls with either acetate or large tertiary amine groups, leading to a significant reduction in complement activation. In addition, these membranes tend to have larger pore size, providing more effective removal of β_2-microglobulin.

Most synthetic membranes (polysulfone, polyacrylonitrile, and polymethylmethacrylate etc…) were originally developed for convective treatments like hemofiltration. Subsequent reductions in membrane thickness have allowed these membranes to be used successfully for hemodialysis, with solute removal occurring by both diffusive and convective transport. Several studies suggest that patients treated with these newer dialyzers have superior clinical outcomes than patients treated with cellulosic dialyzers (Bloembergen, et al. 1999; Koda, et al. 1977).

One aspect of synthetic hemodialyzers that is often overlooked is that these membranes have a very different morphological structure than the cellulose or modified cellulosic materials. Cellulosic membranes have a homogeneous or uniform pore structure throughout the hollow fiber. The AN69 membrane also has a symmetric pore structure (Clark and Gao 2002). In contrast, most other synthetic membranes are asymmetric or anisotropic. These membranes have a thin skin layer approximately 1 μm in thickness on the luminal surface, while the remainder of the membrane has much larger pores and provides the necessary structural support for the hollow fiber. This

asymmetric structure can have a significant affect on the diffusive and convective transport characteristics of the membrane (Boyd and Zydney 1997).

2.1. Properties of Fluids in Hemodialysis

In the hemodialysis operation the main purpose is to clean human blood contaminated by the toxic products of human cells, through a semi permeable membrane and dialysate solution. Either for the optimization of operating conditions or characterization of new membranes, the properties of fluids in both lumen(blood) and shell side(dialysate) should be known. Blood travels down the center of these fibers, and dialysate circulates around the outside of the fibers but inside a plastic casing.

2.1.1. Blood

An average adult has a total blood volume of about 5 L, which is approximately 7% of total body weight. Blood is a dark red, viscous, slightly alkaline suspension (pH 7.4) of cells erythrocytes (red blood cells), leukocytes (white blood cells) and thrombocytes (platelets) suspended in a fluid (plasma). The amount of cells (45% for male, 43% for female) is better known as the hematocrit (Guyton 1986). The composition of blood is shown in Table 2.1.

Table 2.1. The composition of blood.

Parameter	**Value**
Hematocrit	45 ± 7 (38-52%) for males 42 ± 5 (37-47%) for females
pH	7.35-7.45
base excess	-3 to +3
PO_2	10-13kPa (80-100 mmHg)
PCO_2	4.8kPa - 5.8kPa (35-45 mmHg)
HCO_3^-	21mM - 27mM
Oxygen saturation	Oxygenated: 98-99% Deoxygenated: 75%

The main functions of blood include transportation of nutrients from the gastrointestinal system to all cells of the body and subsequently delivering waste products of these cells to organs for elimination. Oxygen (O_2) is carried from the lungs to all cells of the organism by the hemoglobin in the erythrocytes, whereas carbon dioxide (CO_2) is transported back to the lungs for elimination both by the hemoglobin and the plasma. Besides nutrients, numerous other metabolites, cellular products, and electrolytes are transported by the bloodstream.

Additionally, blood has also a function of regulating the body temperature and maintaining the acid-base and osmotic balance of the body fluids. Plasma consists of water (90%), proteins (9%) and inorganic salts, ions, nitrogens, nutrients and gases (1%) (Guyton 1986). There are several plasma proteins with different origin and function, e.g. albumin (69000 Da), α- and β-globulins (80000- 1000000 Da), γ-globulins, clotting proteins, complement proteins (C1 to C9) and plasma lipoproteins.

2.1.2. Dialysate

The dialysis machine mixes a preprepared ‘concentrate’ of electrolytes with treated water to produce dialysis fluid. the composition of dialysis fluid is critical in achieving the desired blood purification and body fluid and electrolyte homeostasis. It contains reverse osmosis water, dextrose and different electrolytes like calcium, magnesium, potassium and sodium chloride and sodium acetate or bicarbonate. Table 2.2 shows the required composition of water used in hemodialysis therapy which is set by Association for the Advancement of Medical Instrumentation (AAMI). Before hemodialysis can be performed, water analysis is performed. Water for hemodialysis generally requires reverse osmosis treatment and a deionizer for “polishing” the water. Organic materials, chlorine, and chloramine are removed by charcoal filtration.

Hemodialysis uses more than 300 litres of water each week. Contamination of water with chemical impurities and micro-organisms carries significant risks. Aluminium causes fracturing osteodystrophy and fatal encephalopathy, chloramines cause haemolysis, and bacteria and endotoxins cause febrile reactions and septicaemia. Use of ultrapure water is crucial in high-flux modes because dialysis fluid is infused directly into the bloodstream by back-filtration and as substitution fluid in on-line

haemodiafiltration. Water is purified using a combination of techniques including softening and de-ionization, carbon adsorption, dual-pass reverse osmosis and ultraviolet irradiation.

Table 2.2. Required composition of water used in hemodialysis therapy set by Association for the Advancement of Medical Instrumentation (AAMI) (Bland and Favero 1993).

Substance	**Concentration (mg/L)**
Aluminum	0.01
Arsenic	0.005
Barium	0.1
Cadmium	0.001
Calcium	2.0
Chloramine	0.1
Chlorine	0.5
Chromium	0.014
Copper	0.1
Fluoride	0.2
Lead	0.005
Magnesium	4.0
Mercury	0.0002
Nitrate	2.0
Potassium	8.0
Selenium	0.009
Silver	0.005
Sodium	70
Sulfate	100
Zinc	0.1

CHAPTER 3

LITERATURE REVIEW

Various efforts are under investigation to synthesize new membrane material which are expected to decrease the treatment time and to increase biocompitability/hemocompatibility of the membranes. In addition, new module designs are considered to increase the efficiency of the hemodialysis operation. The test of performance of new membranes or module designs requires extensive trial and error experimentations. To eliminate this difficulty several mathematical models have been developed to investigate the dialyzer performance and patient's clearance values.

Most of these models defined the mass transfer of toxic compounds through the membrane with an overall mass tranfer coefficient, K_{ov}, involving the blood side, membrane and dialysate side resistances for the given solute (Stiller, et al. 1985; Werynski 1995; Wüpper et al. 1996).

$$N_s = -K_{ov} A_s \Delta\rho_i \tag{3.1}$$

The models based on this approach are far from being accurate since all of the resistances are involved in K_{ov}. In a few studies, the convectional and diffusional mass transfer mechanisms are taken into account separately (Chang 1988; Jaffrin et al. 1981; Kunimoto, et al. 1977; Sigdell 1982), however they assumed the total volumetric flux, J_v constant along the membrane length.

In these studies, the basic, phenomenological description of fluid and solute transport is usually based on linear non-equilibrium thermodynamics (Katchalsky and Curran 1967). The fundamental Staverman–Kedem–Katchalsky–Spiegler approach from the 1960s is used in its current version to define volume, J_V, and solute, N_s, fluxes (i.e. transport rates per unit area), through a flat sheet membrane.

$$J_V = -Lp\left(\frac{dP}{dx} - \sigma RT\frac{d\rho_i}{dx}\right) \tag{3.2}$$

$$N_S = -P_{em}\frac{d\rho_i}{dx} + (1-\sigma)J_V\rho_i \tag{3.3}$$

where ρ_i is the concentration of the solute i, P the hydrostatic pressure, L_p the hydraulic permeability of the membrane, σ the Staverman reflection coefficient, R the gas constant, T the absolute temperature, and P_{em} is the diffusive permeability of the membrane (Spiegler and Kedem 1966). In equations (3.2) and (3.3), gradients (x-direction) are taken perpendicular to the membrane surface.

Deen (1987) has proposed a slightly different expression to describe solute flux through a hollow fiber membrane:

$$N_S = \varepsilon\left[vK_C C - D_\infty K_D \frac{\partial\rho}{\partial r}\right] \tag{3.4}$$

where ε is the local porosity, ρ the local solute concentration, v the local fluid velocity, and D_∞ the Brownian diffusion coefficient of the solute. K_C and K_D are the hindrance factors for convection and diffusion, respectively, and account for the hydrodynamic interactions between the solute and the pore walls.

Zydney et al. (2003) integrated equation (3.4) through each region of an asymmetric hollow fiber membrane consisting of dense and porous layers. The resulting expression is shown in equation (3.5),

$$N_s = \frac{\varepsilon v\phi_1 K_{C_1}\left[\rho_L \exp(K_{C_1} v\delta_1 / K_{D_1} D_\infty) - \rho_S \exp(-(K_{C_2} v\delta_2 / K_{D_2} D_\infty))\right]}{\left(\phi_1 K_{C_1} / \phi_2 K_{C_2}\right) + \exp(K_{C_1} v\delta_1 / K_{D_1} D_\infty) - \left(\phi_1 K_{C_1} / \phi_2 K_{C_2}\right)\exp(-(K_{C_2} v\delta_2 / K_{D_2} D_\infty)) - 1} \tag{3.5}$$

where subscripts '1' and '2' denotes dense and porous layer respectively. In deriving equation (3.5), it is assumed that steady state condition is achieved, thus the solute flux through each region is the same and equal to the overall flux through the membrane. In addition, concentrations on the membrane surfaces in contact with blood (ρ_L) and dialysate (ρ_S) are assumed to be related to bulk concentrations through a linear equilibrium relationship as follow.

$$\phi = \frac{\rho_{r=0}}{\rho_L} = \frac{\rho_{r=\delta_m}}{\rho_S} \tag{3.6}$$

Legallais et. al. (2000) used a similar expression to equation (3.5) in their mathematical model to describe local transmembrane solute flux, *Ns*. They assumed that hemodiafilter operates under steady state conditions, flow rates, concentrations and pressures are uniformly distributed over the cross section and change only along the length of the module. It is further assumed that, axial diffusion is negligible with respect to axial convection and concentrations of the solute at the membrane surface equal to those on the surrounding bulk phase. Based on these assumptions, conservation equations for mass in the blood and dialysate compartments were written as shown below:

$$\frac{d[Q_B \rho_B]}{dx} = -N_{tube} \pi d_B N_s(x) \tag{3.7}$$

and for the solute concentration in dialysate solution:

$$\frac{d[Q_D \rho_D]}{dx} = -N_{tube} \pi d_B N_s(x) \tag{3.8}$$

where N_{tube} is the number of fibers, d_B is the fiber inner diameter, Q_B and Q_D are the volumetric flow rates of blood and dialysate respectively. In addition to mass transfer equations pressure drops in the blood and dialysate compartments were expressed in terms of Hagen-Poiseuille equation and its modified form respectively.

$$\frac{dP_B}{dx} = -\frac{128 \mu_B}{N_{tube} \pi d_B^4} Q_B \tag{3.9}$$

And for dialysate side,

$$\frac{dP_D}{dx} = \frac{-32\mu_D}{S_{eq}(d_{eq})^2} Q_D \tag{3.10}$$

They validated their simulation results with the experimentally calculated clearances of creatinine, vitamin B12 and myoglobin available in the literature. Although calculated clearance values seem to be in good agreement with the experimental data, the results were obtained by correlating diffusive permeability of solute through the membrane. Thus, the results do not represent the predictive ability of their model.

Moreover, it is also assumed in the model that plasma proteins are completely rejected by the membrane. Consequently, comparison of model predictions with experimental data collected using saline solutions does not represent a real test for the predictive ability of the model.

Most of the assumptions used in the model of Legallais et. al. are adapted by Raff and his coauthors (2003) except concentration polarization in blood compartment due to presence of completely rejected molecules is taken into account. The local wall concentration is described by equation (3.11).

$$\rho_w(x) = \rho_b(x) e^{J_v(x)/\beta_B(x)} \tag{3.11}$$

where ρ_w and ρ_b are solute concentrations at the membrane wall and in bulk solution respectively, and β_B is mass transfer coefficient on the blood side.

In their model, convective mass transfer in the blood is taken into account within a mass transfer coefficient calculated by the extended Graetz solution with the local Sherwood number on the blood side. The local mass transfer coefficient on the dialysate side was calculated from the same correlation used for the blood side except that two constants in the correlation were regressed from the clearance data. Based on two regressed parameters, model calculations compare well with the experimental data. However, the predictive ability of the model for different data set was not tested.

There are some other models in the literature which combined simultaneous mass and momentum transfer in both radial and axial directions (Moussy 2000; Noda

and Gryte 1979). Moussy (2000), developed analytical expressions describing convective flow in a continuous arteriovenous hollow fiber hemofilter. In his model, mass transfer in the axial direction is assumed to take place only by convection, while both convective and diffusive mass transfer mechanisms were considered in the axial direction. The species continuity equation for the solute is then given by the equation below:

$$\frac{\partial C}{\partial t} + U\frac{\partial C}{\partial X} + (V - \frac{1}{Pe_R R})\frac{\partial C}{\partial R} = \frac{1}{Pe_R}\frac{\partial^2 C}{\partial R^2} \tag{3.12}$$

and its initial and boundary conditions are:

$$C(0, R, X) = 1 \tag{3.13}$$

$$C(t, R, 0) = 1, \tag{3.14}$$

$$\left(\frac{\partial C}{\partial R}\right)_{R=0} = 0, \tag{3.15}$$

$$\left(\frac{\partial C}{\partial R}\right)_{R=1} = VCPe_R, \tag{3.16}$$

where $C = \rho / \rho_o$, $\tau = V_w t / r_{lum}$, $V = V^* / V_w$, $U = U^* / U_0$, $X = x / L$, $R = r / r_{lum}$, and $Pe_R = V_w r_{lum} / D$ and where ρ is the solute concentration, ρ_o is the bulk concentration, r_{lum} is the iner radius of the fiber, V^* is the radial velocity, V_w is the radial (wall) velocity at the inner radius, U^* is the axial velocity, U_o is the inlet centerline velocity, t is time, L is the length of the fiber, Pe_R is the Peclet number in the radial direction, and D is the solute diffusion coefficient.

In the lumen of the hollow fiber membrane, existing analytical expressions were applied to describe velocity profiles and pressure. For flow in the shell (the extracapillary space separating the fibers), analytical expressions for the radial and axial velocity profiles and pressure distribution were derived by first finding the stream function. The expressions are based on a similarity solution.

Although this model is helpful to describe flow in hollow fiber dialyzers, it is inadequate at elucidating the mass transfer through the porous membrane matrix. The

structural properties of the membrane are very important for describing mass transfer of solutes however these parameters are not taken into account in the model.

In another study, concentration profiles in a countercurrent hollow fiber bundle mass exchanger dialyzer were derived by assuming a uniform distribution of fibers on the dialysate compartment. On the blood side, mass transfer in both radial and axial directions was considered. The fluid velocity for flow through the inside of the hollow fiber was defined by Poiseuille flow, while the velocity profile for the flow through the outside of the fibers was obtained from a previous study. The average radial solute fluxes at the inner and outer surfaces were expressed by the mass transfer coefficients in the bulk phases and the concentration differences between the bulk phase and the surfaces. Eventhough complete set of mass transfer equations were derived on both blood and dialysate compartments and mass transfer coefficients obtained as a function of the fiber packing density, membrane thickness, membrane material and solute type the model has a limited practical usage. This is due to the fact that model neglects the mass transfer resistance through the membrane.

Although some models take into account the accumulation of rejected large molecules on the membrane surface (Chang 1988; Jaffrin, et al. 1981; Kunimoto et al. 1977; Sigdell 1982; Werynski et al. 1995; Wüpper et al. 1997), they generally do not involve the adsorption of these large molecules which causes membrane fouling. Elution from used dialyzers showed that hemodialysis membranes adsorb a lots of proteins (Gachon, et al. 1991). The effect of this adsorbed protein layer on the the flux characteristics and hydraulic permeability of various ultrafiltration membranes are investigated and found to be very significant (Belfort, et al. 1994; Langsdorf and Zydney 1994; Meireles et al. 1991; Nakao et al. 1982). Additional resistance to the mass transfer of solutes caused by the protein fouling is explained by the combination of different types of phenomena. Some authors proposed that the dominant resistance is created by protein blockage of the membrane pores (Nilsson and Hallstrom 1991) or on the contrary, some assumed that the reduction in the solute transfer after protein fouling is controlled by the secondary gel layer formed on the membrane surface (Nakao, et al. 1982). Moreover, in some studies (Boyd and Zydney 1998; Langsdorf and Zydney 1994; Morti, et al. 2003), two layer model is applied to examine the physical properties of the protein layer whose results can be very useful to construct such a theoretical model considering the proteins adsorbed on the membrane as an additional porous layer that contributes the resistance to the solute transfer.

CHAPTER 4

PROTEIN ADSORPTION KINETICS

The medical use of membranes has been evolving since 1940s (Hanft 2002). Today, microfiltration (MF) membranes and ultrafiltration (UF) membranes are widely used as blood-contact devices in blood apheresis and purification for blood collection or disease therapies, e.g. hemodialysis (artificial kidney), plasmapheresis, plasma fractionation, leukofiltration and artificial liver (Schmidt 1996). There are two basic membrane configurations used in blood purification: flat sheet and hollow fiber shapes. And most of them are made of polymeric materials (Hanft 2002).

Unfortunately, just like other protein-contact membranes, blood-contact membranes are faced with a problem of a progressive decline in flux and a change of membrane selectivity. This phenomenon, known as membrane fouling, is mainly attributed to the concentration polarization and protein fouling on the membrane surface, no matter what material the membrane is made of (Basmadjian, et al. 1997; Dionne, et al. 1996; Marshall, et al. 1993; Vanholder 1992).

Concentration polarization, resulting from concentration gradient due to solute accumulation near the membrane surface, is reversible in nature, though it always exists during membrane processing due to the fundamental limitations of mass transfer and the existence of the boundary layer. The concentration polarization, independent of the physical properties of the membrane, reduces permeate flux by offering added hydraulic resistance to the flow of solvent and by causing osmotic backpressure (Wang, et al. 1994). The membrane pore size and porosity are not directly affected by concentration polarization (Marshall, et al. 1993). Concentration polarization can be controlled by means of high shear on the membrane surface, if high shear can be tolerated in operation (Jagannadh and Muralidhara 1996).

Protein adsorption or deposition on the surface or in its pores occurs rapidly within seconds to minutes after the first blood-contact (Huang 1999; Vanholder 1992; Yin, et al. 2000), which leads to a change in membrane behavior. It is irreversible in nature, because fouling is the “coupling” of the adsorbed or deposited protein to the membrane through the intermediate step of concentration polarization (Marshall, et al.

1993). Apart from surface adsorption, pores plugged by adsorbed proteins may be another process affecting efficacy, especially in plasma separators and plasma fractionators with a pore size large enough to allow transmembrane crossing of proteins (Baeyer, et al. 1985).

Compared to concentration polarization, protein adsorption is more complex and is more detrimental to blood apheresis and purification. It is therefore important to investigate its mechanism and various factors affecting protein adsorption. Some good reviews have been published on the protein adsorption in membrane filtrations (Marshall et al. 1993; Fane and Fell 1987), but the blood-contact membrane is not considered. Thus this chapter focuses on the influences of structural parameters and operating conditions on protein adsorption and reviews available protein adsorption models as well.

4.1. Factors Affecting Protein Adsorption

Membrane protein adsorption may be affected by a series of factors (Kim, et al. 1992), e.g. the surface chemistry of the membrane, adsorbed protein size, charge, shape, pH value, and so on. As for the blood-contact membrane, interest is focused on its type and morphology, its hydrophilicity, and operating conditions. In the following section, the influences of these parameters will be reviewed.

4.1.1. Membrane Material and Morphology

It is generally recognized that the surface characteristics of a membrane, which are largely dependent on the membrane material can significantly influence the separation performance of the membrane in terms of both flux and permselectivity. For example, the permeate flux decline almost invariably observed depends on the interactions of solute components with the membrane surface. This is caused by several factors, such as adsorption, plugging of the membrane pores, concentration polarization and gel layer formation, or a combination of some of them. In some cases, accumulation on the membrane surface occurs due to electrostatic interaction between the molecules in solution and the surface of the membrane.

Fujimori et al. (1998) examined the adsorption of albumin, IgG, C3a, interleukin-1β(IL-1β), interleukin-6 (IL-6), human neutrophil elastase (HNE), and tumor necrosis factor α (TNF α) on several types of membranes from dialyzers right

after clinical use. They semiquantitatively graded all these membranes with confocal laser scanning fluorescence microscopy (CLSFM). Their research found that the polyacrylonitrile (PAN) membrane revealed the most abundant adsorption, especially for IL-1β, IL-6, and TNF α. Although a marked elevation of C3a in blood was observed in the cellulose triacetate membrane, considerably more adsorption took place when the polymethylmethacrylate (PMMA) and the PAN membranes were applied.

By means of radioisotope labeling technique and indirect enzyme linked immunosorbent assay, Huang examined three plasma proteins (albumin, immunoglobulin and fibrinogen) adsorption from a single component protein solution or plasma of various dilutions to sulfonated polyethersulfone (SPES), polyethersulfone (PES), polysulfone (PSF), PMMA and cellulose acetate (CA) membranes (Huang 1999). He found that the binding strength of the proteins adsorbed on these membrane surfaces decreased as follows: fibrinogen > albumin > immunoglobulin, and that the extent of clotting factor activation of SPES, PES, PSF and PMMA was lower than that of CA. Sulfonation decreased the ability of PES to activate clotting factor. As these materials' ability to trigger the intrinsic coagulation pathway had relations with Vroman effect, Huang suggested when the Vroman effect took place earlier, more fibrinogen be displaced and the chance of clotting factor to contact the material be bigger (Huang 1999).

Ho and Zydney (1999) studied the effect of membrane morphologies and pore structures on protein adsorption using different track-etched, isotropic and asymmetric MF membranes. They found that the fouling occurred among straight-through pores membranes owing to the pore blockage caused by deposition of large protein aggregates on the surface. The rate of blockage was a function of membrane porosity due to the possibility of multiple pore blockages by a single protein aggregate on high porosity membranes, and membranes with interconnected pores fouled more slowly since the fluid can flow around the blocked pores through the interconnected pore structure. There is evidence that protein is adsorbed within membrane pores, and on the surface as well (Ho 2001; Marshall, et al. 1993).

In UF the amount of protein adsorbed within membrane pores is smaller compared with that on membrane surface (Marshall, et al. 1993). On the other hand, in MF there is greater adsorption within pores, and internal fouling appears to dominate with large pores (Ho 2001). Numerous examples show that membrane fouling is more severe with the pore size increasing. There appears to be an optimum pore size, below

which the membrane resistance restricts permeate flow, and above which severe membrane fouling decreases flux (Marshall, et al. 1993).

4.1.2. Hydrophobicity

One of the main factors enhancing the protein adsorption on the surface is hydrophobic interaction between membrane surface and protein molecules (Feast and Munro 1987; Iaraelachvili 1985). Matthiasson (1983) studied bovine serum albumin (BSA) adsorption to CA, PSF and polyamide membranes using direct measurements of protein uptake, evaluated with 14C-labeled BSA, in combination with studies of the membrane hydraulic permeability before and after adsorption. Adsorption reached the maximum on the hydrophobic PSF membranes, with a surface coverage of 2–50 mg/m^2, and got to the minimum on the hydrophilic CA membranes (approximately 0.5 mg/m^2).

4.1.3. Operating Conditions and Electrostatic Interactions

Operating conditions can also have an effect on the protein adsorption on membranes (Charcosset, et al. 1990). Mineshima and et al. (2001) have found the ratio of the flowrate of the supplied plasma (Q_B) to retained plasma (Q_D) as the most effective operating condition in improving the selectivity of a plasma fractionator between albumin and immunoglobulins. Their results indicated that there is a critical ratio of Q_B/Q_D beyond which membrane fouling could be enhanced and the selectivity of these proteins reduced. Ghosh et. al. (2002) studied BSA fouling on two UF membranes using pulsed injection technique. They found that when the membranes were first exposed to low flux and then to high flux, fouling was occured at a smaller extent.

Fane et al. (1983) performed one of the first quantitative studies of the effect of solution pH on protein (BSA) transmission through semipermeable membranes. BSA transmission at low salt concentrations was greatest near the BSA isoelectric point (pH 4.7) even though the extent of protein adsorption was actually greatest under these conditions. Fane et al. attributed this behavior to conformational changes in the free and adsorbed BSA, although no quantitative analysis of these phenomena was presented. Nakao et al. (1988) evaluated the sieving coefficients of several proteins using both

positively and negatively charged membranes. Protein transmission was generally largest when the solution pH was near the protein isoelectric point, with the greatest rejection seen when the protein and membrane were oppositely charged. However, it was not possible to quantify these effects because the membrane charge was not actually measured in any of the experiments.

Yang and Tong (1997) obtained data for the transport of myoglobin and cytochrome C through hydrolyzed PAN hollow fiber membranes. Protein transmission was greatest at pH near the protein isoelectric point. Yang and Tong attributed the reduction in protein transmission at pH < pI to an increase in protein adsorption, while the reduction at pH > pI was assumed to be due to electrostatic repulsion between the positively charged membrane and the positively charged protein.

Causserand et al. (1996) obtained data for both the sieving coefficients and hindered diffusivity of BSA and a-lactalbumin as a function of solution ionic strength. The data were analyzed using a theoretical model for partitioning of a charged sphere into a slit-shaped pore.

In the model, electrostatic interactions were assumed to occur at constant surface potential (instead of constant surface-charge density), and the surface potential of the membrane was simply set equal to that of the protein. The model and data were in good qualitative agreement suggesting that the effect of the solution ionic strength was primarily due to an alteration in the protein partition coefficient into the membrane pores.

The zeta potential estimated by the streaming potential measurement has been used for the characterization of the membrane fouling by protein (Causserand, et al. 1994; Martin, et al 2002) because the electrostatic interaction between protein and membrane is expected to be a major factor dominating the adsorption behavior. It has been generally observed that the zeta potential of the membrane fouled with protein was similar to that of the protein (Nakamura and Matsumoto 2006). The product of both the zeta potential of membrane and protein molecules was used for an index of the electrostatic interaction between protein and membrane (Fane, et al. 1983; Martinez, et al. 2000). However, the applications of the zeta potential for the fouling prediction or the fouling monitoring are limited because of the lack of the understanding of the configuration of the protein trapped in membrane pore structure and the response of the zeta potential to it.

4.2. Protein Adsorption Models

To elucidate mechanisms and predict trends in membrane fouling, investigators have relied upon four classical models relating microscopic mechanisms of fouling to macroscopic changes in membrane permeability or resistance (Grace 1956; Hermia 1982). Complete blocking assumes that particles seal off pore entrances and prevent flow. Intermediate blocking is similar to complete blocking but assumes that a portion of the particles seal off pores and the rest accumulate on top of other deposited particles. Cake filtration occurs when particles accumulate on the surface of a membrane in a permeable cake of increasing thickness that adds resistance to flow. The standard blocking model describes a fouling mechanism wherein pores constrict and permeability is reduced as foulant particles adsorb on the walls of straight cylindrical pores. The standard model assumes all foulants which enter a pore are deposited and that they accumulate uniformly with axial position. Thus, the standard model, like the other classical models, predicts a membrane capacity independent of flow rate.

Nakamura and Matsumoto (2006) studied adsorption behavior of BSA in MF glass membrane. They suggested that the adsorption should be irreversible and be consist of the two types: the adsorption on clean pore surface, i.e. the primary adsorption, and that on preadsorbed pore surface, i.e. the secondary one. They assumed that the adsorption rate is proportional to the feed rate of BSA, and the proportional coefficient is dependent on the adsorption process. They defined total rate of protein adsorption as the primary and secondary adsorption rates:

$$\frac{\partial q(z,t)}{\partial t} = \frac{\partial q_1(z,t)}{\partial t} + \frac{\partial q_2(z,t)}{\partial t} \tag{4.1}$$

Considering the multilayer adsorption, they prepared following expressions for primary and secondary adsorption rates:

$$\frac{\partial q_1(z,t)}{\partial t} = \Gamma_1 . J(t) . c(z,t) . \frac{1}{a_{v0}} . (1 - \frac{q_1(z,t)}{Q_{\max 1}}) \tag{4.2}$$

$$\frac{\partial q_2(z,t)}{\partial t} = \Gamma_2 . J(t) . c(z,t) . \frac{1}{a_{v0}} . \left(\frac{q_1(z,t)}{Q_{\max 1}} \right) . \left(1 - \frac{q_2(z,t)}{Q_{\max 2}} \right) \tag{4.3}$$

where a_v is the specific surface area based on membrane volume, Q_{max} is the protein adsorption capacity. Subscripts 1 and 2 denote the primary and secondary adsorption, respectively, and q is the amount of protein adsorbed per specific surface area. Γ is the adsorption coefficient, which has the same meaning and dimension of cm^{-1} as the filter coefficient used in Iwasaki's equation (1937).

CHAPTER 5

THEORY

5.1. Whole Body Clearance Model

In order to observe the effects of model parameters on the efficiency of hemodialysis process, it is neccessary to evaluate the concentration values in patient's blood. Therefore, mass balance of toxic compound in total body water is neccessary. The total body water is considered to consist of two compartments; Intracellular water (2/3 of total volume) and extracellular water (1/3 of total volume). As it is schematically represented in Figure 5.1, blood is circulated between the hemodialyzer and extracellular compartment, while the intracellular water is being cleaned by the mass transfer between two compartments.

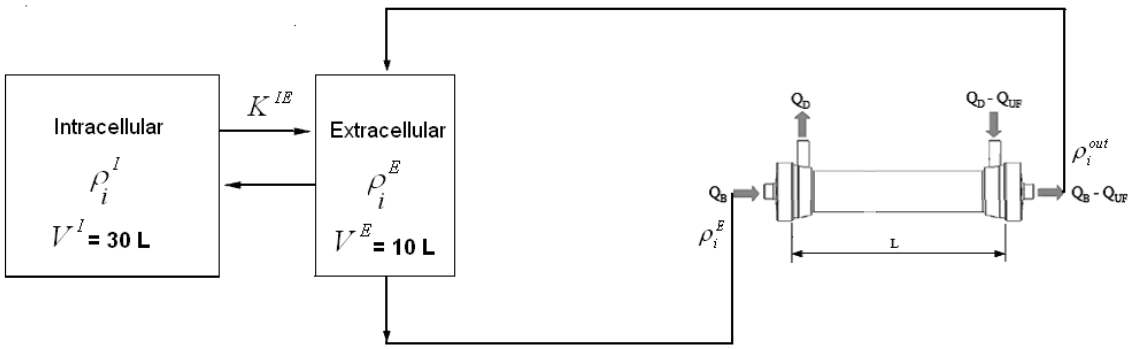

Figure 5.1. Schematic of two compartment whole body clearance model.

Assuming that there is a perfect mixing in both compartments, a mass balance of solute in extracellular water yields:

$$\frac{d(V^E \rho_i^E)}{dt} = (Q_B - Q_{UF})\rho_i^{out} - Q_B \rho_i^E + K_i^{IE}\left(\rho_i^I - \rho_i^E\right) \tag{5.1}$$

and the change of solute concentration in intracellular water is given as:

$$\frac{d(V^I \rho_i^I)}{dt} = -K_i^{IE}\left(\rho_i^I - \rho_i^E\right) \tag{5.2}$$

Not only the performance of the dialyzer, but also the total body weigth of the patient and the clearance between intra and extra- cellular compartments are very important for the overall efficiency of the hemodialysis operation. Average values of 600 mL/min and 40 L are used for intercompartmental clearance of urea(K^{IE}) (Clark, et al. 1999) and total body water (V_{Total}) respectively. Also, intercompartmental clearances of creatinine, inulin and β_2-microglobulin are taken as 275, 90 and 40 mL/min respectively (Clark, et al. 1999) to be able to predict concentrations of these solutes.

Equations (5.1) and (5.2) should be solved together with the model equations derived for solute transport through the dialyzer. Such a coupling is required since inlet concentration for the extracellular compartment, ρ_i^{out}, corresponds to the solute concentration at the exit of the dialyzer. In the following sections, model equations through the dialyzer will be derived.

5.2. Plain Membrane Model

5.2.1. Model Geometry and Assumptions

A typical hollow fiber geometry used for a hemodialysis operation is illustrated in Figure 5.2. In this configuration, blood and synthetic dialysate solution flow through the inside of hollow tubes and outside of the tube walls made from dialysis membranes are shown respectively. The membrane is assumed to have an asymmetric structure with a very thin dense skin layer (δ_{dense}) supported by a thick porous layer (δ_{porous}). Small toxic compounds such as urea and low molecular weight proteins ($< 2x10^4$) can permeate through the membrane, on the other hand, large molecular weight proteins are rejected and then (cannot permeate, thus, they adsorb) accumulate on the surface of the membrane. The thickness of the adsorbed protein layer, $X_p(t)$, changes with time during hemodialysis operation.

Model equations derived here are general in nature and they are based on the following assumptions and restrictions:

1. The dialysis operation runs at pseudo-steady state since protein adsorption at the membrane surface takes place rapidly.
2. There is symmetry in the dialyzer and angular velocity is zero. Axial and radial velocities change both in axial and radial directions.
3. The blood is a binary solution consisting of a toxic compound and a large molecular weight protein.
4. Solute concentration change both in axial and radial directions.
5. The partial specific volumes of the solutes in the blood are independent of concentration and equal to each other so that the density of the mixture remain constant.
6. The shear rates in the hollow fibers and outside of the fibers are low, thus, the blood and the dialysate solution are considered as Newtonian fluids.
7. Adsorbed protein molecules form an additional regularly packed porous layer on the membrane surface.
8. There are no homogeneous reactions in the blood or in the dialysate solution.
9. The diffusion coefficient of the solute in the blood is independent of concentration.
10. Solute transfer in the dialysate side can be expressed with an empirical equation.
11. Since the length of the fiber is much greater than its diameter ($\xi = L >> 2R$) and since the product of Reynolds number and the aspect ratio is very small $R_e \xi << 1$, then lubrication approximation can be used.
12. Dominant mass transfer mechanism in the axial direction is convection, i.e., axial diffusion is assumed to be negligible.

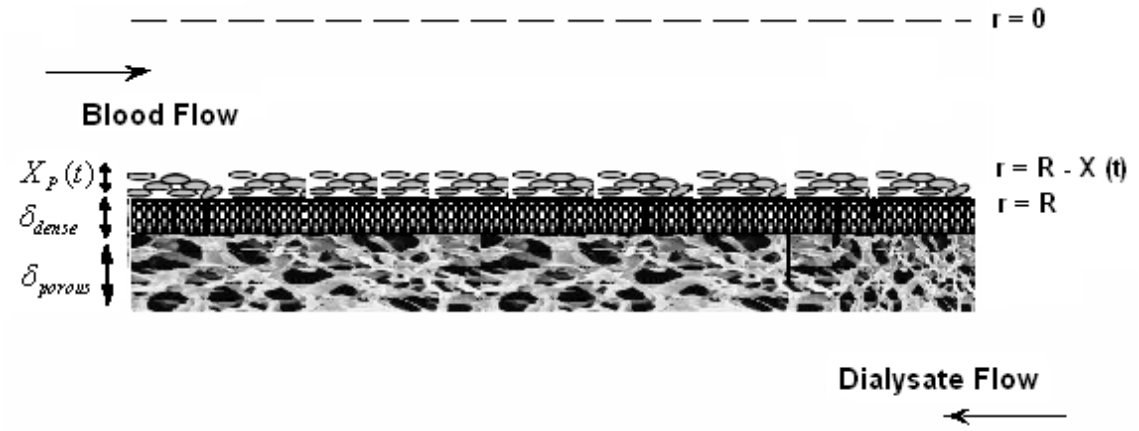

Figure 5.2. Schematic representation of model geometry.

5.2.2. Total Continuity and Conservation of Momentum Equations

Mass transfer of solute through the dialyzer is coupled with momentum transfer. Thus, solute concentrations (ρ_i), axial (U) and radial (V) velocities on the blood side are calculated with respect to radial(r) and axial(z) positions.

$$\rho_i = \rho_i(r,z), \quad U = U(r,z) \quad \text{and} \quad V = V(r,z) \tag{5.3}$$

while pressures on the blood(P_B) and dialysate(P_D) compartments are calculated with respect to axial positions:

$$P_B = P_B(z) \quad \text{and} \quad P_D = P_D(z) \tag{5.4}$$

To facilitate numerical solution of model equations and to make the appropriate simplifications due to the lubrication approximation, they were written in terms of dimensionless variables. All of the variables used in the model both in dimensional and dimensionless forms are listed in Table 5.1.

Total continuity equation can be expressed in dimensionless variables as follows by utilizing first and fifth assumptions listed above:

$$\frac{\partial V}{\partial r} + \frac{V}{r} + \frac{\partial U}{\partial z} = 0 \tag{5.5}$$

Dimensionless forms of the Navier-Stokes equations in radial direction,

$$\frac{\partial P}{\partial r}=\frac{2\xi^2}{r}\frac{\partial}{\partial r}\left(r\mu\frac{\partial V}{\partial r}\right)-\frac{2\xi^2 V\mu}{r^2}+\xi^4\frac{\partial}{\partial z}\left(\mu\frac{\partial V}{\partial z}\right)+\xi^2\frac{\partial}{\partial z}\left(\mu\frac{\partial U}{\partial r}\right)-\mathrm{Re}\,\xi^3\left[V\frac{\partial V}{\partial r}+U\frac{\partial V}{\partial z}\right] \tag{5.6}$$

and in axial direction are:

$$\mathrm{Re}\,\xi\left[V\frac{\partial U}{\partial r}+U\frac{\partial U}{\partial z}\right]=-\frac{\partial P}{\partial z}+\frac{1}{r}\frac{\partial}{\partial r}\left(r\mu\frac{\partial U}{\partial r}\right)+\frac{\xi^2}{r}\frac{\partial}{\partial r}\left(r\mu\frac{\partial V}{\partial z}\right)+2\xi^2\frac{\partial}{\partial z}\left(\mu\frac{\partial U}{\partial z}\right) \tag{5.7}$$

Table 5.1. Dimensional and dimensionless forms of the variables used in model equations.

Model Variables	
Dimensional Forms	**Dimensionless Forms**
r^*	$r=\frac{r^*}{R_i}$
z^*	$z=\frac{z^*}{L}$
U^*	$U=\frac{U^*}{U_{avg}}$
V^*	$V=\frac{V^*L}{U_{avg}R_i}$
P^*	$P=\frac{P^*R^2}{L\mu_p U_{avg}}$
μ^*	$\mu=\frac{\mu^*}{\mu_p}$

Since the length of hollow fibers utilized in hemodialysis operation is much greater than the radius of the fibers $\xi = \frac{L}{2R} >> 1$ and the product of Reynold's number and the aspect ratio is smaller than the unity , $R_e \xi << 1$, lubrication theory becomes valid for describing the flow and mass transfer in a single fibre (Langlois 1964). Based on lubrication approximation, conservation of momentum equations are reduced to following simple forms:

$$\frac{\partial P}{\partial r} = 0 \tag{5.8}$$

and in axial direction,

$$\frac{\partial P}{\partial z} = \frac{1}{r}\frac{\partial}{\partial r}\left[r\mu \frac{\partial U}{\partial r} \right] \tag{5.9}$$

From equations (5.8) and (5.9), the axial velocity is given by the following expression (Morrette and Gogos 1968):

$$U = \frac{\int_r^1 \frac{r'}{\mu} dr'}{\int_0^1 \frac{r^3}{\mu} dr} \tag{5.10}$$

and the radial velocity can be obtained by integrating the overall continuity equation, equation (5.5):

$$V = -\frac{1}{r}\int_0^r r' \frac{\partial U}{\partial z} dr' \tag{5.11}$$

It is evident from equation (5.10) that if the viscosity of the blood is assumed to be constant, then, the axial velocity is no longer a function of the axial position and the radial velocity becomes zero. However, this is not a valid assumption since 98 % of the increase in the plasma viscosity above that of water was found due to the presence of

proteins in blood (George, et al. 2004). Following relation proposed by Pallone et. al. (1987), was used to describe the change in the dimensionless blood viscosity with respect to the protein concentration:

$$\mu = 1 + \left(\frac{\mu_{pR}}{\mu_W} - 1 \right) \frac{\rho_p}{C_{pR}} \tag{5.12}$$

where $\mu_{pR} = 1.22 \times 10^{-3}$ Pa s; $C_{pR} = 70$ g l^{-1} .

5.2.3. Protein Adsorption Model

In the model, it is assumed that large protein molecules retain on the surface, i.e., they cannot diffuse into the membrane pores. In addition, it is assumed that adsorption is irreversible and multilayer type and adsorbed protein molecules form a regular packing as shown in Figure 5.3. The irreversible primary and secondary adsorption mechanisms can be described with the following reactions:

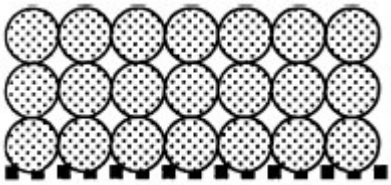

Figure 5.3. Regular packing of adsorbed proteins.

$$S + P \rightarrow P_{ads} \cdot S \qquad \text{(the primary adsorption)} \tag{5.13}$$

$$P_{ads} + P \rightarrow P_{ads} \cdot P_{ads} \qquad \text{(the secondary adsorption)} \tag{5.14}$$

where P and P_{ads} denote free and adsorbed protein molecules, while S represents the surface on which protein molecule adsorbs. The change in total amount of proteins adsorbed with time can be written as follows considering the primary and secondary adsorption rates:

$$\frac{dm_P}{dt} = \frac{dm_{P1}}{dt} + \frac{dm_{P2}}{dt} \tag{5.15}$$

The rate of both primary and secondary adsorption are expected to be high at the early stages of the process then it starts to be slower and finally does not change anymore when the adsorption capacities are reached. Secondary adsorption begins after primary adsorption and it is assumed to be faster as the amount of adsorbed proteins during primary adsorption increases. According to these restrictions the rates of primary and secondary adsorption are expressed by the following equations in a similar manner described by Nakamura et al. (2006):

$$\frac{dm_{p1}}{dt} = N_P A_s \left(1 - \frac{m_{p1}}{Q_{\max 1} A_s} \right) \tag{5.16}$$

$$\frac{dm_{p2}}{dt} = N_P A_s \left(\frac{m_{p1}}{Q_{\max 1} A_s} \right) \left(1 - \frac{m_{p2}}{Q_{\max 2} A_s} \right) \tag{5.17}$$

where m_{p1} and m_{p2} are the amount of adsorbed proteins by primary and secondary adsorption respectively. And Q_{max1} and Q_{max2} are adsorption capacities defined as the maximum amount of protein that can be adsorbed per unit pore surface area. Amount of adsorbed proteins can be written in terms of protein thickness(X_p) as below:

$$m_p = \pi L \left(2R_i X_p - {X_p}^2 \right) \rho_{\substack{ads. \\ layer}} \tag{5.18}$$

where $\rho_{\substack{ads. \\ layer}}$ is density of the adsorbed protein layer and calculated as:

$$\rho_{\substack{ads. \\ layer}} = \left(1 - \varepsilon_p \right) \frac{1}{\hat{v}_p} \tag{5.19}$$

Since the protein molecules are assumed to form a regular packing on the surface, its porosity(ε_p) is 0.4765. $\hat{v}_p$ is the specific volume of the particular protein in blood solution. Utilizing equations (5.15) through (5.19), the change in the protein layer thickness with time is described below:

$$\frac{dX_p}{dt} = \frac{N_P \hat{v}_p}{\left(1 - \varepsilon_p \right)} \left[1 - \left(\frac{m_{p1}}{Q_{\max 1} A_s} \right) \left(\frac{m_{p2}}{Q_{\max 2} A_s} \right) \right] \tag{5.20}$$

where N_p is the total protein flux towards the membrane surface and described in terms of convective and diffusive mass transfer mechanisms in the blood.

5.2.4. Species Continuity Equation

A dimensionless species continuity equation for the toxic solute in the blood can be written as follows:

$$V\frac{\partial \rho_i}{\partial r}+U\frac{\partial \rho_i}{\partial z}=\frac{1}{Pe}\left[\frac{\partial^2 \rho_i}{\partial r^2}+\frac{1}{r}\frac{\partial \rho_i}{\partial r}+\xi^2\frac{\partial^2 \rho_i}{\partial z^2}\right] \tag{5.21}$$

Utilizing assumptions 1, 2, 3, 4, 5, 8, 9 and 12, equation (5.21) can be simplified as follows:

$$V\frac{\partial \rho}{\partial r}+U\frac{\partial \rho}{\partial z}=\frac{1}{Pe}\left[\frac{\partial^2 \rho}{\partial r^2}+\frac{1}{r}\frac{\partial \rho}{\partial r}\right] \tag{5.22}$$

In equation (5.22), $Pe = U_{avg}R_i^2 / D_{AB}L$ is dimensionless Peclet number which is defined as the ratio of convective and diffusive mass transfer. It is evident from equations (5.8) and (5.22) that even though the pressure change in the radial direction becomes negligible with the lubrication approximation, all radial velocity terms persist in the species continuity equation for the solute in the blood.

It is assumed that there is a symmetry along the centerline of the fibers for the solute concentration and the solute flux is no longer assumed to be continuous at the blood-membrane interface due to deposition of proteins on the membrane surface. Hence, following boundary conditions are used in the solution of equations (5.10), (5.11), and (5.22).

$$z^* = 0\,,\ 0 \le r^* \le R_i - X_p(t) \ \rightarrow\ \rho_i = \rho_i^{inlet} \tag{5.23}$$

$$0 \le z^* \le L\,,\ \ r^* = 0 \ \rightarrow\ V = 0 \ \text{ and } \ \frac{\partial \rho_i}{\partial r} = 0 \tag{5.24}$$

$$0 \le z^* \le L,\ r^* = R_i - X_p(t) \ \rightarrow \left(N_i\right)^{Blood} - N_s \frac{R_i}{R_i - X_p(t)} = \frac{dX_p}{dt}\left(\rho_i^{Blood} - \rho_i^{Protein}\right) \tag{5.25}$$

Equation (5.25) was derived from a jump mass balance written for the solute and solute flux through the membrane, N_s, is described according to the following equation (Deen 1987):

$$N_S = K_C J_v \rho_i - \varepsilon K_D D_\infty \frac{d\rho_i}{dr} \tag{5.26}$$

where ρ_i is local solute concentration, ε is membrane porosity, and J_v is solution volumetric flux in the membrane. K_C and K_D are hindrance factors for convection and diffusion respectively accounting for the steric and hydrodynamic interactions between the solute and pore walls. Estimation of these parameters are illustrated in the following sections.

Previously, Morti et al. (2003) derived an explicit expression for the solute flux through a two layer membrane under steady state conditions which is given in equation (3.5). In this study, this expression has been extended for a three layer case in which layer 1 corresponds to porous protein layer while layers 2 and 3 represent dense and porous regions of the asymmetric membrane. For this purpose, if equation (5.26) is integrated over the thickness of each layer and if the solute concentrations at the blood-protein and the membrane –dialysate interfaces are expressed in terms of the external solute concentrations using equilibrium partition coefficients:

$$\phi_1 = \frac{\left(\rho_i\right)^{Protein}\Big|_{r=R-X_p}}{\left(\rho_i\right)^{Blood}\Big|_{r=R-X_p}} \ , \ \phi_2 = \frac{\left(\rho_i\right)^{Membrane}\Big|_{r=R+\delta}}{\left(\rho_i\right)^{Dialysate}\Big|_{r=R+\delta}} \ \text{and} \ \phi_P = \frac{\left(\rho_i\right)^{Protein}\Big|_{r=R}}{\left(\rho_i\right)^{Membrane}\Big|_{r=R}} \tag{5.27}$$

then, the following equation is obtained for the solute flux through the adsorbed protein layer and each region of the membrane.

$$N_s = \frac{\left[\exp(A+B+C)\frac{\rho_{Blood}}{\phi_p} - \rho_{Dialysate}\right] K_{C_2} J_v}{\exp(B)\left[\exp(A)\left[\frac{K_{C_2}}{K_{C_1}} + \exp(C)\frac{K_{C_2}}{\phi_p K_{C_p}} - \frac{K_{C_2}}{\phi_p K_{C_p}}\right] - \frac{K_{C_2}}{K_{C_1}} - \exp(-B) + 1\right]} \tag{5.28}$$

where,

$$A = \frac{\delta_1 K_{C1} J_v}{\varepsilon_1 K_{d1} D_\infty},\ B = \frac{\delta_2 K_{C2} J_v}{\varepsilon_2 K_{d2} D_\infty},\ \text{and}\ C = \frac{X_p K_{Cp} J_v}{\varepsilon_p K_{dp} D_\infty} \tag{5.29}$$

Total volumetric flux, J_v, in equations (5.26) and (5.28) depends on pressure difference between blood and dialysate compartments and hydraulic permeability, L_p, as described below:

$$J_v = L_P\left[P_B - P_D - \pi(z)\right] \tag{5.30}$$

In equation (5.30), blood pressure is calculated from equation (5.9) and oncotic pressure, π(z) is expressed in terms of the protein concentration in blood (Landis and Pappenheimer 1963):

$$\pi(z) = 0.21\rho_P(z) + 1.6\times10^{-3}\rho_P(z)^2 + 9\times10^{-6}\rho_P(z)^3 \tag{5.31}$$

where ρ_P is in g l^{-1} and π is in mm. Hg. The pressure on the dialysate side is dependent on geometry of module and configuration of fibers. The change in dialysate pressure with axial position is expressed with modified form of Hagen-Poiseuille equation (Hosoya and Sakai 1990):

$$\frac{dP_D}{dz} = \frac{-32\mu_D}{S_{eq}(d_{eq})^2} Q_D \tag{5.32}$$

where S_{eq} and d_{eq} are defined as:

$$S_{eq} = \frac{\pi d_{case}}{4} - N_{tube}\pi(R_i - X_p + \delta_1 + \delta_2) \tag{5.33}$$

$$d_{eq} = \frac{4S_{eq}}{\left(2N_{tube}\pi(R_i - X_p + \delta_1 + \delta_2) + \pi d_{case}\right)} \tag{5.34}$$

5.3. Enzyme Immobilized Membrane Model

In this section, model development for urease immobilized hemodialysis membranes is shown. As it can be clearly seen from the schematic of model Figure 5.4, urease enzyme is immobilized on the dense surface of the asymmetric membrane. Similarly, an additional protein layer grows on the surface of the enzyme layer. In this case, the enzyme-protein interactions become important in determining amount of protein adsorbed on the surface.

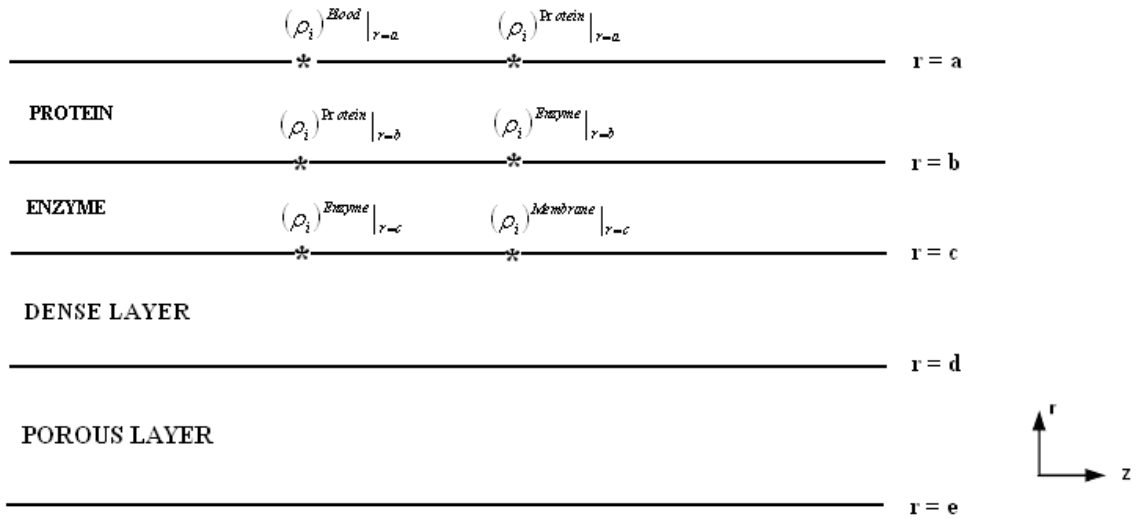

Figure 5.4. Schematic of model geometry of enzyme immobilized case.

The model equations used in the plain membrane case are still valid for the enzyme immobilized membrane case. Therefore, there is no change in total continuity and conservation of momentum equations and they are used with dimensionless variables as in the same form in equations (5.5), (5.10) and (5.11). Urease catalyzes the hydrolysis of urea into carbon dioxide and ammonia. The reaction occurs as follows:

$$(NH_2)_2CO + H_2O \xrightarrow{urease} CO_2 + 2NH_3 \tag{5.35}$$

Species continuity equation is written not only for urea but also for hydrolysis products, CO_2 and NH_3, since it is important to evaluate their levels in blood throughout the hemodialysis operation. Immobilized urease molecules are assumed to form a regular packing on the surface and homogeneous reaction without any side reactions occurs within this layer. It is also assumed that enzyme activity is conserved throughout the process and enzyme molecules do not desorb into the blood.

5.3.1. Species Continuity Equation in Enzyme Layer and Solute Fluxes in Each Layer

In the case of enzyme immobilized membrane, four layers exist between blood and dialysate sides as shown in Figure 5.4. Solute flux through the membrane is described by the same equation (Equation 3.4). Solute flux through the adsorbed protein layer is also defined in the same manner, accounting for both convective and diffusive mechanisms:

$$(N_i)^{Protein} = K_{C_i}^{Protein} J_V \rho_i - \varepsilon_p K_{D_i}^{Protein} D_{\infty_i}^{Protein} \frac{\partial \rho_i}{\partial r} \tag{5.36}$$

Species continuity equation for either reactant or products in enzyme layer is expressed as follows:

$$K_{C_i}^{Enzyme} J_V \frac{\partial \rho_i}{\partial r} - \varepsilon_{enz} K_{D_i}^{Enzyme} D_{\infty_i}^{Enzyme} \frac{\partial^2 \rho_i}{\partial r^2} + \gamma R_{urease} = 0 \tag{5.37}$$

where “i” denotes each species, γ is the stoichiometric coefficients of each species and has the values of -1, 1 and 2 for urea, carbondioxide and ammonia respectively. The reaction rate is defined by the Michaels-Menten in terms of urea consumption rate in equation (5.37).

$$-R_{urea} = \frac{V_{\max} \rho_{urea}}{K_m + \rho_{urea}} \tag{5.38}$$

Boundary conditions at each layer shown in Figure 5.4. are listed in Table 5.2. In order to describe the solute flux through the asymmetric membrane, the explicit expression derived for two layer membranes (Morti, et al. 2003) is used as it is given in the equation (3.5).

Table 5.2. Boundary conditions for enzyme immobilized case.

Position	**Boundary Conditions**	
At r = a	*Continuity of Fluxes*	$(N_i)^{Blood}\big\|_{r=a} = K_{C_i}^{\Pr otein} J_V \rho_i\big\|_{r=a} - \varepsilon_p K_{D_i}^{\Pr otein} \frac{\partial \rho_i}{\partial r}\big\|_{r=a}$
	Thermodynamical Relation	$(\rho_i)^{Blood}\big\|_{r=a} = (\rho_i)^{\Pr otein}\big\|_{r=a} \cdot \phi_1$
At r = b	*Continuity of Fluxes*	$K_{C_i}^{\Pr otein} J_V \rho_i\big\|_{r=b} - \varepsilon_p K_{D_i}^{\Pr otein} \frac{\partial \rho_i}{\partial r}\big\|_{r=b} = K_{C_i}^{Enzyme} J_V \rho_i\big\|_{r=b} - \varepsilon_{enz} K_{D_i}^{Enzyme} \frac{\partial \rho_i}{\partial r}$
	Thermodynamical Relation	$(\rho_i)^{\Pr otein}\big\|_{r=b} = (\rho_i)^{Enzyme}\big\|_{r=b} \cdot \phi_2$
At r = c	*Continuity of Fluxes*	$K_{C_i}^{Enzyme} J_V \rho_i\big\|_{r=c} - \varepsilon K_{D_i}^{Enzyme} \frac{\partial \rho_i}{\partial r}\big\|_{r=c} = N_s$
	Thermodynamical Relation	$(\rho_i)^{Enzyme}\big\|_{r=c} = (\rho_i)^{Membrane}\big\|_{r=c} \cdot \phi_3$

5.3.2. Protein Adsorption Kinetics

To illustrate the influence of enzyme immobilization on the amount of protein adsorbed on the surface, a method proposed for calculating adsorption isotherms for small, globular proteins in aqueous solution was adapted (Nakamura and Matsumoto 2006).

In this method, a linear isotherm is assumed in which the concentration of adsorbed species is directly proportional to the bulk concentration and the proportionality constant is defined as partition coefficient, *K*. The calculation of *K* is based on a collodial approach.

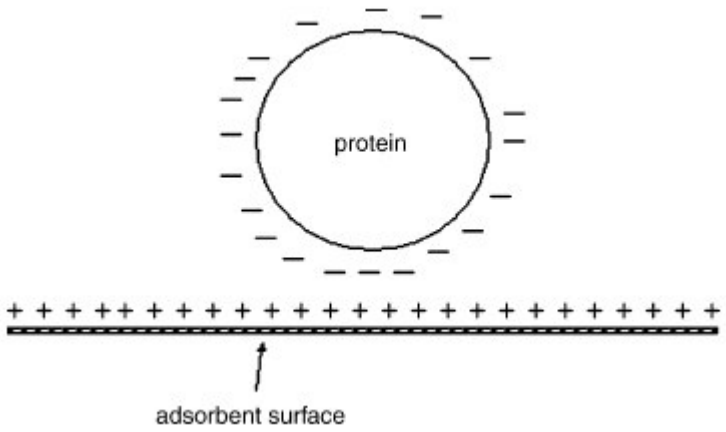

Figure 5.5. Schematic representation of colloidal approach for modeling protein adsorption on a porous surface.

As shown in Figure 5.5, in this approach, the protein is treated as a charged sphere and the adsorbent as a charged surface. Electrostatic and van der Waals interactions between the protein and adsorbent and repulsive interactions between the proteins all influence the adsorption capacity. These non-ideal events can be readily incorporated into the colloidal modeling framework, if the free energy contribution of each known. The colloidal approach based on the thermodynamic relationship for high affinity adsorption is shown in equation below:

$$K = \frac{C_s}{C_b} = \int_{Z_O}^{\infty} \left(e^{-(\Delta G_{total})/(kT)} \right) dz \tag{5.39}$$

where z_0 is distance of closest approach, z is the distance between the surface and the sphere, k is the Boltzmann constant and K is the colloidal equilibrium constant which is the ratio of the concentration of adsorbed proteins to the bulk protein concentration. When the entropic effects are neglected, the total free energy between the protein and the surface is expressed as:

$$\Delta G_{total} = \Delta U^{el}(h) + \Delta U^{vdw}(h) + \Delta H_{pp} \tag{5.40}$$

Here h is the dimensionless gap between the protein and adsorption surface and is a ratio of z/a, where a is the protein radius. $\Delta U^{el}(h)$ is the electrostatic particle surface interaction energy, and $\Delta U^{vdw}(h)$ is the van der Waals interaction energy. ΔH_{pp}

is the enthalpic contribution from repulsive interactions between surface proteins. In the solution of equation (5.40) it is assumed that all of the internal and enthalpic energies are equal to the Gibbs free energy of the corresponding interaction. The electrostatic interaction energy is calculated by the Yukawa's equation (Oberholzer, et al. 1999), and van der Waals interaction energy is calculated by the Hamaker equation. These terms are given below:

$$\Delta U^{el}(h) = kTB_{ps}e^{-\kappa a h} \tag{5.41}$$

$$\Delta U^{vdw}(h) = -\frac{A_{ps}}{6}\left[\frac{1}{h} + \frac{1}{h+2} + \ln\left(\frac{h}{h+2}\right)\right] \tag{5.42}$$

B_{ps} is a dimensionless parameter calculated by the method presented in (Oberholzer, et al. 1997):

$$B_{ps} = \left(\frac{4\pi kT\varsigma\varepsilon_0 a}{e^2}\right)\left(\frac{y_s + 4\gamma\Omega\kappa a}{1+\Omega\kappa a}\right)\left[4\tanh\left(\frac{\psi_s}{4}\right)\right] \tag{5.43}$$

where

$$\gamma = \tanh\left(\frac{\psi_s}{4}\right) \quad \text{and} \quad \Omega = \left(\frac{y_s - 4\gamma}{2\gamma^3}\right) \tag{5.44}$$

ψ_s and y_s are the dimensionless electrical potentials of the adsorption surface and the protein surface. The second bracketed term in equation (5.43) can be considered as effective electirical potential (y_{eff}) of protein surface which can be experimentally measured by zeta potential method. Both ψ_s and y_{eff} are found by the zeta potential measurements available in the literature and scaled by kT/e to be consistent with dimensionless form. ς is the dielectric constant of the solution, ε_o is the dielectric permittivity of free space, e is the electronic charge and κ is the Debye screening length. A_{ps} is the Hamaker constant, which is taken to be 1×10^{-20} J (Sader 1997) for proteins.

To be able to calculate ΔG_{total}, and so equilibrium constant K, the only term missing is the repulsive interactions between adsorbed protein molecules, ΔG_{pp}. Some attempts have been made to estimate ΔG_{pp} in the literature, in which this value is

considered as the heat of adsoption of protein molecules on the surface. However, this approach only takes into account the protein-surface interactions during the adsorption.

In this study, a predictive model has been developed that considers both protein-protein and protein-surface interactions and estimates the position of each particle at any time so that the sum of protein-protein forces determines the repulsive protein free energy.

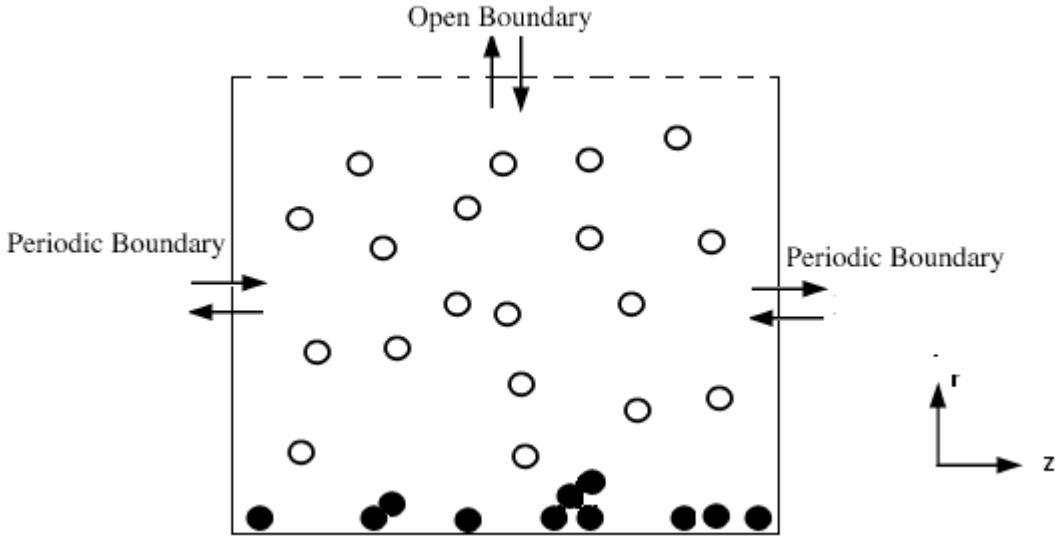

Figure 5.6. Schematic of the simulation box showing the deposition system used in the simulations. Periodic boundary conditions are used in the z directions and the top boundary is an open boundary.

A simulation is performed in two dimensional simulation box shown in Figure 5.6. The simulation box has an open top boundary where the new particles are introduced to the system and a periodic boundary at the left and rigth edges in which the particles can leave the system.

The coordinates of a set of N spherical particles in a dilute suspension are updated in time based on the numerical integration of the Langevin equation (Russel et al. 1989) that represents the force balance for each particle i, $1 \le i \le N$, with mass m_i in the solution:

$$m_i \frac{d^2}{dt^2} r_i = F_i^P + F_i^H + F_i^B \tag{5.45}$$

where r_i is the position vector of the particle, F_i^P is the external force due to protein-protein(p–p) and protein-surface(p–s) interactions, F_i^H is the hydrodynamic drag, and F_i^B is the stochastic (Brownian) force experienced by the particle due to the jostling by solvent molecules. For dilute suspensions, the drag force can be described by Stokes law:

$$F_i^H = 6\pi\mu a \frac{dr_i}{dt} \tag{5.46}$$

where a is the particle radius and μ is the fluid viscosity. For time scales larger than the momentum relaxation time, the particle inertia can be neglected in equation (5.45).

$$m\frac{d^2}{dt^2} r_i \approx 0 \tag{5.47}$$

The motion of the particle can then be given by the following discrete form of the Langevin equation (Gachon, et al. 1991):

$$r_i(t+\Delta t) = r_i(t) + (D\Delta t / k\ T)(F_i^P) + \Delta r_i^B \tag{5.48}$$

where the position vector of a particle at time $t+\Delta t$, $r_i(t+\Delta t)$, is derived from $r_i(t)$ by taking into account the deterministic displacements due to the external force, F_i^P, and the Brownian (random) displacement Δr_i^B corresponding to the timestep Δt. The components of Δr_i^B are chosen from a Gaussian distribution with mean equal to zero and variance given by $\sigma = 2D\Delta t$, where $D = kT/(6\pi\mu\alpha)$ is the Stokes–Einstein diffusion coefficient.

The net force acting on a particle can be calculated as the sum of the p-p and p-s forces based on the Derjaguin-Landau-Verwey-Overbeek(DLVO) theory, which accounts for the long range electrostatic and short range van der Waals interactions. The equations (5.41) and (5.42) are modified for the number of particles more than one and taking the negative gradients of these equations gives the electrostatic and van der Waals forces:

$$F_{ij}^{el} = \frac{\partial E_{ij}^{el}}{\partial r_{ij}} = \frac{B_{pp}}{r_{ij}} \exp\left[-\kappa a(r_{ij} - 2)\right]\left[\frac{1}{r_{ij}} + \kappa a\right] \tag{5.49}$$

$$F_{is}^{el} = \frac{\partial E_{is}^{el}}{\partial h} = B_{ps}\kappa a \exp\left[-\kappa a h\right] \tag{5.50}$$

and the van der Waals forces acting on the particles are:

$$F_{ij}^{vdw} = \frac{\partial E_{ij}^{vdw}}{\partial r_{ij}} = -\frac{A_{pp}}{6}\left[\frac{4r_{ij}}{(r_{ij}^2 - 4)^2} + \frac{4}{r_{ij}^2} - \frac{8}{(r_{ij}^3 - 4r_{ij})}\right] \tag{5.51}$$

$$F_{is}^{vdw} = \frac{\partial E_{is}^{vdw}}{\partial h} = \frac{-A_{ps}}{6}\left[\frac{1}{h^2} + \frac{1}{(h+2)^2} - \frac{h+2}{h}\left(\frac{1}{h+2} - \frac{h}{(h+2)^2}\right)\right] \tag{5.52}$$

where F_{ij}^{el} is the electrostatic force between particles i and j, F_{is}^{el} is the electrostatic force between particle i and the surface, F_{ij}^{vdw} is the van der Waals force between particles i and j, F_{is}^{vdw} is the van der Waals force between a particle i and the surface, B_{pp} and B_{ps} are the Yukawa coefficients, and A_{pp} and A_{ps} are the corresponding Hamaker's constants (units of kT). $r_{ij} \equiv \left|r_i - r_j\right| / a$ is the dimensionless (scaled by particle radius, a) center-to-center distance between particles i and j, h is the dimensionless (scaled by a) surface-to-surface separation distance between particle i and the surface ($h \equiv (r - a)/a$, where r is the r coordinate of the particle).

In the simulation some restrictions are made such as, if the position of the particles are equal or higher than the simulation box boundaries, then particles are terminated. Instead, new particles are introduced keeping the total number of particles constant and they are given the random initial positions. In order to avoid $h=0$ and $r_{ij}=2$ which causes undefined solutions of force equations, the steric exclusion thickness is set to be 0.3 nm (Elimelech, et al. 1995), such that the nearest dimensionless distance between two particles is $r_{ij}^* = 2 + 0.3/a$, and that between the particle and surface is $h^* = 0.3/a$, where the particle radius a should be expressed in nanometers.

The total force acting on a particle can be written as the summation of all p-p and p-s forces on that particle as follow:

$$F_i^{\,p} = F_{is} + \sum_j F_{ij} \tag{5.53}$$

The positions of all particles are estimated by equation (5.48) for each time step. At the point that the total p-p interaction forces reach equilibrium and do not change with time, the iteration is terminated and the free energy of repulsive protein interaction is calculated by total p-p interaction energy due to the final positions of the particles:

$$\Delta G_{pp} = \sum_j \int F_{ij}\, dr_{ij} \tag{5.54}$$

This calculated free energy value is used to find ΔG_{total} in equation (5.39) which allows to estimate equilibrium constant *K*, thus the concentration of adsorbed proteins.

5.4. Estimation of Model Parameters

In this section, the estimation of the parameters used in the model equations for both plain and enzyme immobilized cases is mentioned. Some of the parameters are calculated from the analytical expressions and semi-emprical formulas or they are found directly from the experimental studies available in the literature.

5.4.1. Membrane Characteristics

The structural properties of the membrane such as porosity ε, hydraulic permeability L_p, and pore size λ_s are acquired from the literature for different types of membranes.

Bungay and Brenner (1973) developed analytical expressions for the hindrance factors K_D and convection K_C. These expressions are valid for rigid spherical solutes in uniform cylindrical pores:

$$K_D = \frac{6\pi}{K_t} \tag{5.55}$$

and

$$K_C = \frac{(2-\phi)K_s}{2K_t} \tag{5.56}$$

The equilibrium partition coefficient, ϕ, for a spherical solute in a cylindrical pore is simply (Giddings, et al. 1968):

$$\phi = (1-\lambda)^2 \tag{5.57}$$

where λ is the ratio of the solute to pore radii. The hydrodynamic functions K_t and K_s in equations (5.55) and (5.56) are both expressed as expansions in λ:

$$\begin{bmatrix} K_t \\ K_s \end{bmatrix} = \frac{9}{4}\pi^2\sqrt{2}(1-\lambda)^{-5/2}\left[1+\sum_{n=1}^{2}\begin{pmatrix} a_n \\ b_n \end{pmatrix}(1-\lambda)^n\right] + \sum_{n=0}^{4}\begin{pmatrix} a_{n+3} \\ b_{n+3} \end{pmatrix}\lambda^n \tag{5.58}$$

with the coefficients *a,* and *b,* given in Table 5.3.

Table 5.3. Expansion coefficients for hydrodynamic functions K_t and K_s in equation (5.58).

Subscript n	**a_n**	**b_n**
1	-73/60	7/60
2	77,293/50,400	-2,227/50,400
3	-22.5083	4.0180
4	-5.6117	-3.9788
5	-0.3363	-1.9215
6	-1.216	4.392
7	1.647	5.006

5.4.2. Pore Size of Adsorbed Layer

Pore size of a membrane can be obtained from a manufacturer or experimentally. In this study, both enzyme molecules and adsorbed proteins are assumed to make a regular packing on the membrane surface as shown in Figure 5.7. Area of the pore among the regularly packed molecules can be calculated. However, partition coefficient expression is derived for cylindrical pores and is written in terms solute and pore radius. Therefore, pore size of protein layer is assumed to be equal to radius of a circle that has the same area with the pore between regularly packed molecules.

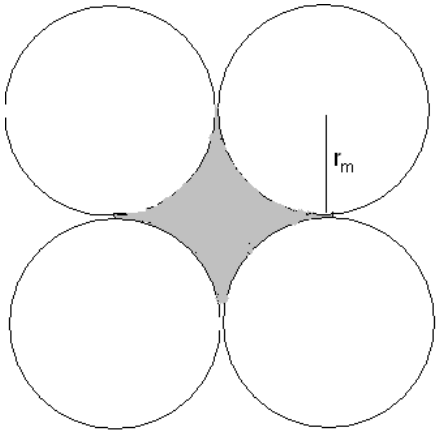

Figure 5.7. Representation of pore between regular packed protein molecules

Then, the pore radius of both enzyme and protein layers can be estimated by the expression below:

$$R_{pore} = r_m \sqrt{\frac{4}{\pi} - 1} \cong 0.523 r_m \tag{5.59}$$

where r_m is the radius of the enzyme molecules or adsorbed proteins on the membrane surface in regular packing.

5.4.3. Mass Transfer Coefficient on Dialysate Side

Analytical and semi-emprical equations exist in the literature to estimate the mass transfer coefficient on dialysate side, although they are derived based on some simplifying assumptions in contradiction with our model, or they are only valid for the given flow rates.

Therefore, a more general expression is needed to observe the effects of operating conditions on the clearances of different molecules. Among the semi-emprical equations for lumen mass transfer coefficient in hollow fiber modules, the equation derived by Dahuron and Cussler (1988) is found to be appropriate for hemodialysis operations since the Reynolds Number (*Re*) calculated is not greater than 15. Equation used for calculating the dialysate mass transfer coefficient(k_D) is given below:

$$S_h = \frac{k_D(d_{hous} + 2\delta)}{D_\infty} = 8.8\left(\frac{d_h}{L}\right)R_e S_c^{\,0.33} \tag{5.60}$$

where *L* is the length of the fiber, δ is membrane thickness, D_∞ is diffusion coefficient in free solution, *Sc* is Schmidt number, and $R_e = d_{hous}U_{avg}\rho/\mu$. Hydraulic diameter(d_h) is defined as:

$$d_h = \frac{d_{hous}^2 - N_{tube}d_o^2}{d_{hous} + N_{tube}d_o} \tag{5.61}$$

where N_{tube} is the number of fibers, d_{hous} and d_o are the inner and outer diameters respectively.

5.5. Numerical Methods

All of the variables are non-dimesionalized and normalized in order to facilitate the numerical calculations. Merely, concentration variables remained dimensional since their magnitude is known to be in the range of magnitude of other variables. All of the numerical solutions are performed in computer software MATLAB 7.0. Having the

model equations expressed in finite difference form, the optimization is performed by Levenberg–Marquardt method in order to converge the optimal solution for all variables.

5.5.1. Transformations for Jump Mass Balance

To facilitate numerical treatment of the moving interface due to protein adsorption, the following coordinate transformation is used:

$$\eta = \frac{r^*}{R_i - X_p(t)} \tag{5.62}$$

where,

$$\text{at } r^* = 0 \rightarrow \eta = 0 \tag{5.63}$$

$$\text{at } r^* = R_i - X_p(t) \rightarrow \eta = 1 \tag{5.64}$$

This new variable is a function of time so all the model equations differ from their previous forms. Ultimate forms of the equations (5.10), (5.11) and (5.22) that are used in the numerical solution are given below:

$$\frac{\partial V}{\partial \eta} + \frac{V}{\partial \eta} + \frac{\eta N_p}{(R_i - X_p)\rho_{\substack{ads.\\layer}} U_{avg}} \left(\frac{\partial U}{\partial \eta}\right) + \frac{\partial U}{\partial z} = 0 \tag{5.65}$$

$$U = \frac{\int_{\eta}^{1} \frac{r'}{\mu} dr'}{\int_{0}^{1} \frac{\eta^3}{\mu} d\eta} \tag{5.66}$$

and species continutiy equation becomes:

$$\left[V + U \frac{\eta N_p L}{(R_i - X_p)\rho_{\substack{ads.\\layer}} U_{avg}} \right] \frac{\partial \rho_i}{\partial \eta} + U \frac{\partial \rho_i}{\partial z} = \frac{1}{Pe} \left[\frac{\partial^2 \rho_i}{\partial \eta^2} + \frac{1}{\eta} \frac{\partial \rho_i}{\partial \eta} \right] \tag{5.67}$$

5.5.2. Numerical Solution Algorithm

Numerical solution is performed using finite difference method. All of the differential equations in the model are written in finite difference form. Central difference approximation is used for defining the first and second order derivatives at each point inside the discretized area as follows:

$$\frac{\partial f}{\partial x}\Big|_{i,j} = \frac{f_{i+1,j} - f_{i-1,j}}{2\Delta x} + O[(\Delta x)^2] \tag{5.68}$$

$$\frac{\partial^2 f}{\partial x^2}\Big|_{i,j} = \frac{f_{i+1,j} - 2f_{i,j} + f_{i-1,j}}{\Delta x^2} + O[(\Delta x)^2] \tag{5.69}$$

Three-point, one-sided forward and backward difference expressions are utilized to evaluate derivatives at the boundaries and with an accuracy of $O[(\Delta x)^2]$. Forward difference expression is,

$$\frac{\partial f}{\partial x}\Big|_{i,j} = \frac{-3f_{i,j} + 4f_{i+1,j} - f_{i+2,j}}{2\Delta x} + O[(\Delta x)^2] \tag{5.70}$$

and backward difference expression is:

$$\frac{\partial f}{\partial x}\Big|_{i,j} = \frac{3f_{i,j} - 4f_{i+1,j} + f_{i+2,j}}{2\Delta x} + O[(\Delta x)^2] \tag{5.71}$$

For the numerical calculations, uniform distribution is used for discretization. The number of grids in both radial and axial directions are decided to be 22, since the change in the results above a grid number of 22 is found to be insignificant. Model equations are normalized to obtain the same order of magnitude for the variables, then, convergence of the equations is easily achieved. The numerical algorithm summarizing the calculation steps is shown with a chart in Figure 5.8.

During the simulations, dimensionless axial and radial velocity components (Equations (5.10) and (5.11)) are transformed into Trapezoidal numerical integration form and involved into the general finite difference solution. Equations (5.9) and (5.22) are solved simultaneously with the Trapezoidal integral velocity equations and given boundary conditions. It is evident that, protein thickness change is considered and it exists in the model as a time dependent equation. Therefore, based on our assumptions, time step(Δt) is determined to be the space time of blood in dialyzer, $\Delta t = \frac{L}{U_{avg}}$.

At each cycle, concentrations of the species, axial and radial velocities both in r and z directions, pressures and volumetric flow rates are calculated so that it is able to find protein flux(N_p) at every axial and radial position. Hence, protein thickness is updated according to equation (5.20) and also the amount of proteins adsorbed in both primary(m_{p1}) and secondary(m_{p2}) adsorption stages is calculated from equations (5.16) and (5.17) respectively at each time cycle. Then these new protein adsorption parameters are used in the next iteration. In the case of enzyme immobilized membrane, adsorption capacities are calculated by the protein adsorption thermodynamic model. The integral in equation (5.39) is calculated numerically by Simpson's 1/3rd rule. Adsorption simulation is performed in computer software MATLAB. Time step for adsorption simulation is taken to be the same with the whole-body clearance model which is equal to space time. The simulation is terminated when the position of the particles reaches equilibrium. The repulsive interaction energy between the proteins is calculated for the ultimate positions of proteins.

As mentioned before, the main goal in these calculations is to make predictions on the concentration levels of solutes in the patient's blood. Therefore, the solute concentration at the dialzyer outlet (ρ_i^{out}) is calculated at each time step and used in the whole-body clearance equations (5.1) and (5.2) so that extra- and intra- cellular solute concentrations can be predicted at any time during hemodialysis.

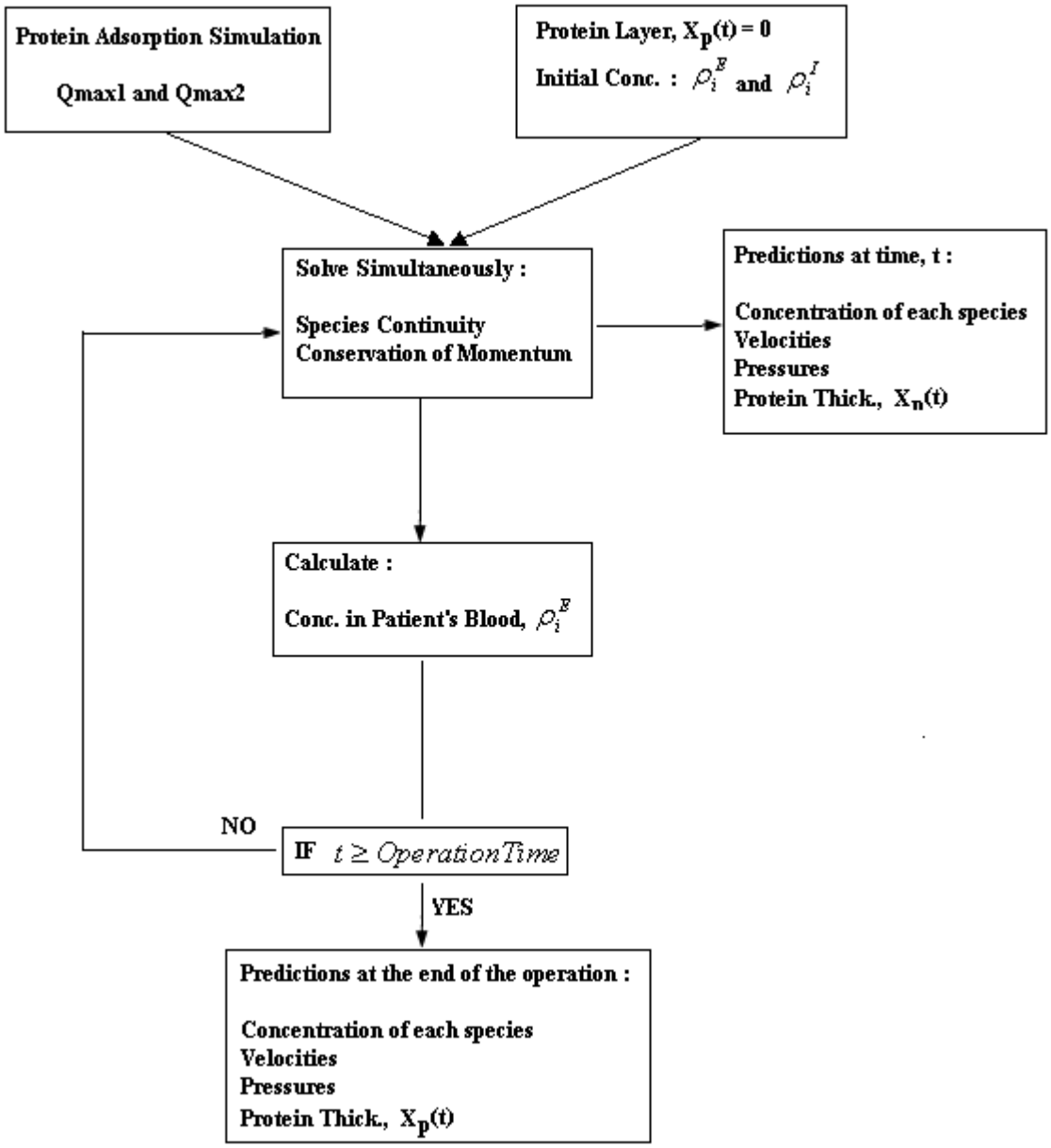

Figure 5.8. Numerical solution algorithm.

CHAPTER 6

RESULTS AND DISCUSSION

6.1. Plain Membrane Results

Model developed in this study was used to predict solute concentrations and velocity profiles at different axial and radial positions in a hemodialyzer. The model results for urea concentration changes in Fresenius 60 type hemodiafilter are shown in Figure 6.1 in which predictions are made at the beginning of the process so that the effect of protein fouling is not significant. The structural properties of the F60 type membrane used in calculations are given in Table 6.1. The simulation results shown in Figures (6.1)-(6.6) are made for the blood flow rate(Q_B) of 200 mL/min and dialysate flow rate(Q_D) of 500 mL/min.

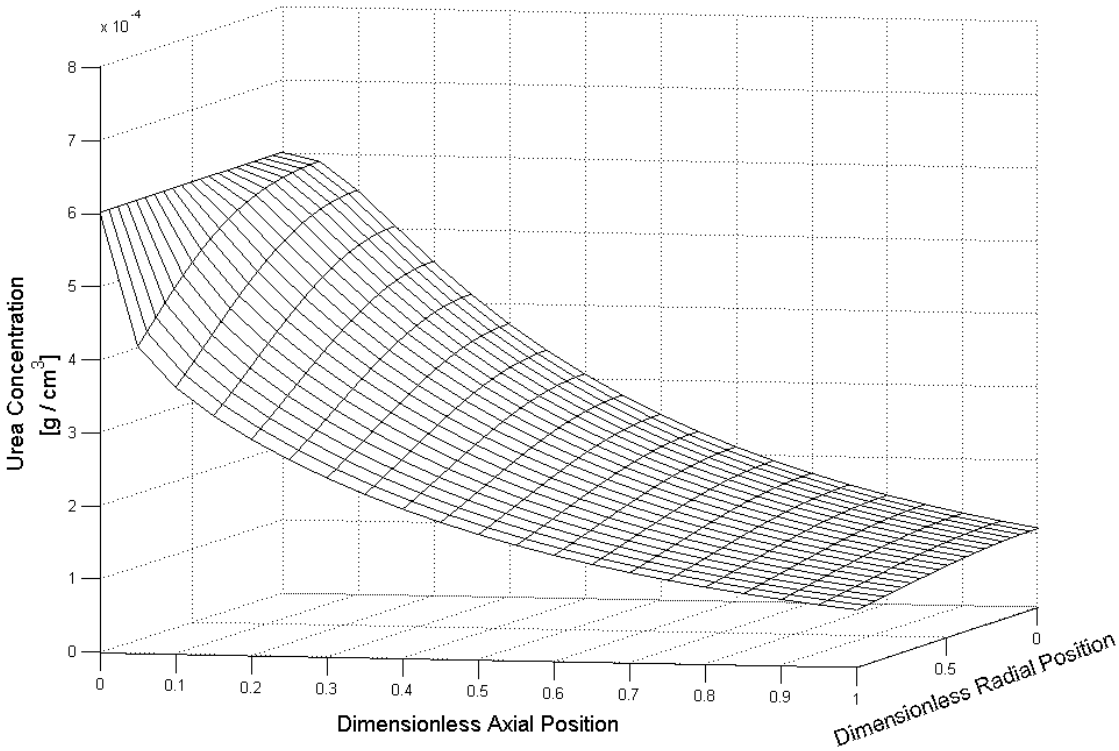

Figure 6.1. Urea concentration at different axial and radial positions.

It is observed that urea concentration decreases dramatically along the length of module, and this change becomes very small being closer to the outlet of the fiber. It is also shown that solute concentration is greater at the center of the fiber and decreases significantly towards the membrane surface at the first half of the module. This concentration difference in radial direction plays an important role in mass transfer of solutes during hemodialysis, thus the assumption that the concentration of solutes are distributed uniformly in cross section can cause inaccurate predictions.

Table 6.1. Structural properties of the F60 type hemodialyzer.

	Effective Length (cm)	**Fiber Radius(μm)**	**Number of Fibers**	**Case diameter(cm)**	**Thickness (μm)**
Fresenius 60 Type Hemodialyzer	22	200	9000	4.0	40
	Membrane Area(m^2)	**Porosity**	**Pore Size(Å)**	**Fraction of Dense Layer**	**Hydraulic Permeability (cm/sec.mmHg)**
	1.25	0.8	7.9	0.0217	3.36×10^{-6}

Since the convection dominates the mass transfer in axial direction, the change in the axial velocity both with axial and radial directions is considered and shown in Figure 6.2. As it is expected, axial velocity is found to be maximum at the center and zero at the membrane surface. Concentration of large blood molecules affect the viscosity of the blood and this causes a small change in axial velocity along the length of fiber. This change is relatively small compared to the change with respect to radial position, however it determines the magnitude of radial velocity which is found to be very effective on protein fouling mechanism.

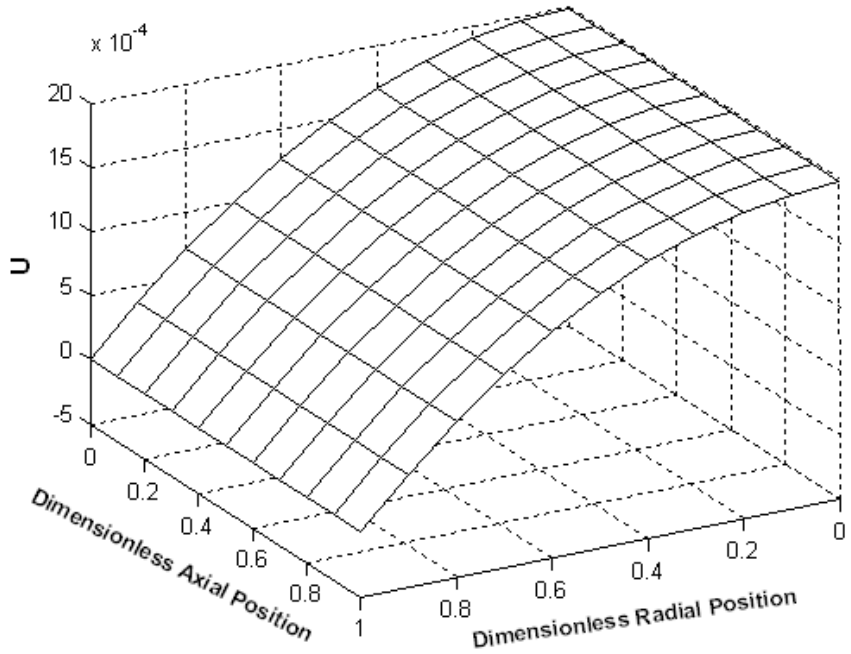

Figure 6.2. Axial velocity change in axial and radial directions.

The dimensionless radial velocity profiles along the fiber length and cross-section are shown in Figure 6.3. (a) and (b) respectively. It is observed that, along the fiber length, radial velocity reaches a maximum point then starts to decrease. This peak point is found to be different for each radial position. The maximum radial velocity is expected to occur at a point close to the inlet and the center of the fibre. Therefore, that is the point where the convectional mass transfer becomes most competitive.

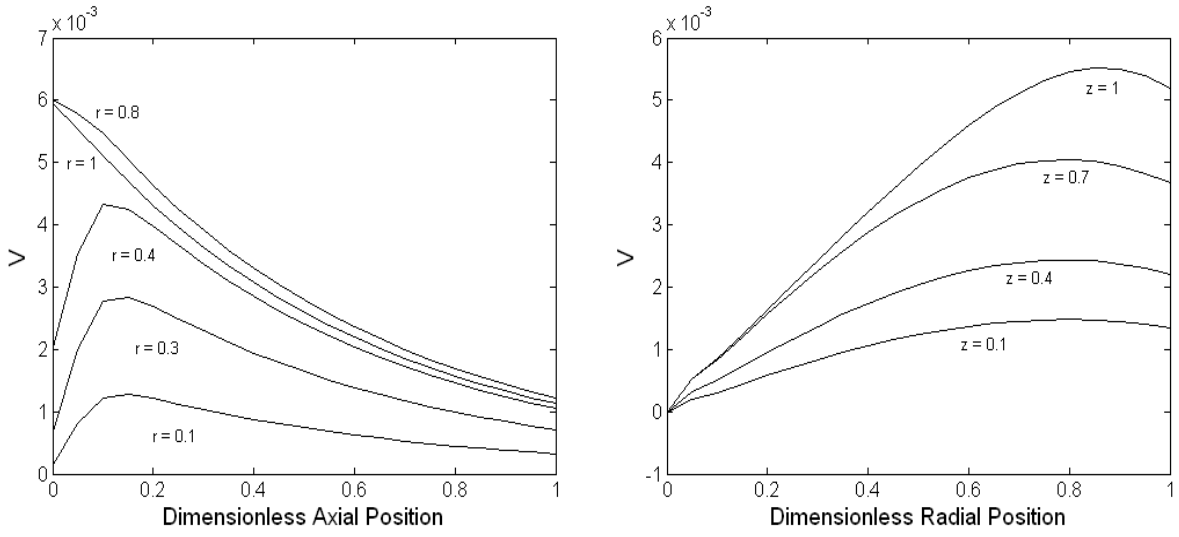

(a) (b)

Figure 6.3. Change of radial velocity along the (a) length of fiber and (b)in cross section

Solute transfer in radial direction is carried out by both convectional and diffusional mechanisms. Therefore the direction and magnitude of radial flow is expected to be determinative on concentration profiles especially for large molecules in blood which can diffuse back from surface to the center. The back-diffusion of large molecules can be explained by the lower concentrations of relatively smaller molecules on the membrane surface because of their high permeability through membrane.

Accumulation and adsorption of protein molecules on the membrane surface is a well-known phenomenon so that there should be a positive net protein flux from center towards the membrane wall. Contributions of mass transfer mechanisms on the protein flux in radial direction are shown in Figure 6.4 for different axial positions. It is evident that, convection is dominating the back-diffusion of proteins in radial direction and net flux is positive at each position along the fiber length. Since protein adsorption is directly proportional with the amount of protein that accumulates on the surface, the magnitude and direction of radial velocity significantly control the rate of protein adsorption.

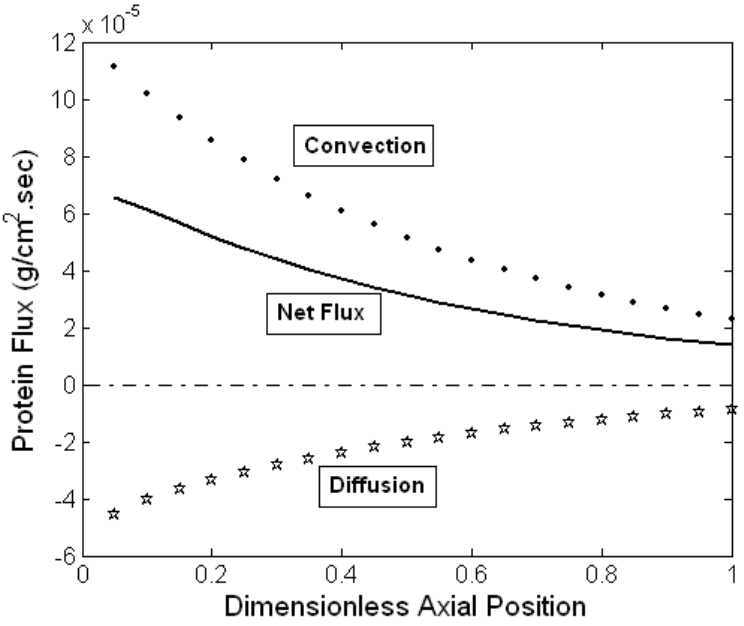

Figure 6.4. Transport mechanisms affecting protein flux.

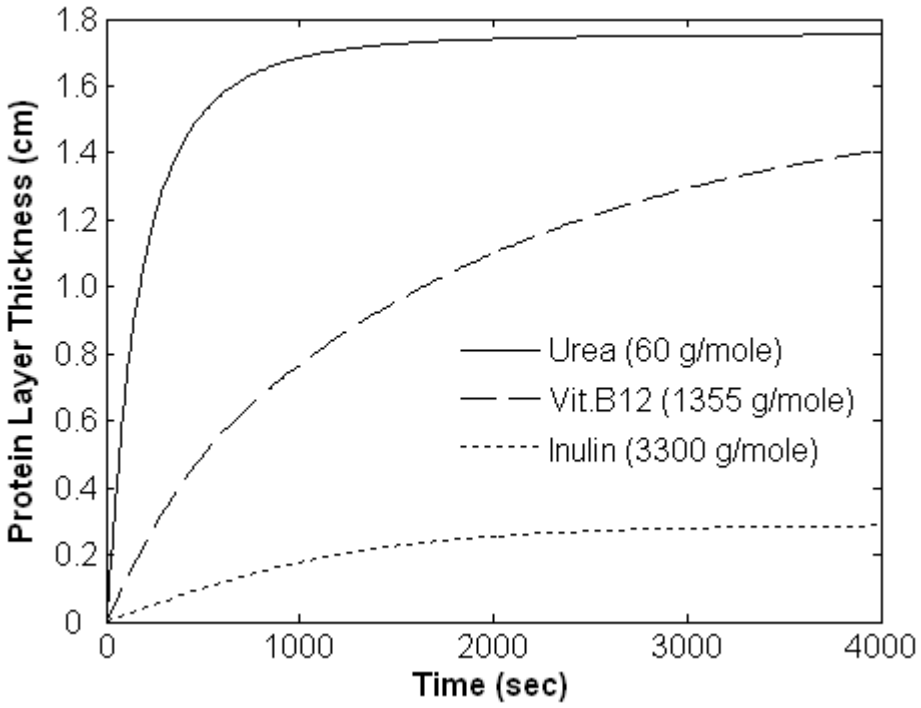

Figure 6.5. Change of length average adsrobed protein layer thickness with respect to time.

In Figure 6.5, it is shown that the rate of accumulation of proteins on the surface depends on the size of solute permeating through the membrane. When the solute size is small, equilibrium protein adsorption capacity is reached within a short period of time. In the case of larger solutes, such as inulin, the rate of accumulation of protein becomes much slower. This is an expected result since the model treats the blood as a pseudobinary mixture. Consequently, slower diffusion of larger solutes results in higher solute or lower protein concentration at the membrane surface.

Since the protein flux towards the membrane surface is not uniform along the membrane length, the rate of adsorption changes with axial position. The change in protein layer thickness in axial direction is shown in Figure 6.6, at each time step during 1 hr hemodialysis. This figure can be considered as the side view of a single sliced fiber where the horizontal lines respresent the thickness of the protein layer which increases as the time passes. It is observed that, at the initial stages of the operation- the lines close to bottom half of the plot-, protein layer thickness decreases through the dialyzer outlet. This is caused by the high convectional protein transport towards the membrane at the positions close to the inlet. On the other hand, as operation time increases, the difference in protein layer thickness between the inlet and outlet of the dialyzer starts to

disappear and finally they come to the same level. This result is expected, since at later times, protein adsorption capacity of the surface is reached.

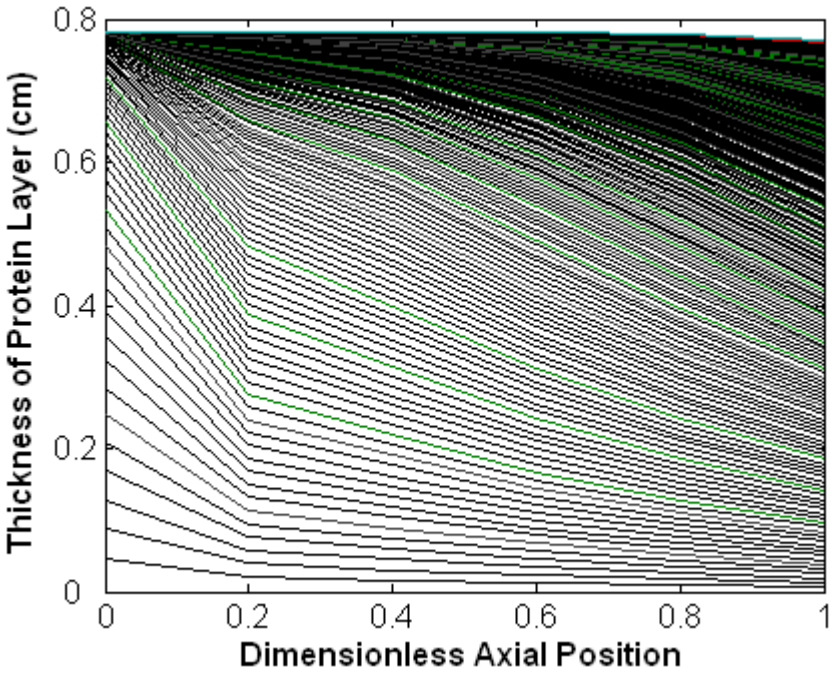

Figure 6.6. Protein layer thickness along fiber length at different times.

6.1.1. The Effect of Parameters on Solute Clearances

In this section, the influences of structural properties of membrane, operating conditions and dimensions of the dialyzer on the solute clearances were investigated. The range of the parameters investigated in the simulations are values typically used for hemodialysis operation or for commercial hemodialyzers. Urea and vit.B12 were used as small and middle molecular weight solutes. Simulation results shown in Figure 6.7 through Figure 6.12 were obtained with the structural properties of F60 type hemodialyzer listed in Table 6.1. Blood and dialysate flow rate values were taken as 200 mL/min and 500 mL/min repectively.

Blood flow rate is found to be very effective on solute clearances of each size. As shown in Figure 6.7, clearance of both model solutes increases with higher blood flow rate. It is observed that a significant concentration difference exists when the blood flow rate is set to 300 mL/min. Although both molecules are considerably affected from this change, it is clear that, especially urea concentration in axial direction starts to decrease exponentially.

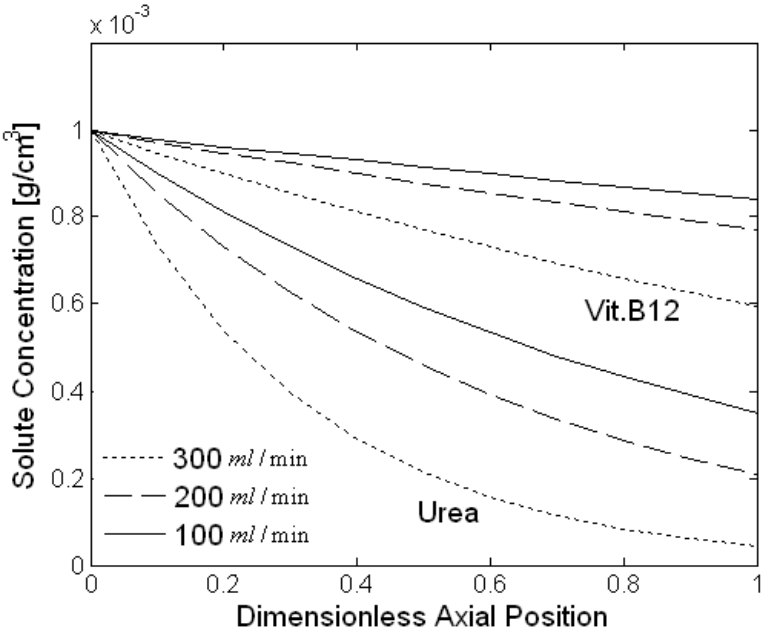

Figure 6.7. Effect of blood flow rate on solute concentration in axial direction.

Obviously, clearance values can be increased by selecting longer dialyzer modules. The model results shown in Figure 6.8 supports this idea. Using a 10 cm module in length does not seem to be adaquate for both urea and vit.B12 clearances.

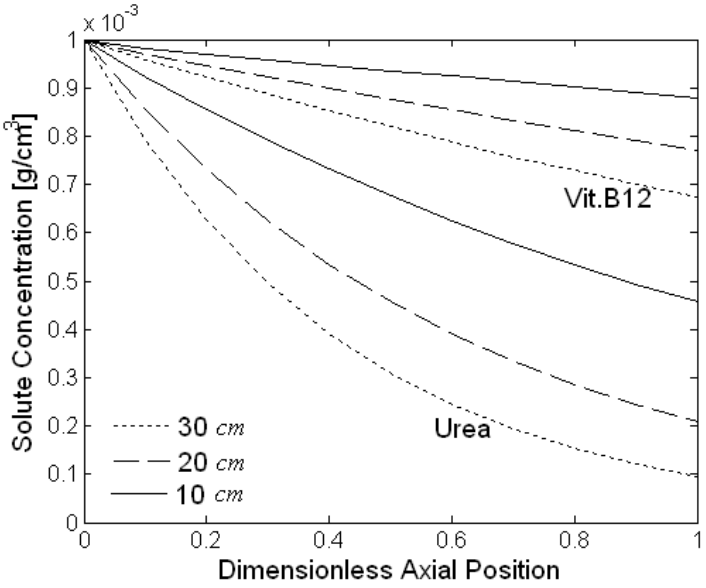

Figure 6.8. Effect of fiber length on solute concentration in axial direction.

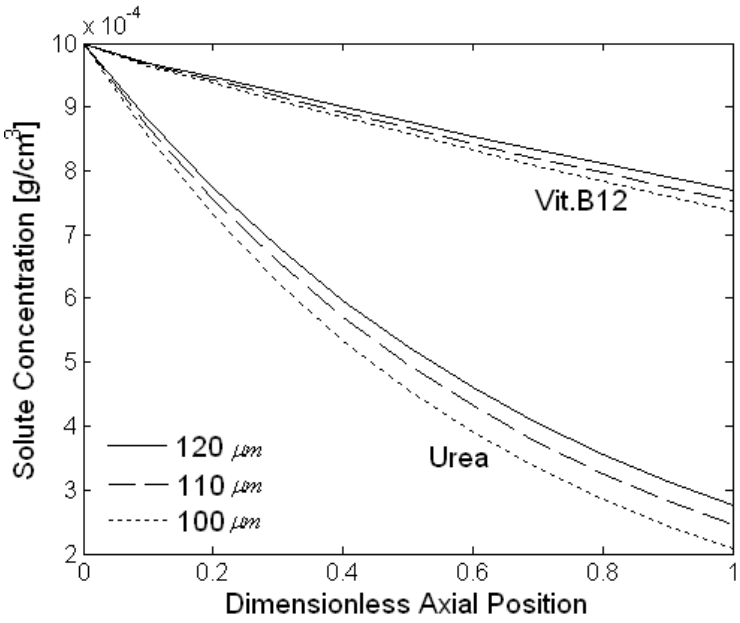

Figure 6.9. Effect of fiber radius on solute concentration in axial direction.

Similarly, fiber radius is also effective on clerances. The solute clearances increases with decreased fiber radius as shown in Figure 6.9. This is caused by the increase in blood velocity which enhances the convective mass transfer in radial direction.

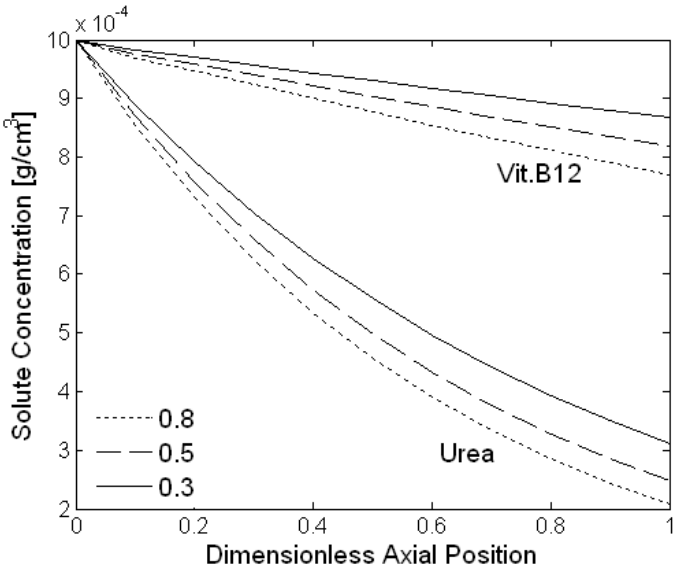

Figure 6.10. Effect of membrane porosity on solute concentration in axial direction.

Solute clearances are also affected by the structure of the membrane. Figure 6.10 illustrates that membrane with higher porosity causes larger solute clearances. Pore size of the membrane does not have any effect on the clearance of urea while it has a small effect on the clerance of larger solute, vit.B12 as shown in Figure 6.11. The increase in pore size has a pronounced effect on the clearance of toxic middle molecular weight proteins.

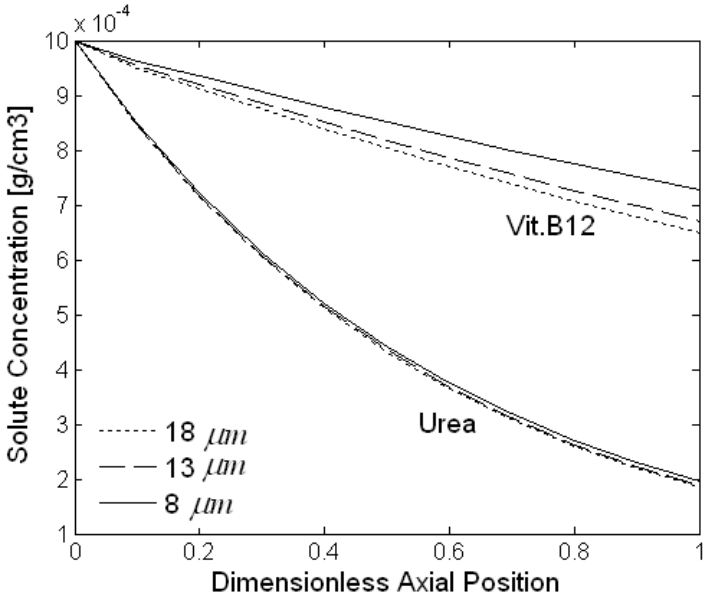

Figure 6.11. Effect of membrane pore size on solute concentration in axial direction.

In dialyzers, both asymmetric and symmetric membranes are used. Figure 6.12 shows that the clearances of both urea and vit.B12 are slightly higher through symmetric membranes. This is due to fact that in the case of asymmetric membranes, pore sizes in the dense layer which is in contact with the blood are much smaller than those in the porous sublayer. Thus, the mass transfer resistance is higher in the case of asymmetric membrane when the pore sizes in the sublayer are the same. Even though, symmetric membrane seems to provide higher clerances, in some cases, asymmetric membranes are used to prevent penetration of large proteins into the pores, thus to minimize internal protein fouling due to clogging of the pores.

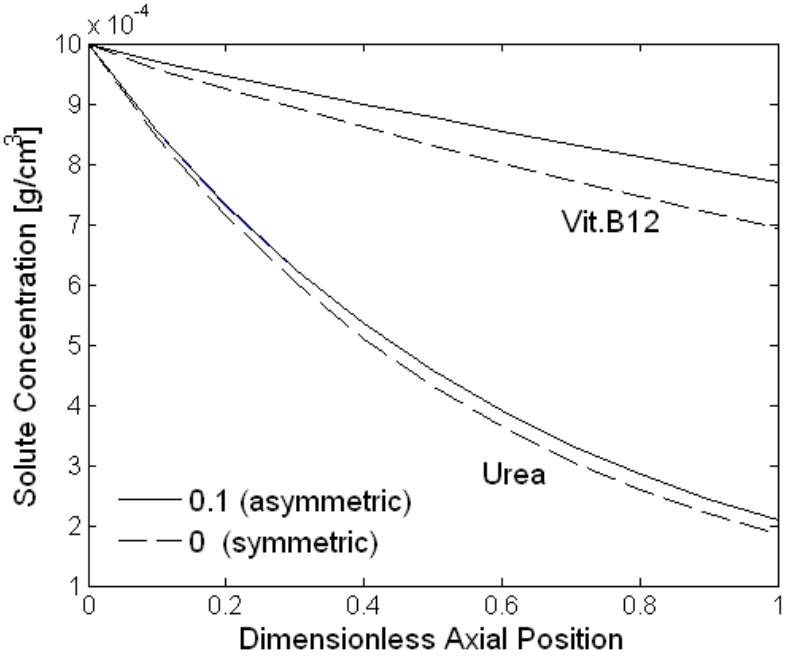

Figure 6.12. Effect of degree of asymmetry on solute concentration in axial direction.

6.1.2. Whole Body Clearances

Clearance value of a dialyzer gives important information about the overall performance of a hemodialysis operation. However, hemodialysis is the combination of dialyzer and intercompartmental clearances as it is illustrated in Figure 5.1. Clinically, the efficiency of the hemodialysis operation is evaluated by checking the solute concentration levels in patient's blood. In this section, model predictions for whole body clearances of urea, vit.B12 and inulin will be presented. Whole body clearance of solutes from the blood at the end of a typical dialysis time of 4 hr.

The effects of structural parameters, operating conditions and dimensions of the dialyzer on the percent removal of different molecules in patient's blood are shown in Table 6.2. The results clearly indicate that the blood flow rate has a significant influence on the clearance of the smallest size solute, urea, while its effect is much smaller on the clearance of larger molecule, inulin. The influence of dialysate flowrate on the clearance of all solutes is smaller, compared to that of the blood flowrate. The increase in the thickness of the membrane causes a decrease in the solute clearance while more porous membrane structure with a larger pore size enhances the solute clearances.

Table 6.2. Effect of different model parameters on % removal of solutes from the blood. *, ≠

Solutes / Parameters	Urea		Vit.B12		Inulin	
Q_B (ml/min)	**With Protein**	**Without Protein**	**With Protein**	**Without Protein**	**With Protein**	**Without Protein**
100	52.61	53.78	38.97	40.60	8.37	10.28
200	69.40	70.22	44.48	45.59	10.75	12.01
300	75.07	75.41	46.57	47.41	11.03	12.10
Q_D (ml/min)						
300	63.37	63.56	36.21	36.83	8.57	9.38
400	66.56	67.06	40.15	40.92	9.59	10.63
500	69.40	70.22	44.48	45.59	10.75	12.01
Thickness(μ)						
20	70.51	71.19	49.95	50.81	16.28	17.24
46	69.40	70.22	44.48	45.59	10.75	12.01
60	68.79	69.25	41.94	42.61	9.02	9.86
Porosity						
0.3	65.97	66.28	33.20	33.88	5.15	5.97
0.5	68.18	68.72	39.71	40.50	7.83	8.79
0.8	69.40	70.22	44.48	45.59	10.75	12.01
Pore Size(Å)						
8	69.13	71.11	37.57	39.24	2.55	3.87
13	69.23	71.08	42.35	43.96	5.54	6.93
18	69.40	70.22	44.48	45.59	10.75	12.01
Fraction of Dense Layer						
0	70.12	70.81	53.67	54.48	21.71	22.80
0.02	69.40	70.22	44.48	45.59	10.75	12.01
0.1	69.38	70.07	43.98	45.01	6.11	7.48
R_{Fibre}(μ)						
100	69.40	70.22	44.48	45.59	10.75	12.01
110	69.54	70.56	46.26	47.68	11.54	13.01
120	70.80	72.13	47.89	49.31	12.12	13.68
L_{Fibre}(cm)						
10	59.44	59.46	29.01	29.02	5.57	5.62
20	69.40	70.22	44.48	45.59	10.75	12.01
30	72.47	73.51	53.68	54.99	12.09	13.55
d_{case}(cm)						
2.5	48.02	48.04	22.75	22.77	5.25	5.41
3.9	69.40	70.22	44.48	45.59	10.75	12.01
4.8	71.36	72.28	48.14	49.52	13.62	14.98

* $\%\ Removal\ of\ Solute = \dfrac{(\rho_i|_{t=0} - \rho_i|_{t=4hr})}{\rho_i|_{t=0}} \times 100$

≠ All other parameters used in the simulations are given in Table 6.1

In addition, % removals of vit.B12 and inulin decrease significantly as the degree of asymmetry of the membrane increases. According to the results in Table 6.2, the influences of structural properties of the membrane on the clearances are more pronounced for larger molecular weight solutes such as inulin.

The most important design parameter for the dialyzer is the effective diameter(d_{case}) among the fibers which has a significant influence on the clearances of all solutes. As seen from Table 6.2, the difference in predicted clearance values by considering or neglecting protein fouling becomes larger as the solute size increases.

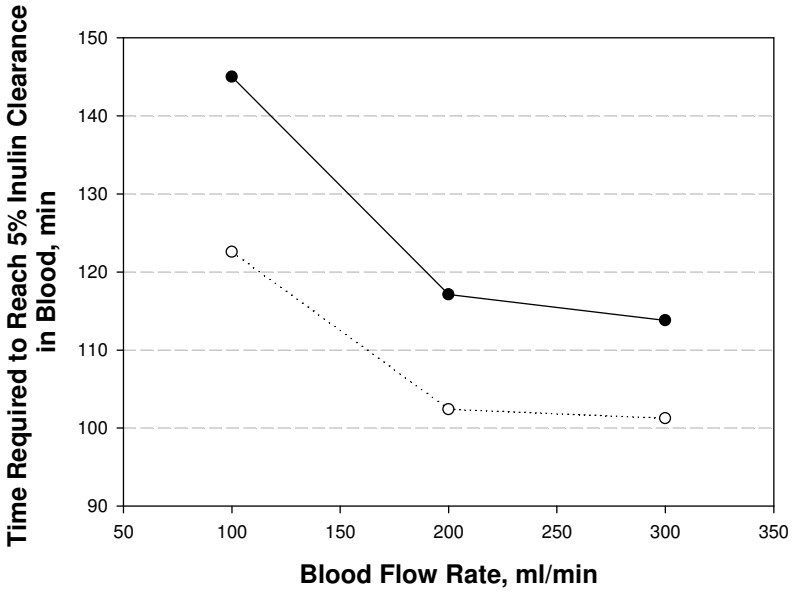

Figure 6.13. Time required to reach 5% inulin clearance at different blood flow rates. Simulations were performed; (○) without protein fouling, (●) with protein fouling.

The influence of protein fouling is more clearly illustrated in Figure 6.13 which indicates that for each blood flow rate, time required to reach 5% inulin clearance is shorter when protein fouling is neglected. This is due to increased mass transfer resistance for solute removals when adsorption of proteins on the membrane surface is considered.

6.1.3. Model Validation

The experimental results available in the literature are used to verify the accuracy of the model developed in this study. Jaffrin et. al. (1981) performed experiments in order to observe the effect of blood flow rate on the clearance of permeable solutes; creatinine, vitamin B12 and myoglobin by using a Hospal Filtral 12 AN69HF type hemodiafilter. The structural parameters are given in Table 6.3. They used saline instead of blood, and the experiments were operated at blood(Q_{Bin}) and dialysate(Q_{Din}) flowrates of 200 mL/min and 500 mL/min respectively. Model predictions and clerance measurements in the experiments are compared in Figure 6.14, where the clearance of the solutes is defined as:

$$CL = \frac{Q_{Bin}C_{Bin} - Q_{Bout}C_{Bout}}{C_{bin}} \tag{6.1}$$

In equation (6.1), C_{Bin} and C_{Bout} correspond to the solute concentrations at the inlet and outlet of the hemodialyzer respectively. It is shown in Figure 6.14, model predictions compare well with the experimental data. The model slightly underestimates the data in the case of myoglobin. This is due to uncertainties in the estimation of diffusion coefficient from Stokes-Einstein equation which is usually approximate for large molecular weight solutes such as myoglobin.

Experimental data and model predictions indicate that increasing blood flow rate from 100 to 500 mL/min enhances the clearance of creatinine by 100%, while it has almost no influence on the clearance of large solute myoglobin. This is due to fact that, clearance of myoglobin is mainly controlled by its transport through the membrane. Thus, the decrease in external mass transfer resistance with increased blood flow rate does not change the overall mass transfer resistance of myoglobin transport.

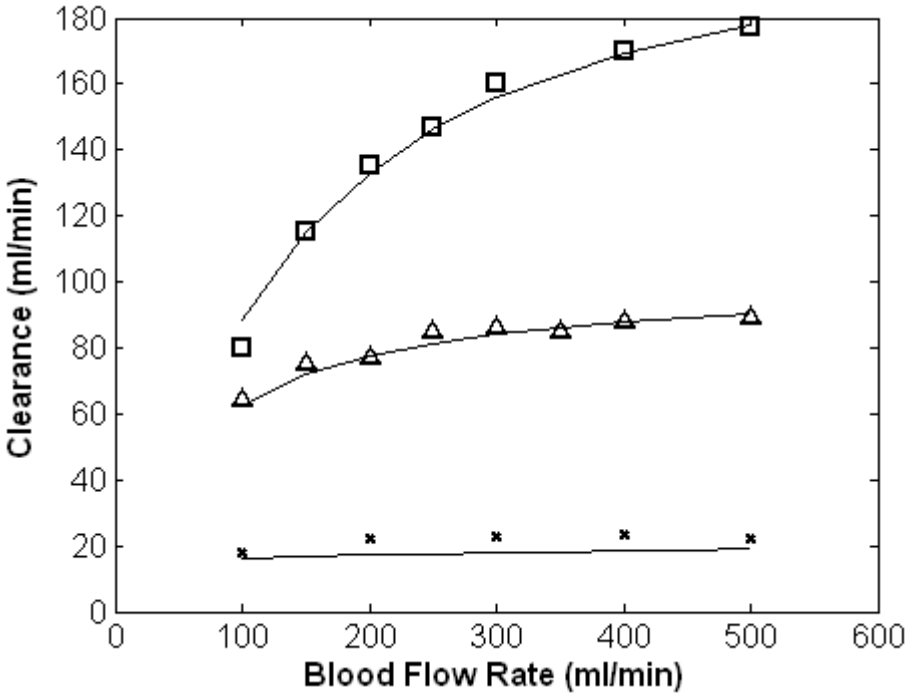

Figure 6.14. Comparison of model results with the experimantal data (Jaffrin, et al. 1981), Q_f = 0 ml/min and Q_d = 500 ml/min for the clearances of molecules ; (□) Creatinine, (Δ) Vit.B12 and (⋆) Myoglobin.

Table 6.3. Structural properties of the Hospal Filtral 12 AN69HF type hemodiafilter.

Hospal Filtral 12 AN69HF Type Hemodialyzer	**Effective Length (cm)**	**Fiber Radius(μm)**	**Number of Fibers**	**Case diameter(cm)**	**Thickness (μm)**
	20	110	8500	3.9	45
	Membrane Area(m^2)	**Porosity**	**Pore Size(Å)**	**Fraction of Dense Layer**	**Hydraulic Permeability (cm/sec.mmHg)**
	1.15	0.8	17.8	0	7.5×10^{-7}

Table 6.4. Influence of protein adsorption on solute clearances.

Clearances (ml/min)		**Experiment**	**Model**
Creatinine	**Saline**	173.3 ± 2.5	171.8
	Plasma	172.2 ± 2.8	170.8
Inulin	**Saline**	95.6 ± 4.1	91.6
	Plasma	91.3 ± 8.4	89.5

Bosch et. al. (1985) measured the clearances of creatinine and inulin by using a Fresenius F60 type module and adjusting the blood and dialysate flowrates at 200 mL/min and 500 mL/min, respectively. To see the influence of proteins in the blood on the solute clearances, experiments were performed for both saline and plasma. Model predictions are in good agreement with the experimental data considering the standard deviations listed in Table 6.4. The clearances of two model molecules are smaller in the case of plasma, where the protein adsorption on the membrane surface takes place. The results have shown that, protein fouling is more effective on larger molecules. In fact, the lower clearance values for plasma is caused by protein fouling as well as the smaller diffusivities of solutes in plasma compared to those in saline solution.

6.2. Enzyme Immobilized Membrane Results

In this section, model predictions for the urease immobilized membrane case are discussed. Clearances of solutes, velocity profiles and pressures are estimated. In addition, since the reaction takes place in the enzyme layer, concentration of the products, ammonia and carbon dioxide are also calculated with respect to time and dimensionless positions.

6.2.1. Prediction of Protein Adsorption Capacities

To illustrate the influence of urease enzyme immobilization on the protein adsorption capacities, electrostatic and van der Waals forces were taken into account by implementing DLVO theory and particle-particle repulsive interaction energy was estimated through an adsorption simulation. It is assumed that immobilized enzyme molecules are uniformly distributed on membrane surface so that protein adsorption capacities are expected to be same at each position on the enzyme layer. The simulation results for BSA adsorption on different porous surfaces are shown in Figures (6.15), (6.16) and (6.17). Parameters and constants used in the simulations are given in Table 6.5.

Figure 6.15 can be considered as a 2-D simulation box where open circles denote the initial position of BSA molecules and stars stand for the positions at the end of 1 hr adsorption. The results show that, approximately half of the BSA molecules are adsorbed after 1 hr.

Table 6.5. Parameters and constants used in simulations at pH=7.3.

Parameters	Symbols	Values
Temperature, (K)	T	310
Boltzmann constant, (j/K)	k	1.380×10^{-23}
Dielectric constant	ς	74.8
Dielectric permittivity of free space, ($C^2/N.m^2$)	ε_o	8.854×10^{-12}
Electron charge, (C)	e	1.602×10^{-19}
Ionic strength, (M)	I	0.001
Closest approach *, (cm)	z_o	0.425×10^{-10}
Debye length, (cm^{-1})	K	8.088×10^{8}
Hamaker constant, (j)	A_{ps}	1×10^{-20}
Protein radius, (cm)	a	29.7×10^{-10}

*(Torrie and Valleau 1980)

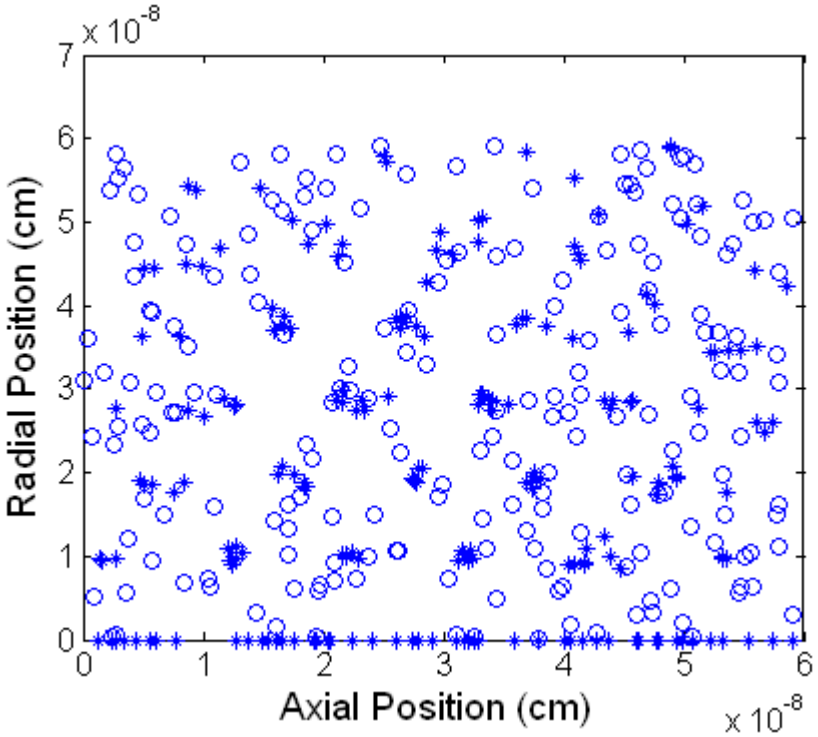

Figure 6.15. Adsorption of BSA on polysulfone membrane.

Figure 6.16 shows the BSA adsorption on urease immobilized membrane. It is found that, urea immobilization on polysulfone membrane causes about 35% decrease in the amount of proteins adsorbed on the surface after 1 hr from the beginning of hemodialysis operation. This result makes sense, because of the highly negative surface

electrical potential of urease compared to polysulfone membrane. Zeta potentials and surface electrical potentials used in the simulations are listed in Table 6.6.

Figure 6.17 shows the secondary adsorption of BSA which refers to the adsorption of BSA molecules on previously adsorbed BSA layer. As time goes to infinity, repulsion interaction free energies of BSA, ΔG_{pp} is estimated as 2.26, 2.42 and 2.68 joules for the polysulfone, immobilized enzyme, and adsorbed protein surfaces respectively. Then, adsorption capacities Q_{max1} and Q_{max2} were estimated by using these free energy values and given in Table 6.7.

Table 6.6. Surface electrical potentials of different types of materials.

Material	**Surface Electrical Potential, (mV)**
AN69 (Thomas, et al. 2000)	-89.0
Polysulfone (Thomas, et al. 2000)	-2.9
Urease (Liang, et al. 2005)	-32.1
Protein (Bowen, et al. 1998)	-25.0

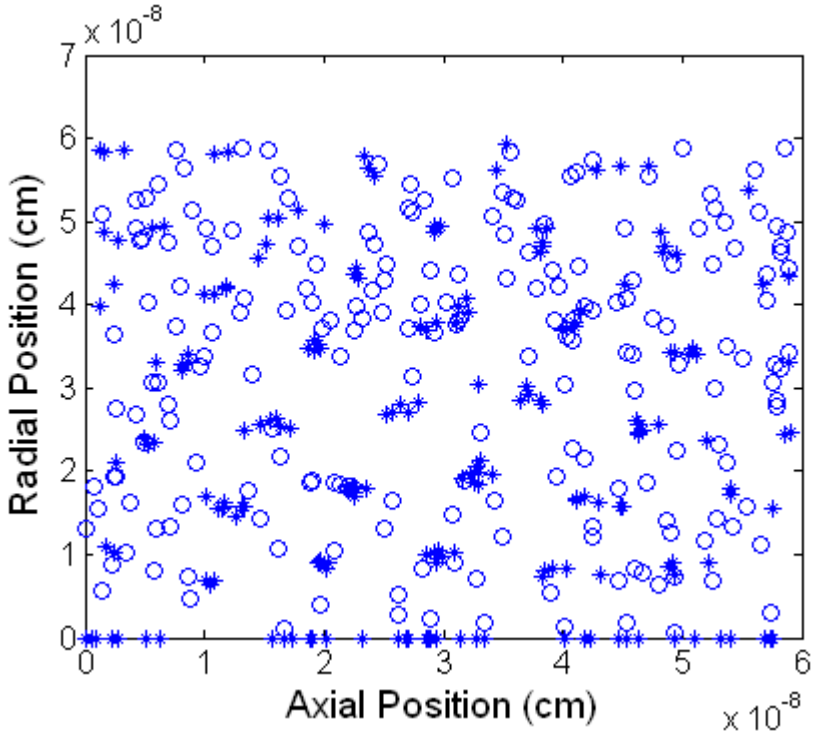

Figure 6.16. Adsorption of BSA on urease immobilized membrane.

The proteins that are not adsorbed tend to come together and coagulate because of the electrostatic and van der Waals interactions. This coagulation may cause some changes in physical properties such as diffusivity and zeta potential of proteins which may affect the protein adsorption capacity. However, particle coagulation is not taken into account by the model.

Table 6.7. Estimated adsorption capacities for different surfaces.

Adsorption Capacity	**Polysulfone Membrane**	**Urease Immobilized Membrane**	**BSA Protein Layer (Q_{max2})**
Q_{max1} (μg/cm^2)	35.1	0.78	15.1

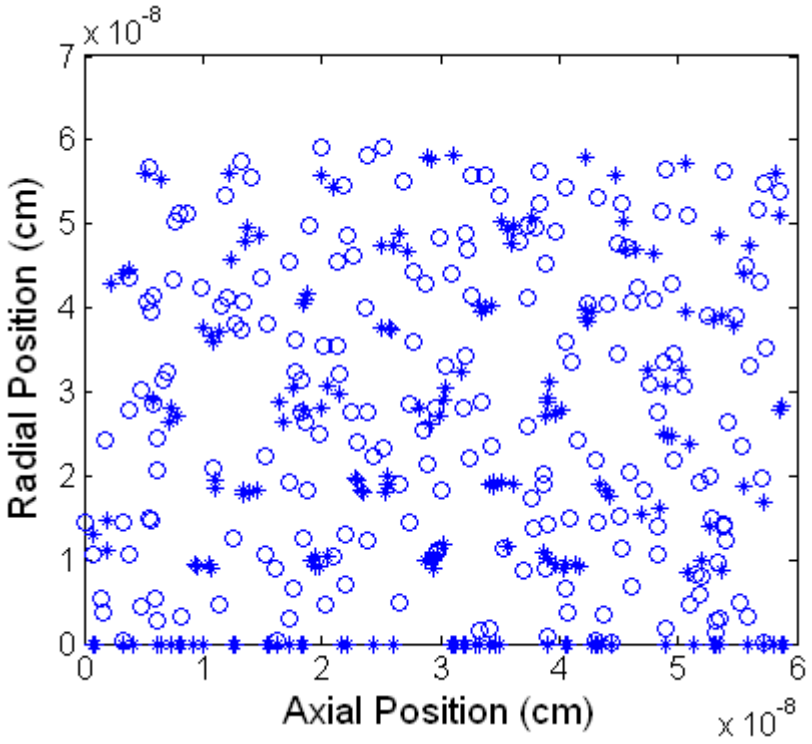

Figure 6.17. Adsorption of BSA on adsorbed BSA layer (secondary adsorption).

It is found that, adsorption capacity of BSA strongly depends on the surface electrical potential. This relationship is illustrated in Figure 6.18, where surface potentials of some commonly used membranes in hemodialysis are indicated. Adsorption capacity increases dramatically as the surface becomes less negatively charged. Q_{max1} for urease is about one-tenth of that for polysulfone membrane. It is also

observed that, after a critical potential value of -25 mV there is no considerable reduction in adsorption capacity.

Although high negative surface electrical potential of the material seems to be an advantage for minimizing protein adsorption, this may cause some undesirable reactions in blood. A previous study has shown that activation of the contact phase of plasmatic coagulation system can cause kallikrein-kinin pathways and as shown in Figure 6.19 the extent of contact phase activation in hemodialysis is strongly related to the density of negatively charged groups on the polymeric surface (Deppisch, et al. 1998). Under the light of these findings, the polymers having highly negative surface electrical potentials like AN69 can lead to serious biocompatibility problems such as kallikrein-kinin pathways which causes dialysis hypertension.

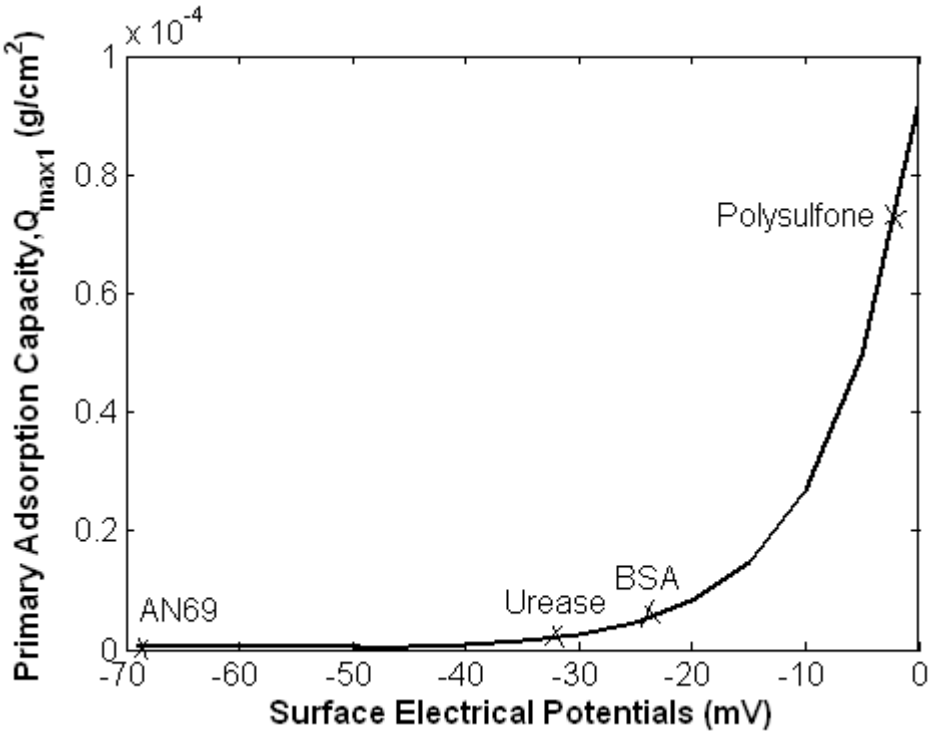

Figure 6.18. Surface electrical potential dependency of primary adsorption capacity.

Not only the surface electrical potential but also the size of the protein influences protein adsorption capacity. Figure 6.20 shows that both primary and secondary adsorption capacities increases exponentially with increased size of the protein.

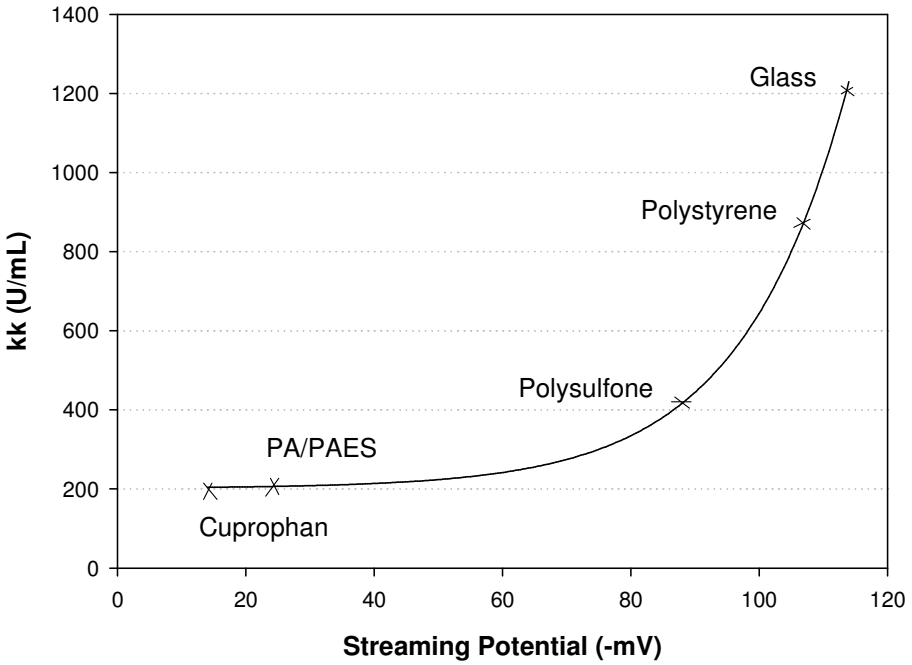

Figure 6.19. Surface induced generation of kallikrein-like activity (kk) versus the streaming potential, as a measure of surface charge, for different materials (Deppisch, et al. 1998).

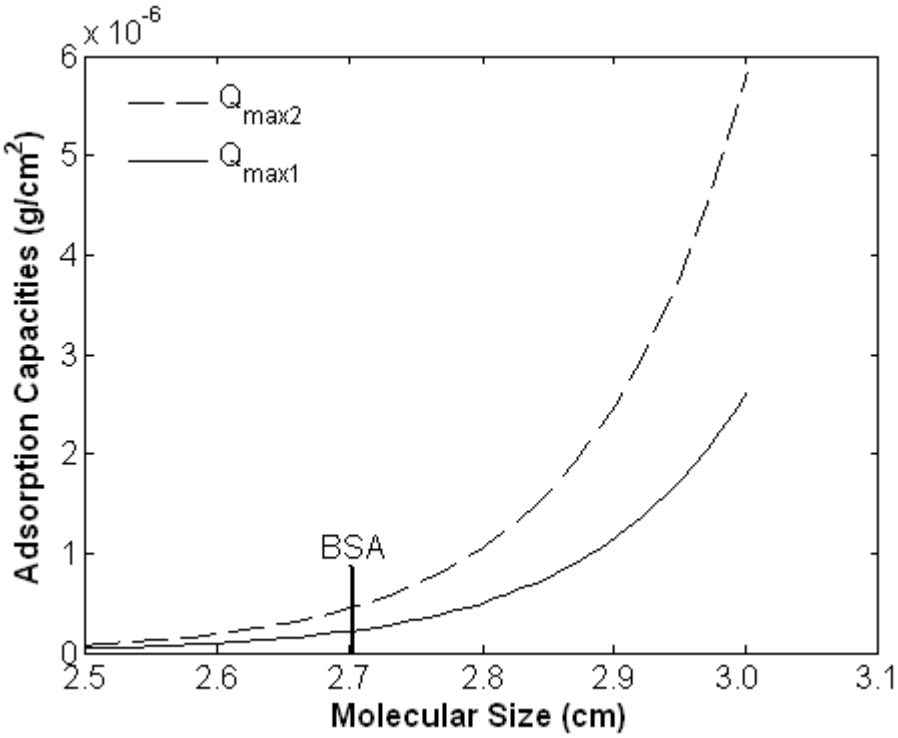

Figure 6.20. Change in primary and secondary adsorption capacities with respect to molecular size.

6.2.2. Predictions of Urea, Ammonia and Carbondioxide Concentration Profiles

In this section, the concentrations of urea, ammonia and carbondioxide were predicted based on the input data listed in Table 6.1 and Table 6.8. The blood (Q_B) and dialysate(Q_D) flow rates were taken as 200 mL/min and 500 mL/min respectively.

The comparison of the urea concentration change along the fiber length for two cases is shown in Figure 6.21. It is obvious that urease immobilization enhances the removal of urea from the blood since urea is consumed by the enzymatic reaction. Lower urea concentrations in the enzyme layer increases the driving force for the transport of urea in the blood. Consequently, in the case of enzyme immobilized membrane urea concentrations are always lower at the same radial position as shown in Figure 6.22.

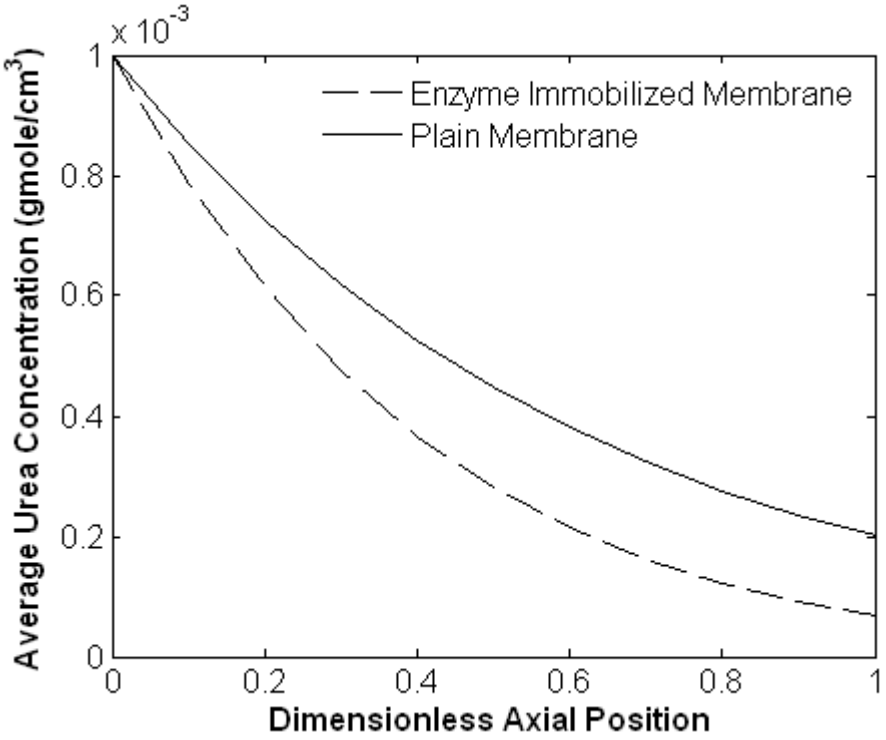

Figure 6.21. The comparison of urease immobilized and plain mambranes with respect to urea concentration change in axial direction.

Table 6.8. Parameters used in enzyme immobilized membrane case simulations.

Parameters	Symbols	Values
Free Diffusion Coefficient of Urea, $cm^2/\sec$	D_{urea}	1.81×10^{-5}
Free Diffusion Coefficient. of Ammonia, $cm^2/\sec$	D_{NH_3}	3.28×10^{-5}
Free Diffusion Coefficient of Carbondioxide, $cm^2/\sec$	D_{CO_2}	2.04×10^{-5}
Porosity of Urease Layer	ε_{Enz}	0.4765
Thickness of Urease Layer, cm	δ_{Enz}	1.31×10^{-5}
Maximum reaction rate, $mmole/cm^3.\sec$	$V_{\max}$	4.8×10^{-7}
Michaelis constant , $mmole/cm^3$	K_m	8.8×10^{-4}

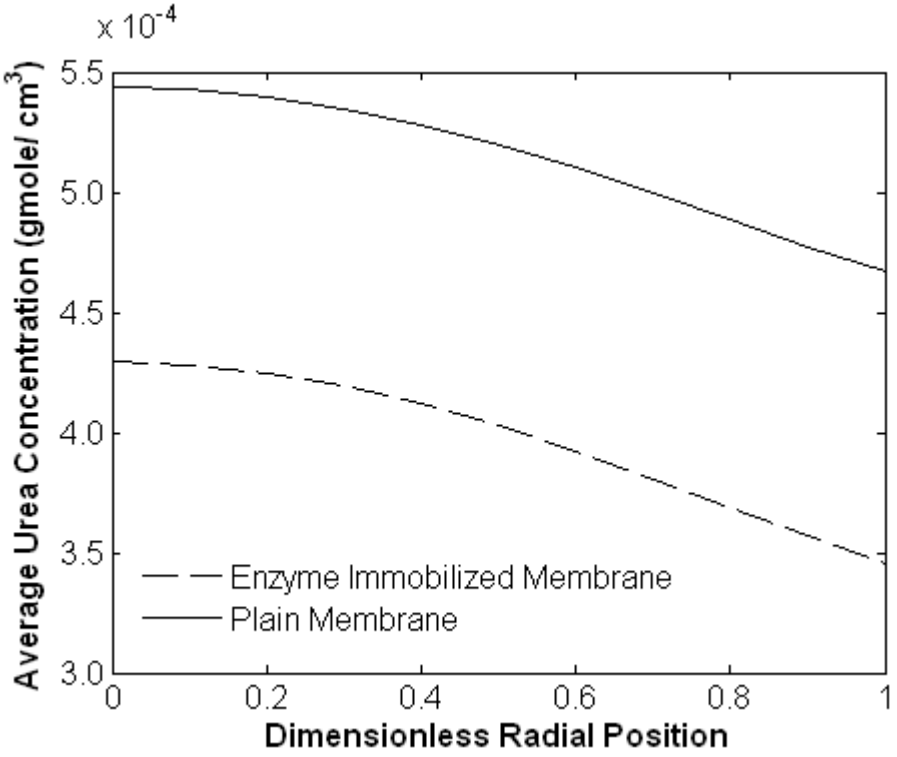

Figure 6.22. Comparison of urease immobilized and plain mambranes with respect to urea concentration change in radial direction.

The concentrations of enzymatic reaction products, ammonia and carbon dioxide, averaged over the cross section are shown in Figure 6.23. This result is obtained at the initial stage of hemodialysis so that the entrance concentrations of NH_3 and CO_2 are zero. At the first half of the fiber, there is a dramatic increase in product

concentrations. As expected, NH_3 molar concentration is higher than that of CO_2 because of the stoichiometric ratio. Along the fiber, the decrease in urea concentration makes the reaction rate slower, thus, less amount of NH_3 and CO_2 are produced. On the other hand, products of enzymatic reaction are also transfered to the dialysate side by both convection and diffusion through the membrane. This explains the decrease in NH_3 and CO_2 concentrations at the second half of fiber as shown in Figure 6.23. In other words, at the second half, mass tranfer towards the dialysate side starts to dominate the production of NH_3 and CO_2. Concentration of NH_3 decreases more sharply, this can be attributed to the higher diffusivity of NH_3 because of its relatively smaller molecular size.

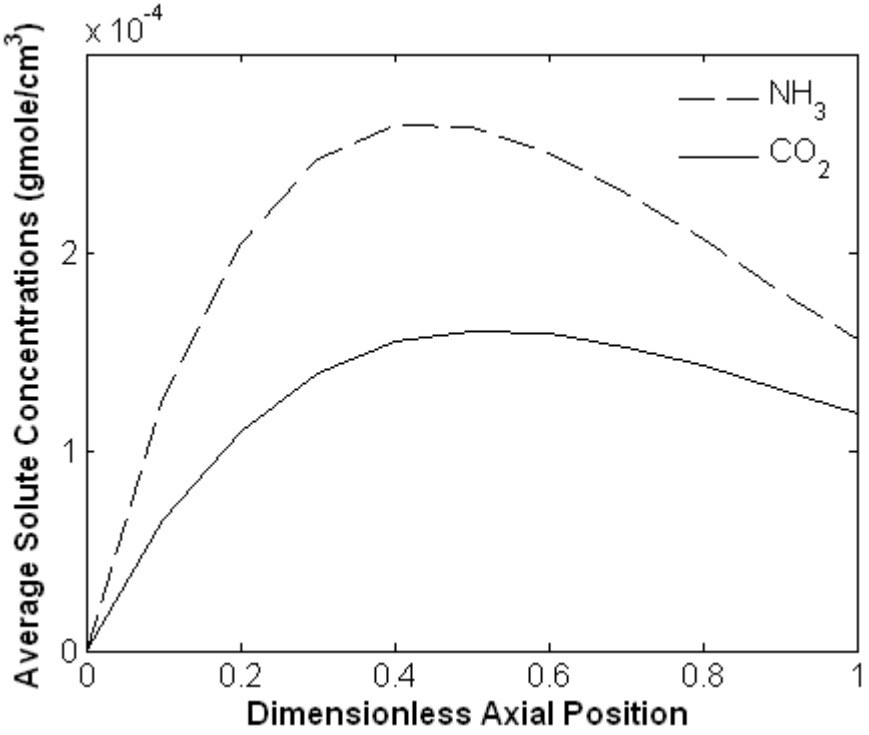

Figure 6.23. Average concentration change of reaction products in axial direction.

As expected, Figures (6.24) and (6.25) show that the concentrations of both NH_3 and CO_2 increases from the center towards the surface of the enzyme layer.

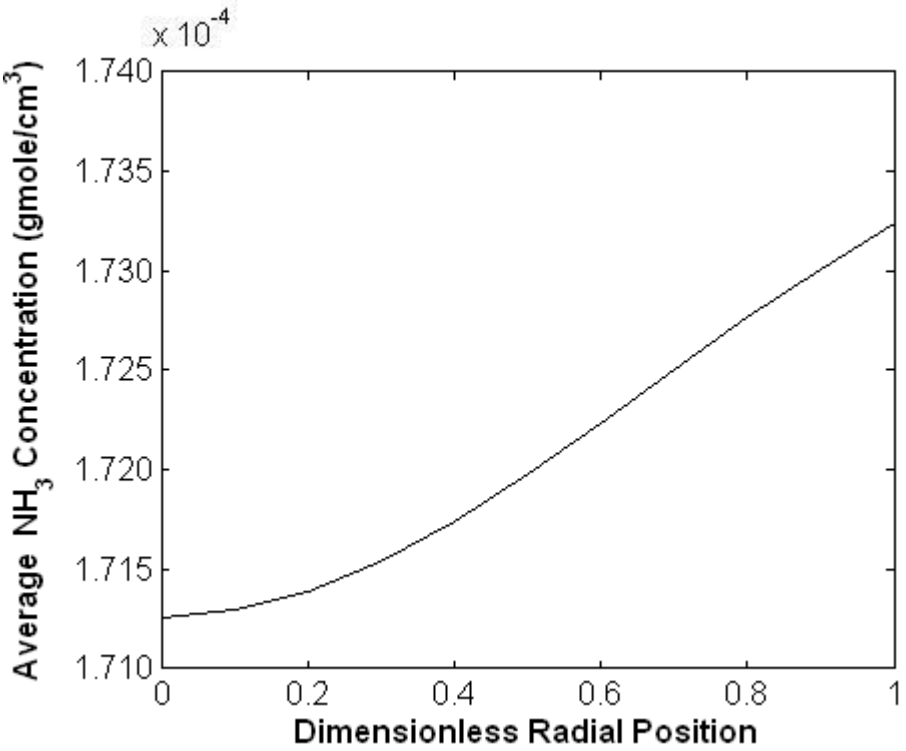

Figure 6.24. Average concentration change of ammonia in radial direction.

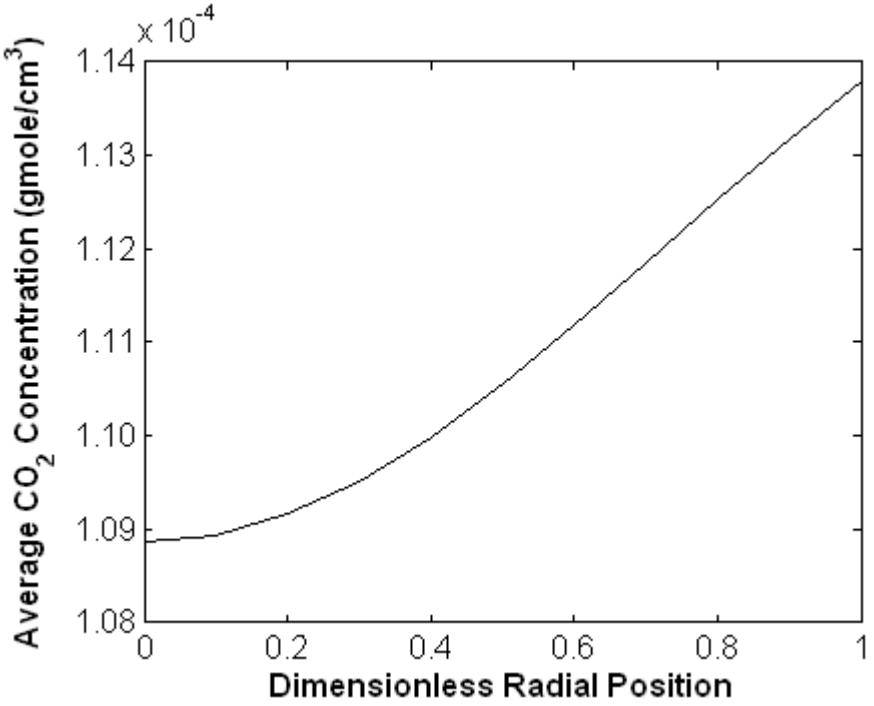

Figure 6.25. Average concentration change of carbon dioxide in radial direction.

Whole body clearance predictions were also made for the enzyme immobilized case. Figures (6.26) and (6.27) show the change in urea, ammonia and carbondioxide concentrations in patient's blood with respect to time. The urea concentration decreases exponentially while NH_3 and CO_2 concentrations increase smoothly during hemodialysis. It can be seen from Figure 6.26, that, enzyme immobilization enhances the urea removal rate, thus, the operation time becomes smaller. It shows that, time required to reduce the urea concentration to 2×10^{-4} gmole/cm^3 in patient's blood is 7000 and 8000 sec in the case of enzyme immobilized membrane and plain membrane respectively.

From clinical point of view, upper limits for NH_3 and CO_2 concentration levels in human blood are determined to be 32 μmole/L and 29 mmole/L, respectively. As shown in Figure 6.27, predicted NH_3 and CO_2 concentrations in patient blood after 2 hr of hemodialysis are found to be between normal levels. Therefore, in the case of enzyme immobilization, accumulation of NH_3 and CO_2 in blood is expected not to cause any health problems during and after hemodialysis.

Figure 6.28 shows the change in average thickness of protein layer with respect to time for enzyme immobilized and plain membrane cases. It is evident that, urease immobilization reduces the protein adsorption during hemodialysis in which protein adsorption ends after 5 min of operation. In the case of plain membrane, the protein adsorption lasts almost to the end of 30 min. The results of both cases agree with the experimental observation that protein adsorption during hemodialysis takes place very rapidly at the first stages of the operation (Basmadjian, et al. 1997; Huang 1999; Vanholder 1992; Yin, et al. 2000). The ultimate thicknesses of adsorbed protein layers were determined as 2.8×10^{-6} cm and 3.7×10^{-5} cm for enzyme immobilized and plain membrane cases, respectively.

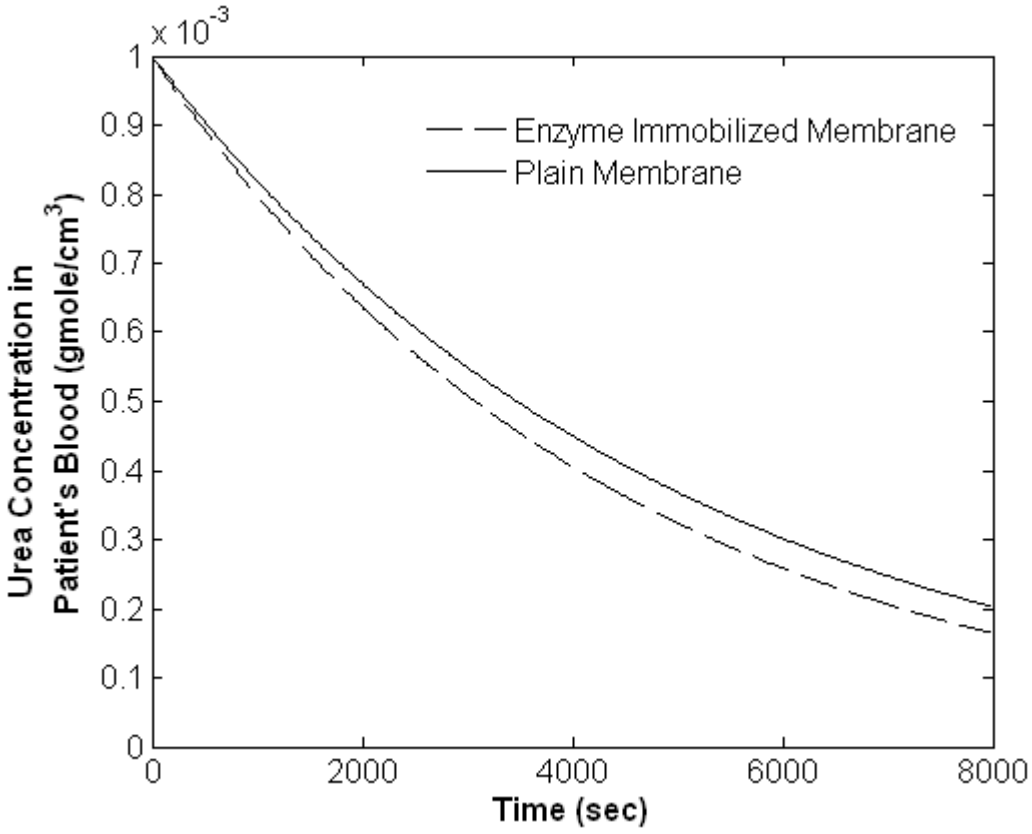

Figure 6.26. Change of urea concentration in patients blood with respect to time.

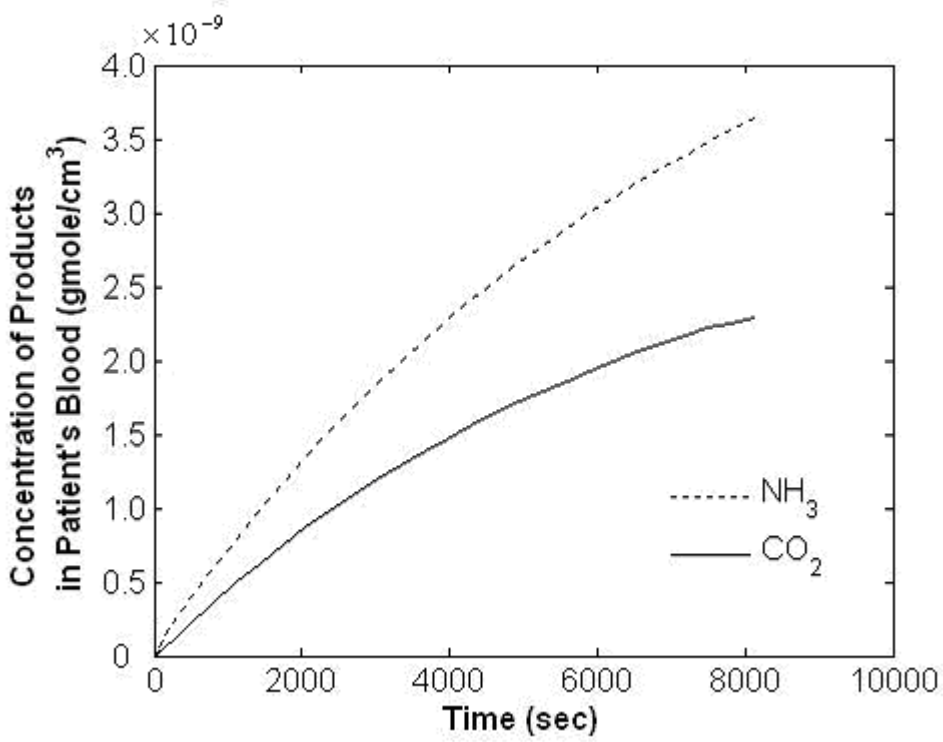

Figure 6.27. Change of product concentrations in patients blood with respect to time.

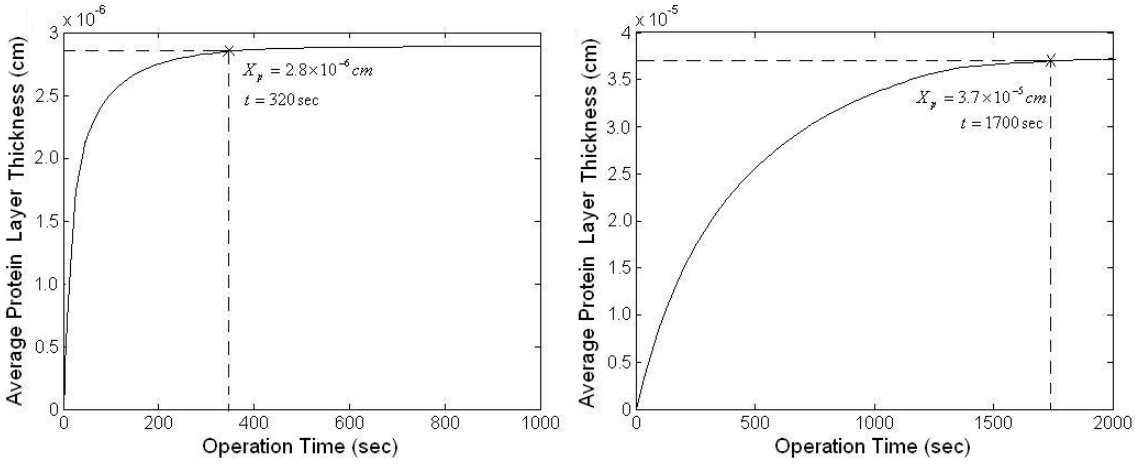

(a) (b)

Figure 6.28. Change of average protein layer thickness with respect to time (a) for enzyme immobilized case and (b) for plain membrane case.

The comparison of percent removal of urea from the patient's blood after 2 hr of hemodialysis in the case of plain and enzyme immobilized membranes are given in Table 6.9. It is observed that, urease immobilization definetely contributes to urea removal from blood at each blood flow rate. Enhancement in the urea removal rate becomes larger with increased blood flow rate and maximum reaction rates.

Table 6.9. Comparion of %urea removal in patient's blood after 2 hr in the case of plain and enzyme immobilized membranes at different blood flow rates and maximum reaction rates.

Q_B (*ml/min*)	**Plain Membrane**	**Urease Immobilized Membrane** $V_{max}=1.6\times10^{-6}$ $(mmole/cm^3.\sec)$	**Urease Immobilized Membrane** $V_{max}=3.7\times10^{-6}$ $(mmole/cm^3.\sec)$	**Urease Immobilized Membrane** $V_{max}= 6.7\times10^{-6}$ $(mmole/cm^3.\sec)$
100	57.76	58.82	59.20	59.31
200	76.29	79.26	80.93	82.44
300	83.13	86.61	88.74	90.95

The maximum reaction rate of enzymes , V_{max}, is strongly influenced by the immobilization method and immobilization conditions. Figure 6.29 shows the influence of V_{max} on predicted product concentrations at the dialyzer outlet. It is clearly seen that

sharp increases in concentrations are observed up to V_{max} values of 1.2×10^{-5} and 4.5×10^{-5} mmole/cm^3.sec for NH_3 and CO_2, respectively.

Reductions in the NH_3 and CO_2 concentrations at the dialyzer outlet can be explained by their transport towards the dialysate solution. As an illustration, NH_3 concentration profiles on both blood and dialysate sides are plotted in Figures (6.30) and (6.31) respectively. Ammonia concentration on the blood side increases up to a certain distance in the dialyzer, then it starts to decrease. The decrease is sharp at high V_{max} values, since urea is consumed more rapidly. 20 fold increase in the V_{max} value does not significantly change the NH_3 concentration at the dialyzer outlet. This is due to the fact that at higher V_{max} values production of ammonia takes place rapidly close to the fiber inlet. Thus the rest of time for blood in dialyzer is spent for the transport of ammonia towards the dialysate side. Figure 6.31 shows that dialysate solution does not contain any NH_3 at the inlet, then, along the fiber length, NH_3 concentration starts to increase with the transfer of produced NH_3 from the blood side. As expected, when V_{max} is higher, more ammonia is found on dialysate side.

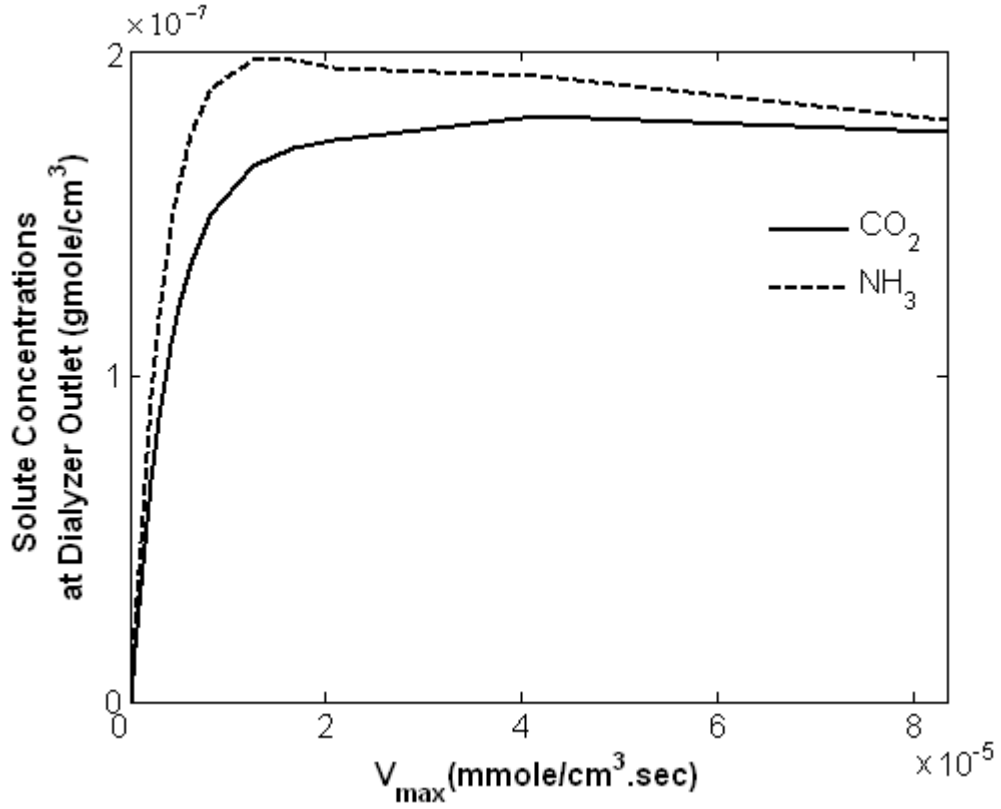

Figure 6.29. Product concentrations at dialyzer outlet for different V_{max}.

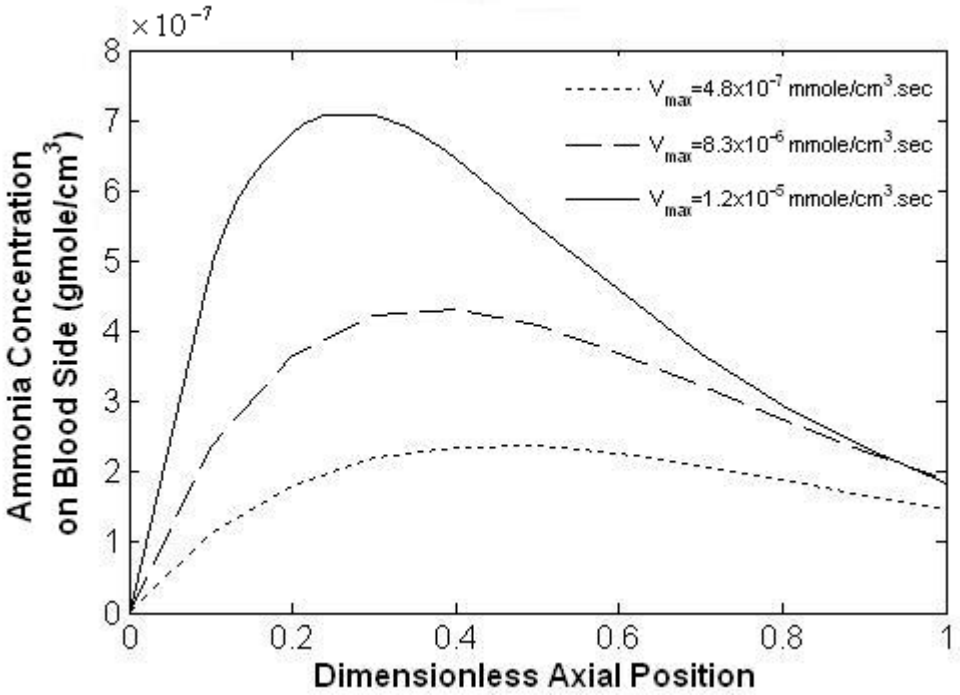

Figure 6.30. Ammonia concentration change in axial direction for different V_{max} values.

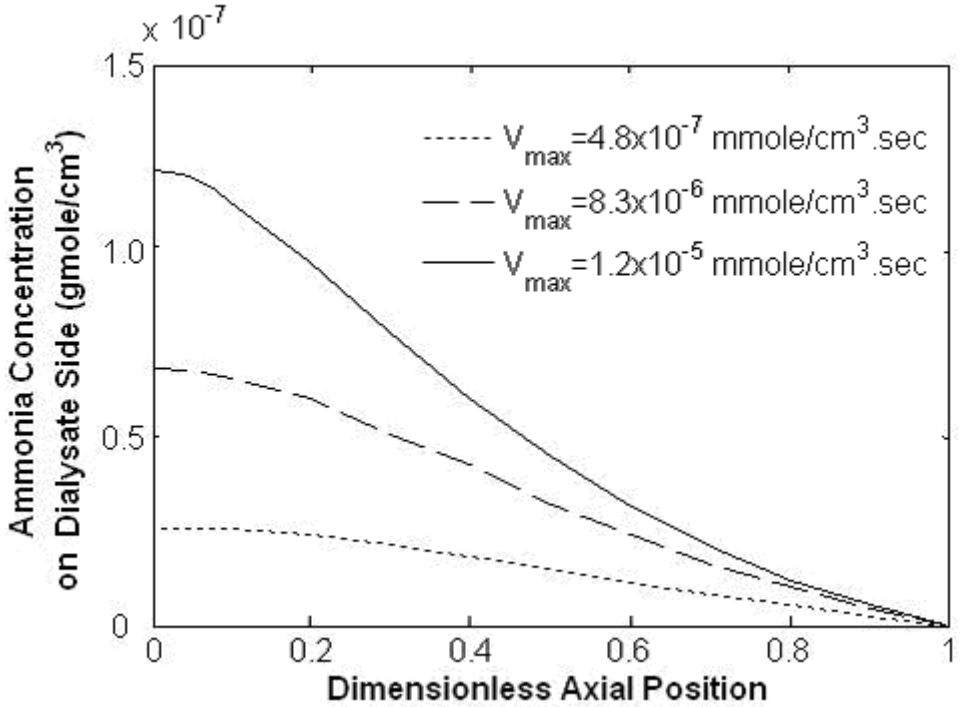

Figure 6.31. Ammonia concentration in dialysate along the module length for different V_{max} values.

CHAPTER 7

CONCLUSION

The model developed in this study can be used to predict the solute concentrations, pressure and velocity profiles as well as the adsorbed protein layer thickness as a function of time during the hemodialysis operation. Model predictions have shown that, solute concentrations in the radial direction that are usually assumed to be uniform in other studies change non-linearly. In addition, existence of radial velocity plays an important role in convective transport of protein molecules from blood to the membrane surface. It is shown that protein flux towards the membrane layer is dominated by the convection. The proteins rejected by the membrane adsorb, thus, form an additional porous layer on the membrane and make considerable resistance to the mass transfer of solutes.

Model predictions have shown that the blood and dialysate flowrates are effective for the clearances of all solute sizes. On the other hand, structural parameters of the membrane have more influences on the removal of large molecular weight solutes. Longer dialyzers with smaller fiber radius enhance the solute clearances. In addition, the free spacing among the fibers can also be adjusted as an effective design parameter to increase the rate of removal of solutes.

The model has been extended to investigate the influence of urease immobilized membrane on the overall efficiency of the hemodialysis operation. The predictions have shown that, urease immobilization enhances the rate of removal of urea. In addition, the protein adsorption capacity of the polysulfone membrane, chosen as a model system in the simulations, decreases significantly. The protein adsorption capacities of polysulfone and urease immobilized polysulfone membranes were calculated as 35.1 $\mu g/cm^2$ and 0.78 $\mu g/cm^2$ respectively. Molecular simulations performed for protein adsorption have shown that, protein adsorption capacity of a surface strongly depends on its electrical potential. Adsorption capacities were found to increase dramatically, as the surface becomes less negatively charged.

The accuracy of the model predictions were tested with two different sets of experimental data. The agreement was found to be satisfactory for each data set. Thus, it is fair to conclude that the model developed in this study can be used as a tool by

clinicians to investigate the influences of blood and dialysate flowrates or by researchers either to optimize module design or the structure of the membrane.

To our knowledge, this is the first predictive model which takes into account not only simultaneous mass and momentum transfer but also the adsorption of large proteins. In the future, the model can be further extended to consider the internal fouling phenomena inside the membrane caused by the adsorption of middle molecular weight proteins. It may also be useful to include an expression for calculating the hydraulic permeability of the membrane in the presence of an adsorbed protein layer.

REFERENCES

Baeyer H. V, Kochinke R, Schwerdtfeger R. 1985. Cascade plasmapheresis with online membrane regeneration: laboratory and clinical studies. J. Membr. Sci. 22 : 297.

Baeyer H. V, Lajous-Petter A, Debrandt W, et al. 1988. Surface reactions on blood contact during hemodialysis and haemofiltration with various membrane types. J. Membr. Sci. 36 : 215.

Basmadjian D, Stefon M. V, Baldwin S. A. 1997. Coagulation on biomaterials in flowing blood: some theoretical considerations. Biomaterials 18 : 1511.

Belfort G, Davis R, Zydney A.L. 1994. The behavior of suspensions and macromolecular solutions in crossflow microfiltration. J. Membrane Sci. 96 : 1–58.

Bland L. A, Favero M. S. 1993. Microbiologic aspects of hemodialysis systems. In AAMI Standards and Recommended Practices. Association for the Advancement of Medical Instrumentation 257–265.

Bloembergen W, Hakim R, Stannard D, et al. 1999. Relationship of dialysis membrane to cause-specific mortality. Am. J. Kidney Dis. 33.

Bosch T, Schmidt B, Samtleben W, Gurland H. J. 1985. Effect of protein adsorption on diffusive and convective transport through polysulfone membranes. Contr. Nephrol. 46 : 14–22.

Bowen W. R, Pan L.C, Sharif A. O. 1998. Predicting equilibrium constants for ion exchange of proteins colloid science approach. Colloids and Surfaces A: Physicochemical and Engineering Aspects 143 : 117–131.

Boyd R. F, Zydney A. L. 1997. Sieving characteristics of multilayer ultrafiltration membranes. J. Membr. Sci. 131 : 155.

Boyd R. F, Zydney A. L. 1998. Analysis of Protein Fouling During Ultrafiltration Using a Two-Layer Membrane Model. Biotechnology and Bioengineering. 59 : 451-460.

Bungay P. M, Brenner H. 1973. The motion of a closely fitting sphere in a fluid filled tube. Int. J. Multipk. Flow 1 : 25-56.

Causserand C, Meireles M, Aimar P. 1996. Proteins transport through charged porous membranes. Trans IChemE. 74 : 113–122.

Causserand C, Nystrom M, Aimar P. 1994. Study of streaming potentials of clean and fouled ultrafiltration membranes. J. Membr. Sci. 88 : 211–222.

Chang Y. L, Lee C. J. 1988. Solute transport characteristics in hemodiafiltration, J. Membr. Sci. 39 : 99–111.

Charcosset C, Jaffrin M.Y, Ding L. 1990. Time and pressure dependence of sieving coefficients during membrane plasma fractionation. ASAIO Trans. 36 : 594.

Chen J.-P, Chiu S.-H. 2000. Enzym. Microb. Technol. 26 : 359.

Chibata I, eds.1975. Immobilized Enzyme. Kodansha.

Clark W. R, Gao D. 2002. Properties of membranes used for hemodialysis therapy. Seminars Dialysis 15 : 191.

Clark W. R, Leypoldt J. K, Henderson L. W. 1999. Quantifying the effect of changes in the hemodialysis prescription on effective solute removal with a mathematical model. J Am Soc Nephrol 10 : 601-609.

Dahuron L, Cussler E. L. 1988. Protein extraction with hollow fibres. AIChE J. 34.

Deen W. M. 1987. Hindered transport of large molecules in liquidfilled pores. AIChE J. 33 : 1409.

Deppisch R, Storr M, Buck R, Gohl H. 1998. Blood material interactions at the surfaces of membranes in medical applications, Separation and Purification Technology 14 : 241–254.

Dionne K.E, Cain B.M, Li R.H, Bell W. J. 1996. Transport characterization of membranes for immunoisolation. Biomaterials 17 : 257.

Elimelech M, Gregory J, Jia X, Williams R. A. 1995. Particle Deposition and Aggregation Measurement, Modeling and Simulation. Oxford : Butterworth–Heinemann.

Eloot S. 2005. Experimental and Numerical Modeling of Dialysis.

Fane A. G, Fell C. J. D. 1987. A review of fouling and fouling control in ultrafiltration. Desalination 62 : 117.

Fane AG, Fell C, Walters A. G. 1983. Ultrafiltration of protein solutions through partially permeable membranes – The effect of adsorption and solution environment. J. Membrane Sci. 16 : 211–224.

Feast W. J, Munro H. S. 1987. Polymer Surfaces and Interfaces. Chichester: Wiley.

Fujimori A, Naito H, Miyazaki T. 1998. Adsorption of complement, cytokines, and proteins by different dialysis membrane materials: evaluation by confocal laser scanning fluorescence microscopy. Artif. Organs 22 : 1014.

Fukui S, Chibata I, Suzuki S, eds. 1981. Enzyme Technology. Tokyo: Kagaku Dojin.

Gachon A. M. F, Mallet J, Tridon A, Deteix P. 1991. Analysis of proteins eluted from hemodialysis membranes. J Biomater. Sci. Polym. 76 (2) : 263.

Ghosh R. 2002. Study of membrane fouling by BSA using pulsed injection technique. J. Membr. Sci. 195 : 115.

Giddings J. C, Kucera E, Russell C. P, Myers M. N. 1968. Statistical theory for the equilibrium distribution of rigid molecules in inert porous networks. Exclusion chromatography. Pkys. Ckem. 72 : 4397-4408.

Godjevargova T, Gabrovska K. 2003. J. Biotech. 103 : 107.

Grace H. P. 1956. Structure and performance of filter media. AIChE J. 2 : 307.

Guyton A. C. 1986. Textbook of medical physiology. Philadelphia : WB Saunders Company.

Hanft S. 2002. C-208R Key Medical Membrane Devices for the New Millennium. Business Communications Company Inc.

Hermia J. 1982. Constant pressure blocking filtration laws-application to power-law non-Newtonian fluids. Trans. IchemE 60 : 183.

Ho C.-C, Zydney A. L. 1999. Effect of membrane morphology on the initial rate of protein fouling during microfiltration. J. Membr. Sci. 155 : 261.

Ho C.-C. 2001. Effect of membrane morphology and structure on protein fouling during microfiltration. Diss. Abstr. Int. 62 : 2403.

Hosoya N, Sakai K. 1990. Backdiffusion rather than backfiltration enhances endotoxin transport through highly permeable dialysis membranes. Trans. ASAIO 36 : 311–313.

Huang J. 1999. Investigation of Biocompatibility of Polyethersulfone and Sulfonated Polyethersulfone used as Blood Purification Membranes. China: Sichuan University Dissertation.

Iaraelachvili J. N. 1985. Intermolecular and Surface Forces. London: Academic Pres.

Iwasaki T. 1937. Some notes on sand filtration. J. Am. Water Works Assoc. 29 : 1591–1602.

Jaffrin M.Y, Gupta B. B, Malbrancq J. M. 1981. A one-dimensional model of simultaneous hemodialysis and ultrafiltration with highly permeable membranes. J. Biomech. Eng. 103 : 261–266.

Jagannadh S. N, Muralidhara H. S. 1996. Electrokinetics methods to control membrane fouling. Ind. Eng. Chem. Res. 35 : 1133.

Katchalsky A, Curan P. 1967. Nonequilibrium Thermodynamics in Biophysics. Cambridge : Harvard University Pres.

Kim K. J, Fane A.C, Fell C. D, Joy D. C. 1992. Fouling mechanisms of membranes during protein ultrafiltration. J. Membr. Sci. 68 : 79.

Kim K. J, Fane A. G, Nystrom M, Pihlajamaki A. 1997. Chemical and electrical characterization of virgin and protein-fouled polycarbonate track-etched membranes by FTIR and streaming-potential measurements. J. Membr. Sci. 134 : 199–208.

Koda Y, Nishi S, Miyazaki S, Haginoshita S. 1997. Switch from conventional to high-flux membrane reduces the risk of carpal tunnel syndrome and mortality of hemodialysis patients. Kidney Int. 52 : 1096.

Kunimoto T, Lowrie E. G, Kumazawa, et al. 1977. Controlled ultrafiltration (UF) with hemodialysis (HD): analysis of coupling between convective and diffusive mass transfer in a new HD-UF system. Trans. ASAIO 23 : 234–241.

Kuwayhara T, Markert M, Wauters J. P. 1989. Proteins adsorbed on hemodialysis membranes modulate neutrophil activation. Artif. Organs 13 : 427.

Landis E. M, Pappenheimer J. R. 1963. Handbook of Physiology, , Washington, DC: Am. Phys. Soc.

Langlois W. E. 1964. Slow Viscous Flow. New York: 201-221.

Langsdorf L. J, Zydney A. L. 1994. Effect of blood contact on the transport properties of hemodialysis membranes: A two-layer membrane model. Blood Purif. 12 : 292–307.

Legallais C, Catapano G, Harten B. V, Baurmeister U. 2000. A theoretical model to predict the in vitro performance of hemodiafilters. J. Membr. Sci. 168 : 3–15.

Lin C.-C, Yang M.-C. 2003. Biomaterials 24 : 1989.

Lipps B, Stewart R, Perkins H, Holmes G, et al. 1969. The hollow fiber artificial kidney. Trans. Am. Soc. Artif. Intern. Org. 13 : 200.

Mahliçli F.Y, Preparation and Characterization of the Membranes, Master Thesis, İzmir Institute of Technology, (2007).

Marshall A. D, Munro P. A, Trägårdh G. 1993. The effect of protein fouling in microfiltration and ultrafiltration on permeate flux, protein retention and selectivity: a literature review. Desalination 91 : 65.

Martin A, Martinez F, Calvo J. I. 2002. Protein adsorption onto an inorganic microfiltration membrane: solutesolid interactions and surface coverage. J. Membr. Sci. 207 : 199–207.

Martinez F, Martin A, Pradanos P. 2000. Protein adsorption and deposition onto microfiltration membranes: the role of solute-solid interactions, J. Colloid Interf. Sci. 221 : 254–261.

Martino S. D, El-Sheriff H, Diane N. 2003. Appl. Catal. B: Environ. 46 : 613.

Matthiasson E. 1983. The role of macromolecular adsorption in fouling of ultrafiltration membranes. J. Membr. Sci. 16 : 23.

Meireles M, Aimar P, Sanchez V. 1991. Effects of protein fouling on the apparent pore size distribution of sieving membranes. J. Membrane Sci. 56 : 13–28.

Mineshima M, Yokoi R, Horibe K. 2001. Effects of operating conditions on selectivity of a plasma fractionator in double filtration plasmapheresis. Ther. Apher. 5 : 444.

Morrette R. A., Gogos C.G. 1968. Viscous dissipation in capillary flow of rigid PVC and PVC degradation. Polymer Engng. Sci. 8 : 272-280.

Morti S, Shao J, Zydney A. L. 2003. Importance of asymmetric structure in determining mass transport characteristics of hollow fiber hemodialyzers. J. Membrane Sci . 224 : 39–49.

Mosbach K, eds. 1976. Immobilized enzyme. Methods in Enzymology: Academic press.

Moussy Y. 2000. Bioartificial Kidney. I. Theoretical Analysis of Convective Flow in Hollow Fiber Modules: Application to a Bioartificial Hemofilter, Biotechnology and Bioengineering. Biotechnology and Bioengineering 68 (2) 142-152.

Nakamura K, Matsumoto K. 2006. Properties of protein adsorption onto pore surface during microfiltration: effects of solution environment and membrane hydrophobicity. J. Membr. Sci. 280 : 363–374.

Nakao S, Osada H, Kurata H, Suru T, Kimura S. 1988. Separation of proteins by charged ultrafiltration membranes. Desalination 70 : 191–205.

Nakao S, Yumoto S, Kimura S. 1982. Analysis of rejection characteristics of macromolecular gel layer for low molecular weight solutes in ultrafiltration. J. Chem. Eng. 15 : 463–468.

Nilsson J, Hallstrom B. 1991. Deviations in the fouling resistance of UF membranes due to clean membrane permeability variations. J. Membrane Sci. 67 : 177–189.

Noda I, Gryte C. C. 1979. Mass Transfer in Regular Arrays of Hollow Fibers in countercurrent Dialysis. Aiche Journal 113-122.

Oberholzer M. R, Lenhoff A. M. 1999. Langmuir 15 : 3905.

Oberholzer M. R, Wagner N. J, Lenhoff A. M. 1997. J. Chem. Phys. 107 : 9157.

Pallone T. L, Petersen J. 1987. A mathematical model of continuous arteriovenous hemofiltration predicts performance. Trans. ASAIO 33 : 304–308.

Pandya P, Farrington K. 2003. Haemodialysis. Medicine 66-69.

Raff M, Welsch M, Göhl H, et al. 2003. Advanced modeling of highflux hemodialysis. J. Membr. Sci. 216 : 1–11.

Russel W.B, Saville D.A, Schowalter W. R. 1989. Colloidal Dispersions. Cambridge: Cambridge Univ. Pres.

Sader J. E. 1997. J. Colloid Interface Sci. 188 : 508.

Schmidt B. 1996. Membranes in artificial organs. Artif. Organs 20 : 375.

Sigdell J. E, Tersteegen B. 1986. Clearance of a dialyzer under varying operating conditions. Artif Organs 10 : 219-225.

Sigdell J. E. 1982. Calculation of combined diffusive and convective mass transfer. Int. J. Artif. Organs 5 : 361–372.

Spiegler K. S, Kedem O. 1966. Thermodynamics of hyperfiltration (reverse osmosis): criteria for efficient membranes, Desalination 1. 311–326.

Stiller S, Mann H, Brunner H. 1985. Backfiltration in hemodialysis with highly permeable membranes. Contr. Nephrol. 46 : 23–32.

Thomas M, Valette P, Mausset A. L, Dejardin P. 2000. High molecular weight kininogen adsorption on hemodialysis membranes: influence of pH and relationship with contact phase activation of blood plasma. Influence of pre-treatment with poly(ethylenamine). The International J. of Art. Organs, 23 : 20-26.

Torrie G. M , Valleau J. P. 1980. J. Chem. Phys. 73 : 5807.

Truskey G. A, Fan Y, Katz D. F. 2004. Transport Phenomena in Biological Systems. Prentice Hall : 104.

Uragami T. 1986. Bio Ind. 3 (22) : 33.

Van Waeleghem J. P, Lindley E. J. 2000. Management of the vascular access in Europe. Part I - A study of centre based policies. EDTNA/ERCA J. 26 : 28-33.

Vanholder R. 1992. Biocompatibility issues in hemodialysis. Clin. Mater. 10 : 87.

Wang Y, Howell J. A, Field R. W, Wu D. 1994. Simulation of cross-flow filtration for baffled tubular channels and pulsatile flow. J. Membr. Sci. 95 : 243.

Werynski A, Wanieski J. 1995. Theoretical description of mass transport in medical membrane devices, Artif. Organs 19 (5) : 420–427.

Woffindin C, Hoenich N. A. 1995. Hemodialyzer performance: a review of the trends over the past two decades. Artif. Org. 19 : 1113.

Wüpper A, Dellanna F, Baldamus C. A, Woermann D. 1997. Local transport processes in high-flux hollow fiber dialyzers. J. Membr. Sci. 131 : 181–193.

Wüpper A, Woermann D, Dellanna F, Baldamus C. A. 1996. Retrofiltration rates in high-flux hollow fiber hemodialysers: analysis of clinical data. J. Membr. Sci. 121 : 109–116.

Yang M. C, Tong J. H. 1997. Loose ultrafiltration of proteins using hydrolyzed polyacrylonitrile hollow fiber. J Membrane Sci 132 : 63–71.

Yin G, Janson J.-C, Liu Z. 2000. Characterization of protein adsorption on membrane surface by enzyme linked immunoassay. J. Membr. Sci. 178 : 99.

Zhao Z.-P, Wang Z, Wang S.-C. 2003. Formation, charged characteristic and BSA adsorption behavior of carboxymethyl chitosan/PES composite MF membrane. J. Membr. Sci. 217 : 151–158.

Zhenpeng L, Chaoyang W, Zhen T. 2005. Bio-catalytic nanoparticles with urease immobilized in multilayer assembled through layer-by-layer technique. Reactive & Functional Polymers 63 : 85–94.